UNIVERSIDADE FEDERAL DE SANTA CATARINA
CENTRO TECNOLÓGICO
PROGRAMA DE PÓS-GRADUAÇÃO EM ENGENHARIA QUÍMICA

Karla Pollyanna Vieira de Oliveira

^{3L}BNC Platform: an innovative stacked-multilayered BNC scaffold for studies of multi-cell co-culture in compartmentalization

FLORIANÓPOLIS
2022

Karla Pollyanna Vieira de Oliveira

^{3L}BNC Platform: an innovative stacked-multilayered BNC scaffold for studies of multi-cell co-culture in compartmentalization

Thesis submitted to the Program of Doctorate in Chemical Engineering of the Federal University of Santa Catarina to obtain the title of Doctor in Chemical Engineering
Advisor: Prof. Dr. Luismar Marques Porto (UFSC)
Co-advisors: Dra. Fernanda Vieira Berti (Biocelltis Biotecnologia)
Prof. Dra. Maryam Tabrizian (McGill University)

Florianópolis
2022

Ficha de identificação da obra elaborada pelo autor,
através do Programa de Geração Automática da Biblioteca Universitária da UFSC.

Oliveira, Karla Pollyanna Vieira de
3LBNC Platform : an innovative stacked-multilayered BNC scaffold for studies of multi-cell co-culture in compartmentalization / Karla Pollyanna Vieira de Oliveira ; orientador, Luismar Marques Porto, coorientadora, Fernanda Vieira Berti, 2022.
118 p.

Tese (doutorado) - Universidade Federal de Santa Catarina, Centro Tecnológico, Programa de Pós-Graduação em Engenharia Química, Florianópolis, 2022.

Inclui referências.

1. Engenharia Química. 2. Triple cell co-culture. 3. 3D model. 4. Bacterial nanocellulose. 5. Breast cancer. I. Porto, Luismar Marques. II. Berti, Fernanda Vieira. III. Universidade Federal de Santa Catarina. Programa de Pós Graduação em Engenharia Química. IV. Título.

Karla Pollyanna Vieira de Oliveira

^{3L}BNC Platform: an innovative stacked-multilayered BNC scaffold for studies of multi-cell co-culture in compartmentalization

O presente trabalho em nível de doutorado foi avaliado e aprovado por banca examinadora composta pelos seguintes membros:

Profa. Maryam Tabrizian, Dra.
McGill University

.

Prof. Alexander Birbrair, Dr.
Universidade Federal de Minas Gerais

Profa. Ana Paula Immich Boemo, Dra.
Universidade Federal de Santa Catarina

Julia de Vasconcellos Castro, Dra.
MassBiologics

Certificamos que esta é a **versão original e final** do trabalho de conclusão que foi julgado adequado para obtenção do título de doutora em Engenharia Química.

ICP-Edu
Documento assinado digitalmente
Debora de Oliveira
Data: 07/03/2022 17:09:58-0300
CPF: 728.453.929-15
Verifique as assinaturas em https://v.ufsc.br

_____

Coordenação do Programa de Pós-Graduação

ICP-Edu
Documento assinado digitalmente
Luismar Marques Porto
Data: 07/03/2022 16:54:07-0300
CPF: 380.494.909-63
Verifique as assinaturas em https://v.ufsc.br

_____

Prof. Luismar Marques Porto, Dr.
Orientador

Florianópolis, 2022

Every great advance in science has issued from a new audacity of imagination.

John Dewey

Acknowledgement

ACKNOWLEDGEMENT

This being research performed in two different countries – Brazil and Canada, my gratitude needs to be expressed in the two languages used by my audiences.

First, I would like to thank my mentors. My advisor (Dr. Porto) and my co-advisor (Dra. Tabrizian) for accepting to guide me and for the opportunity of being part of your great teams at UFSC and McGill University.

My co-advisor Dra. Berti would be deserving a special chapter in my thesis. I may have already told you, but I'd like to reinforce my gratitude for all the "rescue operations", for orienting me, and for your ability to share your passion about science. It's inspiring and I want to be sure that you know that I'm very thankful, from the bottom of my heart!

I'm also very thankful for the teams I worked with. In Brazil, my special thanks go to Stefanie Mandrik (for accepting to be my undergrad assistant for a short-time and helping me with many experiments) and to Giovana Fucina (for being a tireless source of encouragement and discussions). For the Canada' team, I can say that I had the privilege of being part of a great family with which I had lots of fun and lots of discussions that made me think about my research and made me a better scientist. Additionally, I'm very thankful for your help, Michael Yitayew, with all confocal experiments. It was not easy but I'm glad that I could count on you.

Both institutions in which I conducted this research, UFSC and McGill, deserve a big thank you, as well as the financing agencies from Brazil (CAPES) and Canada (CIHR). Specifically, from UFSC, I would like to thank you the secretary Edevilson Silva, for all help in bureaucracy.

Then, it's important to acknowledge my friends. All of them had an important role in my journey and nominating each one could make me sound ungrateful. There were so many! In Brazil, Canada, and other parts of the world!

However, I want to express my thanks to two girls, for their role in my stay in Canada. First, I would like to say thank you to you, Vandrize Meneghini, because without your suggestions, I would never have tried the selective process to go to McGill. Then, I want to thank you so much, Claudia Zwarg, for being such a great friend even before we met. Without you, my stay would be quite different and I'm sure I could have "panicked" in some moments.

My psychologist also had a big role in this process and deserves special thanks. With so many things going on, I'm pretty sure that you were extremely important to keep my sanity intact (or should I say: to keep my craziness under control? LOL). So, thank you very much, Eliane de Campos. For all.

My final thanks go now to my parents. Mom, dad... Thank you. I feel privileged for being your daughter and receiving all support from you both. I can't count how many times you were essential to keep me on track and make me feel better just for being myself. You both are a blessing in my life. Thank you, for everything!! I love you and I want to dedicate this achievement to you both and to Léo (wherever he may be, I know that is happy for me too).

AGRADECIMENTOS

Como esse trabalho foi realizado em dois países – Brasil e Canadá, meus agradecimentos merecem ser expressos em ambas as línguas utilizadas pela minha audiência.

Em primeiro lugar, gostaria de agradecer aos meus mentores. Ao meu orientador (Dr. Porto) e à minha coorientadora (Dra. Tabrizian) pelo aceite em me guiar nos caminhos científicos e pela incrível oportunidade de ter participado de seus respectivos times na UFSC e na McGill University.

Minha coorientadora Dra. Berti merece um capítulo especial nessa tese. Talvez eu tenha lhe dito, mas gostaria de reiterar minha profunda gratidão por todas as "operações de resgate", pela orientação, e por sua habilidade em compartilhar seu amor pela Ciência. É inspirador e quero ter certeza de que você saiba o quanto sou grata, do fundo do meu coração!

Agradeço também a ambos os times com os quais trabalhei. No Brasil, meu agradecimento vai especialmente à Stefanie Mandrik (por ter aceitado me acompanhar nesse projeto enquanto realizava sua iniciação científica e por ter me ajudado com tantos experimentos) e à Giovana Fucina (por todas as discussões e por todo encorajamento). Quanto ao time canadense, posso dizer que tive o privilégio de fazer parte de uma família com a qual me diverti muito e tive incontáveis discussões que me ajudaram a pensar melhor sobre minha pesquisa e me tornar uma cientista melhor. A você, Michael Yitayew, meu agradecimento por todos os experimentos de microscopia confocal. Não foi fácil, mas fico muito feliz que pude contar com você.

É importante agradecer a ambas as instituições nas quais essa pesquisa foi conduzida, UFSC e McGill, bem como à CAPES (Brasil) e CHIR (Canadá). Além disso, gostaria de agradecer nominalmente ao secretário do PosENQ, Edevilson Silva, por toda ajuda fornecida para sanar as burocracias.

A seguir, é importante agradecer a todos os meus amigos. Todos tiveram um papel muito importante em minha jornada e nomeá-los poderia fazer com que eu soasse ingrata. Eles foram tantos! No Brasil, Canadá e em outras partes do mundo!

No entanto, gostaria de expressar meus agradecimentos a duas amigas em particular que tiveram um papel muito importante para minha estadia no Canadá. Primeiro, quero agradecer a você, Vandrize Meneghini, porque se não fossem suas sugestões, eu nunca teria tentado o processo seletivo para fazer parte do meu

doutorado na McGill. A seguir, agradeço à você, Claudia Zwarg, por ser uma amiga incrível mesmo antes de nos conhecermos. Sem você, minha estadia teria sido diferente e tenho certeza de que teria ficado um pouco desorientada em alguns momentos.

Minha psicóloga também teve papel muito importante nesse processo e merece um agradecimento especial. Com tantas coisas acontecendo, tenho certeza de que você foi extremamente importante para manter minha sanidade intacta (ou deveria dizer: para manter minha loucura sob controle? LOL). Por isso, muito obrigada Eliane de Campos. Por tudo.

Finalmente, quero agradecer aos meus pais. Mãe, Pai… Muito obrigada. Sinto-me privilegiada por ser sua filha e por receber tanto suporte de ambos. Perdi a conta das vezes em que vocês foram essenciais para me ajudar a me manter na linha e das vezes em que me fizeram sentir amada, só por ser eu mesma. Vocês dois são uma bênção na minha vida. Muitíssimo obrigada, por tudo! Amo vocês dois e gostaria de dedicar essa realização a vocês e ao Léo (que de onde quer que esteja, sei que também está feliz por mim).

ABSTRACT

Cell culture 3D models are a well-established field since many works had proved that cells cultured in plates (2D environment) differ from what is seen *in vivo*. Consequently, different 3D models have been proposed but they have important drawbacks such as the lack of more than 2 cell types co-culturing, and the absence of cell support as promoted *in vivo* by ECM and of molecular biology analysis. In this work, we report the production, characterization, and validation of a pristine stacked-multilayered nanocellulose-based scaffold that has an optical translucid format. The platform was made by statically culturing *K. hansenii* ATCC 23769 in DMCM media and adding further media in defined time-points. The formed structure presented layers of BNC connected by regions of the lower density of nanofibers (interlayers). The pore size of layers and interlayers were significantly distinct and allowed co-culture of the triple-negative breast cancer cell line (MDA-MB-231) and two tumor-associated cells (BC-CAFs and M2 macrophages). Cells remained viable and metabolic activity during the whole period of analysis (up to 15 days). Confocal microscopy showed no characteristics of cell invasion, although BC-CAFs and MDA-MB-231 cells were frequently seen in the same region due to limitations of our system. The gene expression of three important BC genes (*Junb,* E-cad, and DUSP5) was evaluated and showed similar patterns to what is described *in vivo* but this analysis requires improvement for further applications. It is the first time that those pristine and translucent multi-compartmentalized BNC platforms were proposed and validated *in vitro*. Additionally, it is the first time that a triple and independent co-culture model is proposed in hydrogels, opening possibilities of applicability in several studies of cell signaling.

Keywords: Breast cancer. Bacterial nanocellulose. Triple co-culture. 3D Model.

RESUMO EXPANDIDO

Introdução

Os modelos de cultivo celular em 3D são largamente estudados na literatura pois muitos trabalhos provaram que células cultivadas em placas (ambiente 2D) diferem do observado *in vivo*. Consequentemente, diferentes modelos 3D têm sido propostos, mas apresentam importantes desvantagens, como a falta de co-cultura de mais de 2 tipos celulares, a ausência de suporte celular como promovido pela ECM *in vivo* e ausência de análises de biologia molecular. Neste trabalho, relatamos a produção, caracterização e validação de um arcabouço à base de nanocelulose bacteriana empilhado em multicamadas que possui um formato óptico translúcido.

Objetivos

O presente trabalho teve por objetivo criar um arcabouço tridimensional robusto para cultivo de três importantes tipos celulares encontrados em tumores mamários triplo-negativos (célula tumoral, fibroblastos associados a tumor e macrófagos associados a tumor) a partir de multicamadas de nanocelulose bacteriana (BNC) a fim de permitir interação entre as células de forma similar ao observado *in vivo*.

Metodologia

A ^{3L}BNC Platform foi produzida a partir do cultivo estático de 2,5% (v/v) de *Komagataeibacter hansenii* ATCC 23769 em meio mínimo (DMCM), seguido de adição de 750µL de meio nos dias 7 e 14 após início do experimento. Essa metodologia foi adaptada para produção de *scaffolds* de uma ou duas camadas de BNC. As amostras foram submetidas à purificação e caracterização quanto às dimensões tridimensionais, tamanho de poros, transparência, permissividade à glicose, e ensaios reológicos correspondentes. Para os ensaios biológicos, foram inoculadas/injetadas células tumorais (MDA-MB-231), fibroblastos associados a tumor (CAFs) e macrófagos do tipo M2. Análises de viabilidade celular, microscopia confocal e expressão gênica foram realizadas em diferentes tempos de (1, 5, 10 e 15 dias após início da co-cultura tripla).

Resultados e Discussão

As amostras de ^{3L}BNC apresentaram diâmetro médio de 14.6 ± 0.2mm e altura média total de 7.0 ± 0.6mm. Foi possível visualizar regiões com menor densidade de nanofibras, as quais foram chamadas regiões intercamadas. Estas apresentaram altura média de 0.42 ± 0.04mm, confirmando a reprodutibilidade do método. Todos os diferentes modelos de *scaffolds* apresentaram translucidez e as amostras de ^{3L}BNC apresentaram transmitância de 47,6% a 50,6%, com valores médios de transparência de 7,0±0.2%. Foram observados poros maiores na região intercamadas (2.386 ± 0.981µm) quando comparado às camadas de hidrogel, porém menores que o tamanho celular. No entanto, tais características não inviabilizaram a passagem de nutrientes (nesse caso glicose) pela estrutura do material, tampouco inibiram o crescimento celular. As células permaneceram viáveis e com atividade metabólica durante todo o período de análise (até 15 dias). A microscopia confocal não mostrou características de invasão celular, embora as células BC-CAFs e MDA-MB-231 tenham sido frequentemente observadas na mesma região devido a limitações do nosso sistema. A expressão gênica de três importantes genes do BC (*Junb, E-cad* e DUSP5) foi

avaliada e apresentou padrões semelhantes ao descrito *in vivo*, mas esta análise requer aprimoramento para futuras aplicações.

Considerações Finais

O arcabouço ^{3L}BNC Platform foi padronizado e validado *in vitro*, sendo a primeira vez que uma plataforma composta de hidrogeis empilhados de nanocelulose bacteriana (BNC) é produzida de forma pristina (isto é, sem adição de outros compostos). Outro ponto relevante diz respeito ao meio de cultivo em que a bactéria *K. hansenii* foi cultivada (meio DMCM), um meio simples e quimicamente definido e que confere características ópticas à BNC. No arcabouço desenvolvido, foram cultivados simultaneamente diferentes tipos celulares que atuam no tumor mamário triplo negativo, porém estas células não permaneceram compartimentalizadas devido a limitações técnicas. A expressão dos genes foi compatível com o descrito na literatura para pacientes com essa patologia, mas esta análise requer aprimoramento para futuras aplicações. É a primeira vez que essas plataformas BNC multicompartimentadas puras e translúcidas foram propostas e validadas *in vitro*. Além disso, é a primeira vez que um modelo de co-cultura triplo é proposto em hidrogeis, abrindo possibilidades de aplicabilidade em diversos estudos de sinalização celular.

Palavras-chave: Câncer de mama. Celulose bacteriana. Cultura celular tripla. Modelo 3D.

LIST OF FIGURES

LIST OF TABLES

LIST OF ABBREVIATIONS AND ACRONYMS

µL	Microliter
µm	Micrometer
16S	Ribosome subunit
2D	Two-dimensional
3D	Three-dimensional
ABIF	Advanced Bioimaging Facility
AFM	Atomic force microscopy
APCs	Presenting-antigen cells
ATCC	American Type Culture Collection
BC	Breast cancer
Bcs	Cellulose synthase
BME	Biomedical Engineering Department
BNC	Bacterial nanocellulose
BOD	Bio-Oxygen Demand
BSC	Biological Safety Cabinet
C	Family of chemokine
CAFs	Cancer-associated fibroblasts
CBM	Carbohydrate binding module
CC	Family of chemokine
CCT	Coleção de Cultura Tropical (acronym in Portuguese meaning Tropical Collection Culture)
CD31	The cluster of differentiation 31
CD86	The cluster of differentiation 86
CM	Conditioned media
cm	Centimeter
CO_2	Carbon dioxide
CSC	Cancer stem cell
CSF-1	Colony stimulatory factor 1
CX3C	Family of chemokine
CXC	Family of chemokine
DE	Differential expression
DMCM	Defined Minimal Culture Medium
DMEM	Dulbecco's Modified Eagle Medium
ECM	Extracellular matrix

EHS	Engelbreth-Holm-Swarm murine sarcoma
EMT	Epithelial-to-mesenchymal transition
EOMA	Mouse Hemangioendothelioma Endothelial cell line
ER	Estrogen receptor
FAP	Fibroblast associated protein
FBS	Fetal bovine serum
FGF	Fibroblast growth factor
FN	Fibronectin
FSP1	Fibroblast-specific protein 1
g	Gram
G	Gauge
g/L	Gram per liter
GAG	Glycosaminoglycan
GO	Gene ontology
GPa	Gigapascal
h	Hour
hASCs	Human adipose-derived stem cells
HER2	Human epidermal growth factor receptor 2
hMSCs	Human mesenchymal stem cells
HNSSC	Head and neck squamous cell carcinoma
HS	Hestrin-Scharam medium
HUVECs	Human umbilical vein endothelial cells
IARC	International Agency for Resarch on Cancer
IL-6	Interleukin 6
IL-10	Interleukin 10
IL-12	Interleukin 12
ILT3	Myeloid inhibitory receptor LILRB4
INCA	Institute Nacional do Câncer (acronym in Portuguese meaning Cancer National Institute)
SINOVA	Secretaria de Inovação (acronym in Portuguese meaning Innovation Secretary)
InteLab	Laboratório de Tecnologias Integradas (acronym in Portuguese meaning Integrated Technologies Laboratory)
ITH	Intratumor heterogeneity
kV	Kilovolts

LAMATE	Laboratório de Materiais Elétricos (acronym in Portuguese meaning Electrical Materials Laboratory)
LAMEB	Laboratório Multiusuários de Estudos em Biologia (acronym in Portuguese meaning Multiuser Biology Studies Laboratory)
LCME	Laboratório Central de Microscopia Eletrônica (acronym in Portuguese meaning Central Laboratory of Electron Microscopy)
LIDI	Laboratório de Imunobiologia (acronym in Portuguese meaning Immunobiology Laboratory)
LiEB	Laboratório Integrado de Engenharia Biológica (acronym in Portuguese meaning Integrated Laboratory of Biological Engineering)
MC3T-E1	Murine osteoblastic cell line
MCF-7	Human breast cancer cell line which acronym means Michigan Cancer Foundation-7
MD-1	Protein expressed by the gene Ly-86
MDA-MB-231	Human breast cancer cell line, triple-negative and highly invasive
min	Minute
mm	Millimeter
MMPs	Metalloproteinases
mRNA	Messenger RNA
MSC	Mesenchymal stem cell
MTS	3-(4,5-dimethylthiazol-2-yl)-5-(3-carboxymethoxyphenyl)-2-(4-sulfophenyl)-2H-tetrazolium
N_2	Nitrogen
NaOH	Sodium hydroxide
NK	Natural killer cell
nm	Nanometer
NO	Nitric oxide
OsO_4	Osmium tetroxide
PANC-1	Human pancreatic cell line
PMA	Phorbol 12-myristate 13-acetate
PBS	Phosphate buffered saline
PCR	Polymerase chain reaction
PG	Proteoglycan
pH	Hydrogen potential
Ph.D.	Doctor of Philosophy
PR	Progesterone receptor

PTX	Paclitaxel
qPCR	Quantitative PCR
RNA	Ribonucleic acid
ROS	Reactive oxygen species
RP105	Cluster differentiation 180 (CD180)
RPMI-1640	Cell culture medium developed at the Roswell Park Memorial Institute
rRNA	Ribosomal ribonucleic acid
RT	Reverse transcription
SEI	Secondary electron image
SEM	Scanning electron microscopy
SH-SY5Y	Human neuroblastoma cell line
SP	São Paulo
subs/tumor	Substitutions per tumor
T-47D	Human breast cancer cell line, derived from metastatic site
TAM	Tumor-associated macrophage
TCM	Tumor-conditioned media
TGFβ	Transforming growth factor beta
Th1	T helper cell of type 1
TME	Tumor microenvironment
TNBC	Triple-negative breast cancer
TNFα	Tumor necrosis factor alpha
U87	Human primary glioblastoma cell line
UFSC	Universidade Federal de Santa Catarina (acronym in Portuguese meaning Federal University of Santa Catarina)
UV	Ultraviolet radiation
v/v	Volume per volume
VEGF	Vascular endothelial growth factor
WHC	Water holding capacity
WHO	World Health Organization
XRD	X-ray diffraction
αSMA	Alpha smooth muscle actin

CONTENT

Introduction and Justification

1 INTRODUCTION AND JUSTIFICATION

Breast cancer (BC) affects thousands of women annually and is one of the leading causes of female death in the world. Its genetic heterogeneity imposes limitations on the use of drugs to fight against the disease.

Much of what we already know about BC and its treatment was based on research of cells cultured in plates (2D environments), but they do not reflect the complexity found *in vivo*. In fact, in 2D, cells are in contact with a flat surface on the bottom, laterally with other cells, and grow in monolayers, having free access to nutrients. However, *in vivo* (a 3D environment), cells are surrounded by the extracellular matrix, and receive nutrients based on its position in the tissue which reflects differences of cells' properties (such as migration, drugs' resistance, and gene expression) comparing with cells cultured in plates.

To surpass these problems, researchers have been developing 3D models that better mimic *in vivo* environments and there is a massive diversity of materials that allows researchers to observe the effect of three-dimensionality on cell cultures. Among these materials, the natural biopolymer called bacterial nanocellulose (BNC) has gained attention thanks to its biological properties such as the absence of toxicity and immunogenicity, and its high biocompatibility.

BNC is suitable for tissue and tumor engineering studies and its properties are constantly enhanced by addition of other components. However, BNC has never been used for growing triple co-culture, especially in its pristine form, which make us question if it would be possible to create tumoral co-culture system that allows studying molecular characteristics of the tumor. We believe so, and this project intends to be a proof of concept.

We took advantage of the support given by matrices (in this case, BNC) to study ability of compartmentalizing cells (of the breast cancer environment) in chamber and realize multiple downstream analysis. The characteristics studied took into consideration important properties of the tumor environment and the results brought us confidence that this platform is compatible with multiple applications, such as personalized medicine. Our intention was to offer a tool for other researchers to answer their own questions.

2 OBJECTIVES

2.1 General

The main objective of this project is to develop a robust 3D platform cell culture formed by multilayers of bacterial nanocellulose (BNC) that allows mimicking interactions of triple-negative breast cancer (TNBC) cells and tumor-associated cells (CAFs and TAMs).

2.2 Specific

The specific goals of this thesis comprise:

- Standardize and produce tridimensional structures made up of three compartmentalized layers of BNC (^{3L}BNC Platform) in a defined culture medium (DMCM);
- Analyze the physical properties of the platform such as structure and nutrient permeability;
- Evaluate the ability of cells to live and grow into the scaffold;
- Triple co-culture of cells into the ^{3L}BNC Platform and verify their interaction and migration towards to each other;
- Verify gene expression of tumor progression in cells cultured into ^{3L}BNC Platform.

3 STATE-OF-THE ART

3.1 Cancer

3.1.1 The context

Cancer (also known as malignant tumor or neoplasia) is a generic name given to more than a hundred diseases that have in common the abnormal cell growth beyond tissue boundaries, possibly spreading into organs and causing metastasis (INCA, WHO). These diseases are caused by somatic cell mutations that usually confer advantages to the mutated cells and allow them to evade the rules of cell proliferation (MARTINCORENA et al., 2017).

According to the International Agency for Research on Cancer (IARC/WHO http://gco.iarc.fr/), the cancer incidence reached 18.1 million new cases and 9.6 million deaths, corresponding to an increase of 1,6 million of deaths in 2018. Only in Brazil, it is expected 559,371 new cases of cancers to both sexes (ONCOGUIA). Regarding mortality, this number is 243,588 (ONCOGUIA).

Taking attention to the costs of treatment, prevention and physical disabilities caused by cancers, approximately US$1.16 trillion were invested only in 2010 (WHO). The most three incident cancer types in 2018 were: lung, female breast, and colorectum cancers ((INCA), 2017). Together, they account for one-third of cancer incidence and mortality worldwide (ONCOGUIA).

Breast cancer (BC) is the most diagnosed cancer in women (approximately 24.2%), causing 15% of death worldwide. In Brazil, it was estimated to affect 59,700 women in the biennium 2018-2019 with a frequency of 56.33 cases per 100,000 women and an estimated death of 15,593 patients ((INCA), 2017).

Similarly, BC comprises a group of heterogeneous diseases that show distinct behaviors due to the variation of clinical and morphological aspects, as well as different genetic signatures and therapeutic responses (INCA). Despite the current knowledge about BC, there is not a full agreement between researchers about their types and subtypes due to differences in classifier methods and their parameters.

Indeed, many studies have been published revisiting the current classifications and/or proposing a better classificatory system (ELIAS, 2010;HE et al.,

2018;STEWART; WILD, 2014;WEIGELT, B et al., 2008;WEIGELT, Britta; BAEHNER; REIS-FILHO, 2010;YERUSHALMI; HAYES; GELMON, 2009).

Regarding the molecular method, researchers usually agree to divide BC into luminal, basal, and triple-negative breast cancer (TNBC). The TNBC does not have the receptors often found in BCs (estrogen receptor (ER) and progesterone receptor (PR)), and do not overexpress the human epidermal growth factor 2 (HER2) (BARECHE et al., 2018). For this reason, TNBC has the worst prognosis among BCs and shows the higher mortality rate. Furthermore, TNBC patients cannot benefit from target-therapies commonly used (WAHBA; EL-HADAAD, 2015).

It is noteworthy that even TNBC is a heterogeneous group of illnesses which comprises different subtypes and accounts for approximately 20% of all breast carcinomas in the world (FORNIER; FUMOLEAU, 2012;GONÇALVES et al., 2018). However, similarly to BC, subdividing TNBC is a target of debate (BARECHE et al., 2018;LEHMANN et al., 2011) and much of this divergence derives from new approaches of molecular biology such as genome and transcriptome sequencing.

3.1.2 Biological aspects

Despite being a rather heterogeneous group of sicknesses, all cancers have in common the existence of genome mutations (CASWELL; SWANTON, 2017;NOWELL, 1976), which are not always shared among patients of the same cancer type (GREAVES; MALEY, 2012). As a result, patients with the same type of cancer can have different groups of mutations, phenotypically undistinguished, which may explain the differences observed in the treatment's response with the same drug (SANNACHI et al., 2018).

As first proposed by Nowell (1976), the mutations are accumulated through the time, following some evolutionary principles, in a process of diversification and selection (MARTINCORENA et al., 2017). These mutations take advance of genomic instability and can be divided into the following: a) passenger and driver mutations; and b) common, shared and privates' mutations. Passenger mutations have no effect on fitness (VOGELSTEIN et al., 2013) but evolutionary cancer studies suggest that their accumulation can help cancer progression (MARTINCORENA et al., 2017).

Furthermore, if passenger mutations appear in the same genome of the driver mutations, it is possible to observe a clonal expansion (called the hitchhiker effect).

Driver mutation, on the other hand, confers increasing fitness and usually causes clonal expansion (MARTINCORENA et al., 2017). Driver mutation can vary from 1 substitution per tumor (in thyroid cancer) to 10 subs/tumor (in colorectal cancer), but its average is 4 drivers' subs/tumors (MARTINCORENA et al., 2017).

Mutations alter more than clonal fitness and cause heterogeneity to neoplasia, which can be traced to reveal the history of a patients' tumor (CASWELL; SWANTON, 2017;GREAVES; MALEY, 2012;NOWELL, 1976;SWANTON, 2012). In other words, the phylogeny of a tumor (the order that mutations occur and the relationship among clones and subclones) can be estimated applying appropriate methods and bioinformatics tools to a suitable number of biopsies from the same patient (GREAVES; MALEY, 2012;JIANG et al., 2016). For instance, Nik-Zainal and colleagues (2012) developed an algorithm to analyze 21 BC sequencing, inferring their evolutionary history and reconstructing a phylogenetic tree; NAVIN and coworkers (2011) considered evolution of tumor breast through single-cells sequencing, after cell sorting; and many other studies about this field can be found everywhere (greatly reviewed by SCHWARTZ; SCHÄFFER, 2017).

Actually, the clonal evolution and the intratumor heterogeneity (ITH) have been topic of multiple articles (BURRELL et al., 2013;CASWELL; SWANTON, 2017;GRZYWA; PASKAL; WŁODARSKI, 2017). This attention is explained by the fact ITH is dynamic, evolves over time (STANTA; BONIN, 2018;SWANTON, 2012), and can so high that it resembles different patients, more than adjacent areas of the same tumor, directly affecting cancer treatment decisions, as well as patients' surveillance (FARHANGFAR et al., 2013;RYE et al., 2018;STANTA; BONIN, 2018).

Regarding the common mutations, they normally occur early in the tumor's history and are observed in all branches (GRZYWA; PASKAL; WŁODARSKI, 2017). Shared mutations, on the other hand, are found only in some regions, while the private mutations appear later and are branch-specific (GRZYWA; PASKAL; WŁODARSKI, 2017).

Another important aspect of the cancer studies encompasses the tumor microenvironment (TME), which means the interaction of tumor cells and the circumvent milieu (BALKWILL; CAPASSO; HAGEMANN, 2012;YUAN et al., 2016). This topic will be covered later in this thesis.

In a seminal work, Hanahan and Weinberg (2000) discussed the existence of six cancers hallmarks: (1) sustaining proliferative signaling – the most fundamental aspect of cancers; (2) evading growth suppressors; (3) activating invasion and metastasis; (4) enabling replicative immortality – ability that contrasts to the natural existence of a limited number of cell divisions; (5) inducing angiogenesis – to maintain energy sources; and (6) resisting cell death. In 2011 they reviewed their previous work and added two emerging hallmarks: deregulating cellular energetics and avoiding the immune system (HANAHAN; WEINBERG, 2011).

3.1.3 Tumor microenvironment (TME)

The microenvironment is a complex system (**Figure 1**) (BALKWILL; CAPASSO; HAGEMANN, 2012;YUAN et al., 2016). The relevance of this microsystem was first proposed in 1889 by Paget through the “seed and soil” theory but did not receive much attention at the time (PAGET, 1889). This scenario changed from the 2010s and now there are multiple surveys about the interaction between tumor cells and ECM (DELNERO; SONG; FISCHBACH, 2013;HANAHAN; WEINBERG, 2011b;PETERSEN et al., 1992;TIBBITT; ANSETH, 2009;WALKER; MOJARES; HERNÁNDEZ, 2018); between tumor cells and adjacent stromal cells (HANAHAN; WEINBERG, 2011;KAMINKA et al., 2015); and between tumor cells and immune cells (YAVUZ et al., 2019). These aspects will be discussed in the following topics.

Figure 1: The tumor microenvironment at a glance.

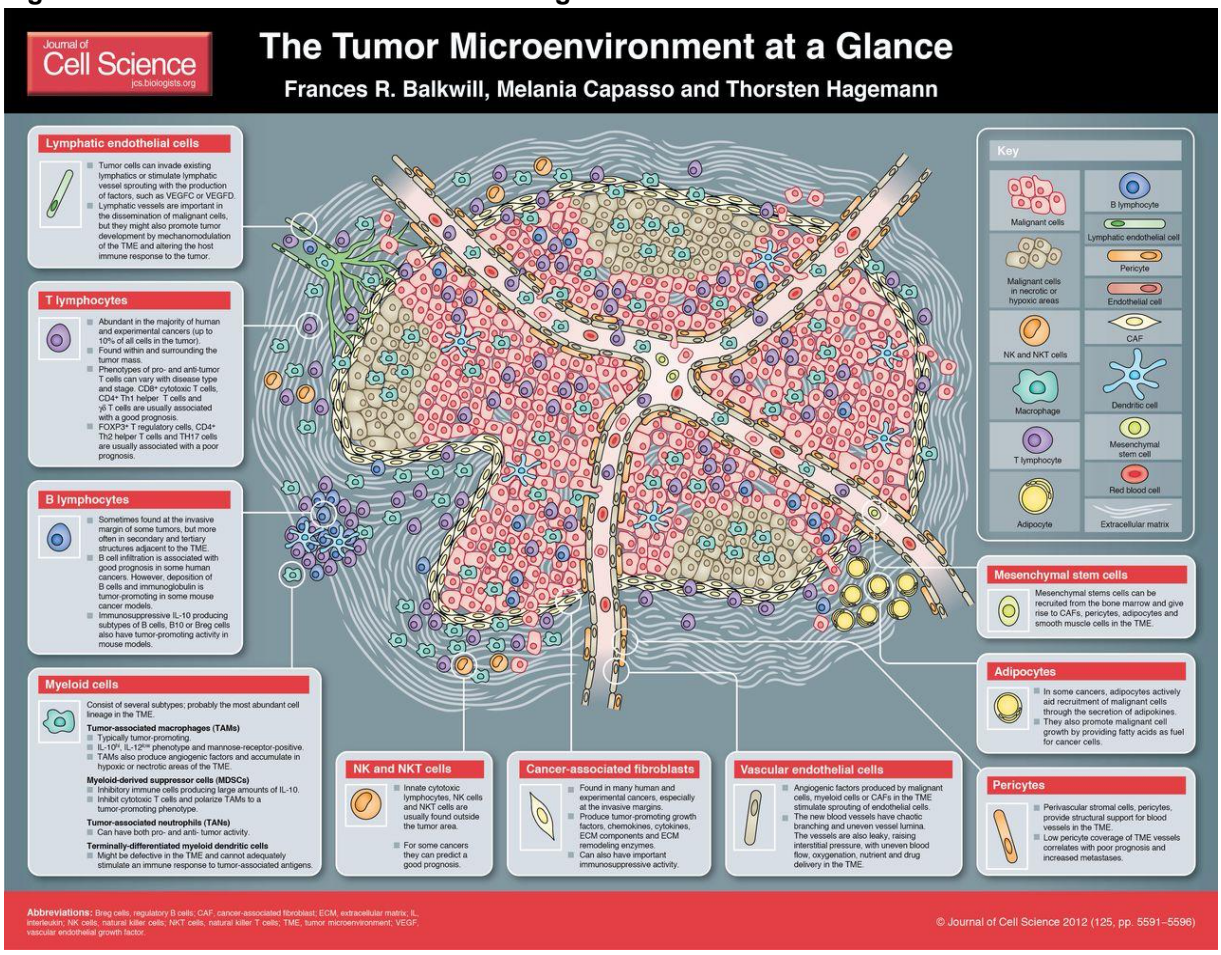

(BALKWILL; CAPASSO; HAGEMANN, 2012)

3.1.3.1 Extracellular matrix (ECM)

ECM is a non-cellular entity made of insoluble and interlocked macromolecules secreted for cells (HUANG et al., 2017) to offer them structural and mechanical support. In general, the ECM molecules can be divided into two categories: proteins and glycosaminoglycans (GAGs). The first category includes collagen, elastin, laminin, and fibronectin (FN).

ECM has different composition according to the tissue and organ it derives (BEACHLEY et al., 2015). Additionally, it regulates cell growth, motility, differentiation, and survival (PICKUP; MOUW; WEAVER, 2014).

The variation in ECM composition affects their properties, including cancer prognosis and ability to produce metastasis (BEACHLEY et al., 2015;BONNANS;

CHOU; WERB, 2014;KULAR; BASU; SHARMA, 2014) (**Figure 2**), as exemplified by the rising tumorigenesis and metastasis in higher collagen densities (PROVENZANO et al., 2008) and the involvement of fibronectin (FN) with distant metastasis derived from breast carcinomas (FERNANDEZ-GARCIA et al., 2014).

Figure 2: ECM composition and its relation to breast cancer.

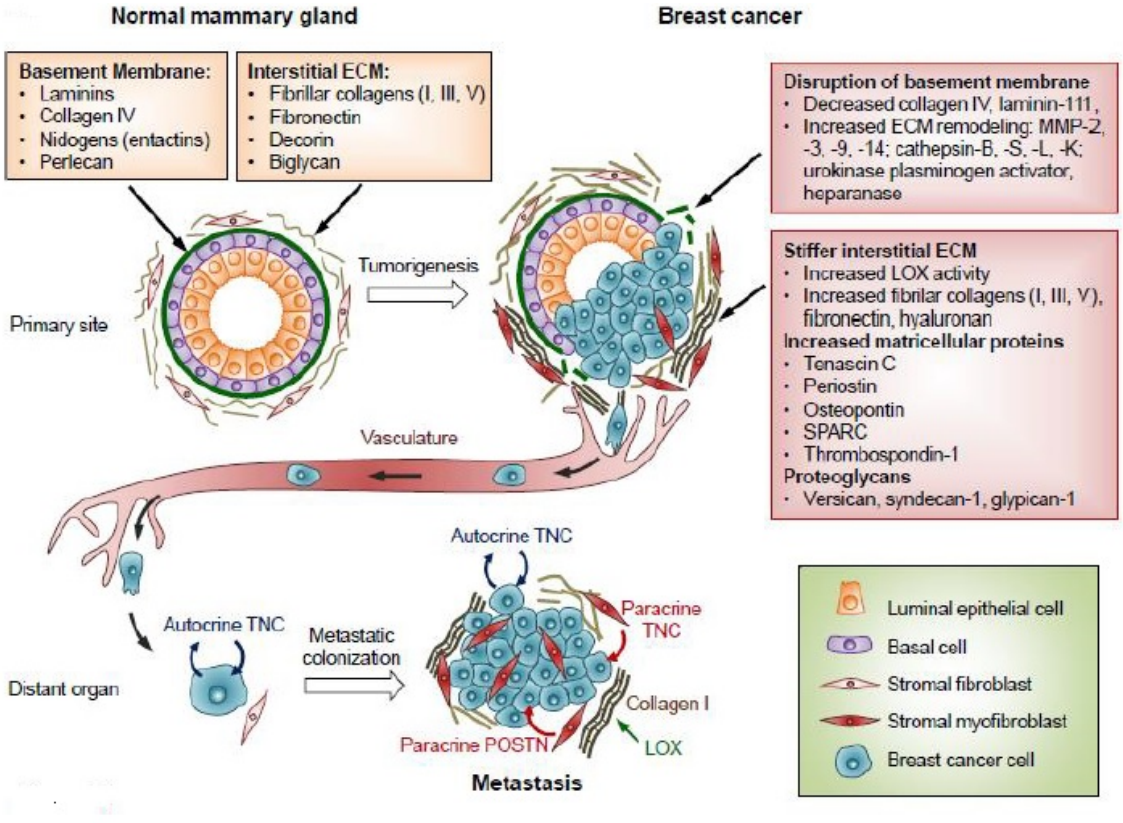

(INSUA-RODRÍGUEZ; OSKARSSON, 2016)

3.1.3.2 Stromal cells

Stromal cells, their function is to connect tissues and provide nutrition and support to an organ. Regarding cancer, they can act in tumor initiation, progression, and metastasis, which transform them into prospective therapeutic targets (ROMA-RODRIGUES et al., 2019;ZHANG, J.; LIU, 2013). Stromal cells include mesenchymal cells (KALLURI; ZEISBERG, 2006), mast cells, adipocytes, fibroblasts (the major subject of this topic), and immune cells such as macrophages (which will be covered in the next section) (LITTLEPAGE; EGEBLAD; WERB, 2005).

Fibroblasts are extended cells in a spindle-like shape that exhibit potential to planar polarity and are important players in the deposition of ECM-constituents such as collagens, laminin, and fibronectin (KALLURI, 2016;KALLURI; ZEISBERG, 2006).

They also secrete matrix metalloproteinases (MMPs) – ECM-degrading proteins that preserve their homeostasis, but whose role in metastasis dissemination has also been indicated (CATHCART; PULKOSKI-GROSS; CAO, 2015;COX, G.; O'BYRNE, 2001;DAS et al., 2017;WEBB et al., 2017). In the normal tissues, fibroblasts occur at the interstitial space without association with the base membrane but embedded in the ECM (KALLURI, 2016). However, when involved with cancer progression, they become cancer-associated fibroblasts – CAFs (ANDERBERG; PIETRAS, 2009;KALLURI, 2016;ÖSTMAN; AUGSTEN, 2009;SHIGA et al., 2015).

CAFs are indefinitely activated fibroblasts that display different molecular variation according to their origin, comprising different subtypes (BARTOSCHEK et al., 2018;LEBLEU; KALLURI, 2018). Furthermore, it is speculated that CAFs' role in pro-tumorigenesis might be different according to the type of tumor once it has been shown that resident fibroblasts exhibit anatomic origin-specific transcriptomes (RINN et al., 2006).

Today, although imprecise (due to the absence of CAFs' specific markers), these cells are often characterized by expression of α-smooth-muscle actin (αSMA), fibroblast-activated protein (FAP), fibroblast-specific protein-1 (FSP1), vimentin and absence of the expression of CD31 and cytokeratin (SHIGA et al., 2015). When activated, through epigenetic regulation, CAFs proliferate intensively, synthesize high amounts of ECM, secrete cytokines and chemokines, recruit immune cells, and apply physical forces that change the tissue architecture (KALLURI, 2016).

The involvement of fibroblasts in the development of the tumor has been largely described and includes cancer-initiation (SASAKI et al., 2014;YOSHIDA et al., 2019), progression (DIMANCHE-BOITREL et al., 1994;OLUMI et al., 1999) and metastasis (KWA; HERUM; BRAKEBUSCH, 2019). Their source, on the other hand, is not well elucidated. The shreds of evidence suggest that they can derive from local fibroblasts (MITRA et al., 2012), endothelial-cells (ZEISBERG et al., 2007), bone-marrow precursors (DIREKZE et al., 2004;ISHII et al., 2003;MISHRA et al.,

2008;QUANTE et al., 2011), and epithelial-to-mesenchymal transition (EMT) cells (KALLURI; ZEISBERG, 2006;RADISKY; KENNY; BISSELL, 2007).

Studies demonstrate that CAFs promote cancer support conditions in a paracrine mode, by secreting many factors (such as EGFs, TNFα, TGFβ, IL-6, VEGFs, FGFs, SDF-1, amongst others) (GAO et al., 2019;JOHANSSON et al., 2012;LEBLEU; KALLURI, 2018;OLUMI et al., 1999;QUANTE et al., 2011;WEI et al., 2018;YOSHIDA et al., 2019) but in return, they receive stimuli from the tumor cells to proliferate and differentiate (BARCELLOS-DE-SOUZA et al., 2016;MITRA et al., 2012;SHIGA et al., 2015;VU et al., 2019).

Indeed, the differentiation of adipose tissue-derived stem cells (hASCs) into CAFs was possible by their growing with conditioned medium (CM or TCM – tumor-conditioned medium) from the MDA-MB-231 and MCF-7 breast cancer cell lines (JOTZU et al., 2010)). Furthermore, TCM derived from a culture of MDA-MB-231, PANC-1 and U87 (all breast cancer cell lines) also allowed human bone marrow-derived mesenchymal stem cells (hMSCs) to express CAF phenotype (MISHRA, 2008).

Notwithstanding, the impact of CAFs in tumors surpasses the involvement with a cancer cell and, it has been revealed their ability to recruit immune cells and act on M2 macrophage-differentiation (YAVUZ et al., 2019).

3.1.3.3 Immune cells

The literature attributes to the Greek physician Claudius Galenus the first comparison between cancer and inflammation (TRINCHIERI, 2011). However, it was the pathologist Rudolf Virchow who, in 1863, noted leukocytes into neoplastic tissues and concluded that the observed cellular infiltrate would be the origin of the tumor (GONZALEZ; HAGERLING; WERB, 2018;SHALAPOUR; KARIN, 2015). Although it was a wrong assumption, this work was important to supporting to a century later discovery of Dvorak (1986), who observed some basic features shared between inflammation and cancer, such as tissue-infiltrating cells (such as mastocytes, lymphocytes, and macrophages) (GONZALEZ; HAGERLING; WERB, 2018). Since then, the role of inflammation and the immune cells in cancer progression has been

the theme of several studies (CRUSZ; BALKWILL, 2015;GRETEN; GRIVENNIKOV, 2019;MURATA, 2018).

In fact, regulating the immune system is pivotal to the development of a tumor and acts as a fine-tuned orchestra. During the early stages of cancer, innate immune cells are responsible for eliminating mutated cells by liberating cytokines that induce pore-formation in the tumor cell membrane (provoking death) after the recognition of non-self-patterns presented by antigen-presenting cells (APCs) (GONZALEZ; HAGERLING; WERB, 2018). As the tumor progresses (and the less immunogenic clones become more abundant), the configuration of the neoplasia changes and immune cells are replaced (**Figure 3**) (GONZALEZ; HAGERLING; WERB, 2018).

Figure 3: Roles of innate immunity in cancer.

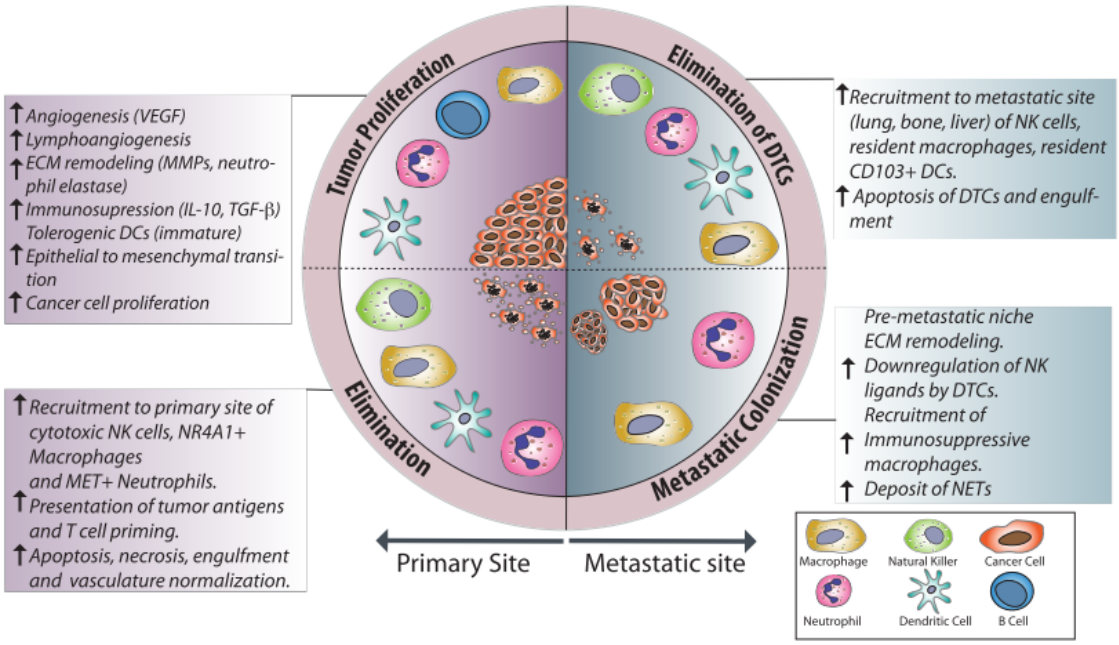

(GONZALEZ; HAGERLING; WERB, 2018)

One important immune cell that participates in all neoplastic cycles and acquires a central role in progression and metastasis is the macrophage (**Figure 3**), that can comprise more than 50% of a tumor mass (KELLY et al., 1988). Macrophages differ from their precursor monocytes by the ability to infiltrate tissues (YANG et al.,

2014). When activated, macrophages can exhibit specialized phenotypes such as M1 and M2.

M2 is a non-inflammatory tumor-associated macrophage (TAM), derived from both monocytes and embryonic macrophages, that exhibit an opposite cytokine pattern from its counterpart (IL-10^{high}, IL-12^{low}, $ILT3^{high}$, $CD86^{low}$) and that exerts a fundamental part on cancer development (DULUC et al., 2009;GONZALEZ; HAGERLING; WERB, 2018;UPADHYAY et al., 2018). Moreover, the switching between both phenotypes is also possible (DAVIS et al., 2013;YAVUZ et al., 2019;YU et al., 2016).

In fact, TAMs are recruited to the tumor by chemokines (that are divided into 4 subclasses: CXC, CC, C and CX3C) and by cytokines (such as colony-stimulating factor-1 or CSF-1) and promote tumor growth through secreting growth factors that act on the proliferation, invasion, vascularization, metastasis and ECM remodeling (ARAS; RAZA ZAIDI, 2017;MURDOCH; GIANNOUDIS; LEWIS, 2004;ZHANG, B. et al., 2012). This recruitment is proved by the multiple studies were researchers differentiate macrophages in TAMs through culturing them with different tumor conditioned media (TCM), including melanoma (WANG, T. et al., 2012), breast cancer (BENNER et al., 2019;CASSETTA et al., 2019;SOUSA et al., 2015), endometrial cancer (CASSETTA et al., 2019), and colon cancer (SAWA-WEJKSZA et al., 2018) and also by studies were TAM-conditioned media was used to culture cancer cells (LITTLE et al., 2019).

In a similar experiment, Yavuz and coworkers (2019) demonstrated that CAFs-derived media was also important to educate macrophages to differentiate from the M1 phenotype to M2. This result is in accordance with previous works from Takahashi et al. (2017) and Cohen et al. (2017), who was able to induce TAMs' differentiation through culturing tumor and admixing CAFs.

3.1.4 Cell signaling

The interaction with surrounding cells can occur directly or indirectly. The former regards physical contact through tight, gap or anchoring junctions (HUANG et al., 2017). The last is favored by mechanical communication through fibrous ECM and by cell signals (HUANG et al., 2017).

Cell signaling mechanisms can be autocrine, paracrine, endocrine or juxtacrine (**Figure 4**). The last can be exemplified by the effect of secreted chemoattractant CCL8 by TNBC on fibroblasts (FARMAKI et al., 2016) and is usually realized by culturing cells in conditioned media (CM) – the medium derived from another cell culture. Nonetheless, this technique has some limitations, such as the absence of a continuous and dynamic feedback that affects the whole microenvironment.

Figure 4: Different types of cells signaling.

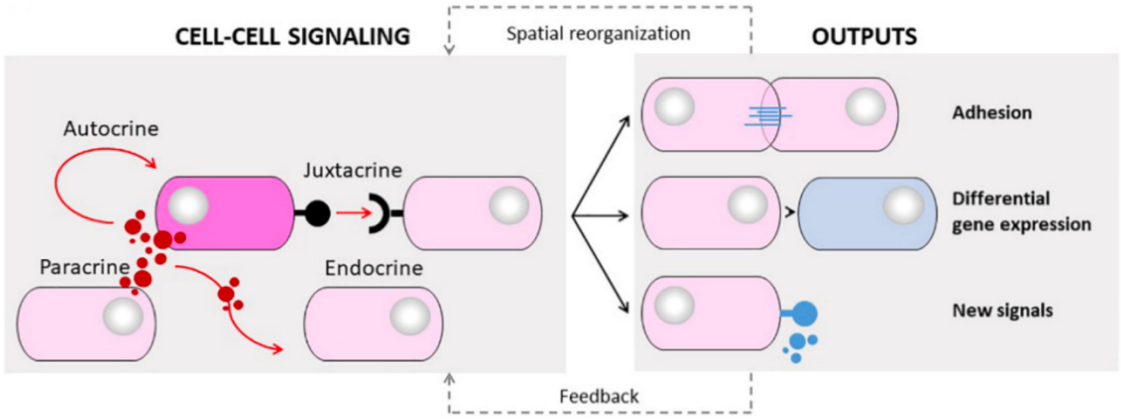

(COLOMBO; CATTANEO, 2021)

In fact, Camargo and colleagues (2021) showed that growth factors secreted by carcinoma cells cultured in decellularized bladder scaffolds differ from cells cultured on plastic dishes, which highlighting the importance of 3D architecture to paracrine signals' studies.

3.1.5 Soluble factors

Soluble factors exist in gradients due to a combination of cell secretion, protein diffusion, proteoglycan-mediated stabilization, and depletion in neighboring cells (RUBASHKIN; OU; WEAVER, 2014; CARMONA-FONTAINE et al., 2017;LYSSIOTIS; KIMMELMAN, 2017).

These factors include basic nutrients (glucose, amino acids and oxygen) and signaling molecules (growth factors, cytokines, hormones and other small molecules) (HUANG et al., 2017). The most known effect of nutrients' gradient regards to oxygen:

hypoxic cells perform anaerobic glycolysis and discard lactate which is used by normoxic cancerous cells that increase intake of lactate and utilizes it to mitochondrial metabolism (LYSSIOTIS; KIMMELMAN, 2017). Moreover, metabolites' gradients (such an association of high doses of lactate and hypoxic conditions) can affect spatial patterning of cells in a MAPK/ERK signaling way (CARMONA-FONTAINE et al., 2017).

In BC, studying nutrient and metabolites gradients were realized in a two-dimensional model named REEC - restricted exchange environment chambers (GILMORE et al., 2021) and spheroids, especially for address drug-metabolism questions (reviewed by: HAN; KWON; KIM, 2021). Nonetheless, this is the first time that a 3D biopolymer is used for culturing more than 2 cell types, which gives a live cell feedback in a paracrine way.

3.2 3D cell culture models and their significance

2D is mostly referred to cells grown in monolayers, in plates of polystyrene or in glasses surfaces and exhibits important differences to 3D methods (**Table 1**). In 2D, cells interact with a basal surface (plate) and with other cells laterally (RUBASHKIN; OU; WEAVER, 2014) and are equally exposed to nutrients, metabolites, and signaling molecules (KAPAŁCZYŃSKA et al., 2018).

Table 1: Proposed advantages and disadvantages of different 3D cell culture methods.

Type of culture	2D	3D
Time of culture formation	● Within minutes to a few hours	● From a few hours to a few days
Culture quality	● High performance, reproducibility, long-term culture, easy to interpret, simplicity of culture	● Worse performance and reproducibility, difficult to interpret, cultures more difficult to carry out
In vivo limitation	● Cells shape is flat and elongated since the cells can only grow and expand in two dimensionally ● Cells grow in a monolayer on the plate	● Natural cell shape is preserved and cell growth ● Cells grow into 3D aggregates/spheroids ● Spheroids contain multiple layers

Cells interaction	• Cell junctions are less common and less accurately represent real junctions • Deprived cell-ECM interactions, no *in vivo*-like microenvironment and no “niches”	• Proper interactions of cell-cell and cell-extracellular environment, environmental “niches” are created • Cells communicate through exchange ions, small molecules, and electrical currents
Characteristics of cells	• Changed morphology and way of divisions; loss of diverse phenotype and polarity	• Preserved morphology and way of divisions, diverse phenotype, and polarity
Access to essential compounds	• Unlimited access to oxygen, nutrients, metabolites and signaling molecules (in contrast to *in vivo*) • This causes more cells to be in the same stage of cell cycle	• Variable access to oxygen, nutrients, metabolites and signaling molecules (same as in vivo) • The core cells often remain inactive since they receive less oxygen and growth factors from the medium • This process resembles the core cells in tumor cells, making it possible to mimic the behavior and structure of a tumor cell *in vivo*
Molecular mechanisms	• Changes in gene expression, mRNA splicing, topology, and biochemistry of cells	• Expression of genes, splicing, topology and biochemistry of cells as *in vivo*
Response to stimuli	• Inaccurate representation of response to mechanical stimuli of cells • Cells cannot experience gravity since they are unable to expand into the third dimension	• Accurate response to mechanical stimuli of cells • Cells can experience gravity giving a more accurate representation of a cell *in vivo*
Drug sensitivity	• Cells often have little resistance to drugs making it appear as though drugs administered to the cells were a successful treatment	• Cells often have more resistance to drug treatment • Drug metabolism is much better

	● Drugs are not well metabolized	● Gives a more accurate representation of the drug's effects
Cost of maintaining a culture	● Cheap, commercially available tests and the media	● More expensive, more time-consuming, fewer commercially available tests

(Modified from: JENSEN; TENG, 2020;KAPAŁCZYŃSKA et al., 2018)

In three-dimensional *in vivo* environments, cells are embedded in and surrounded by the extracellular matrix (ECM) (RUBASHKIN; OU; WEAVER, 2014) that make them interact with the microenvironment in which they exist. This microenvironment comprises neighboring cells, soluble factors, the ECM and biophysical fields (HUANG et al., 2017). All these actors play important role on cell's behavior as explored in the previous sections.

Seeking to mimic *in vivo* characteristics, different 3D cell culture methods have been developed such as forced-floating, hanging drop, matrices, and microfluidics. These methods have different advantages and drawbacks and for this reason there is not a "perfect" model for all purposes.

In cancer studies, 3D models offer important tools for understanding the mechanisms of tumor progression (FERREIRA; GASPAR; MANO, 2018;HORNING et al., 2008;PULS et al., 2017;REIS et al., 2017;XIONG et al., 2013) and for drugs development, since cells grown in this context usually exhibit more resistance to treatment (BIELECKA et al., 2017;IMAMURA et al., 2015;LOVITT; SHELPER; AVERY, 2018;MELISSARIDOU et al., 2019). These disparities are caused by: a) the inability of cells cultured in 2D to keep their natural morphology; b) variation in the organization of their surface receptors; c) cell cycle synchrony; and d) differences in their local pH due to unnatural shape.

Although this important disparity between both culture environments, 2D systems remain vastly used in the initial steps of drug discovery, what explain the high cost of this type of research in comparison to the low rate of anticancer drug's approval

on clinical stages due to collateral effects not predicted on the previous stages of the study and the high cost of this type of research (BRESLIN; O'DRISCOLL, 2013).

Breslin and O'Driscoll (2013) compared pros and cons of the 3D methods in the light of anticancer drug screening and presented an informative table to summarize their findings (**Table 2**).

Table 2: Proposed advantages and disadvantages of different 3D cell culture methods.

Method type	Advantages	Disadvantages
Forced-floating	● Relatively simple ● Inexpensive ● Suitable for high-throughput testing ● Spheroids produced are easily accessible	● Variability in cell size and shape if not as fixed cell no/well ● DIY plate-costing is relatively labor-intense
Hanging drop	● Inexpensive if using standard 96-well plate ● Homogeneous spheroids suitable for high-throughput testing ● Spheroids produced are easily accessible	● More expensive if using specialized plates ● Labor intensive if preparing plates in-house ● Small culture volume makes medium exchange, without disturbing cells, difficult (proposed easier handling with commercially available formats)
Agitation-based approaches	● Simple to culture cells ● Large-scale production relatively easily achievable ● Motion of culture assists nutrient transport ● Spheroids produced are easily accessible	● Specialized equipment required ● No control over cell no./size of the spheroid (can be overcome by additional culture steps) ● Time-consuming for HTS due to extra step required for homogeneous spheroids ● Cell possibly exposed to shear force in spinner flasks (may be problematic for sensitive cells)
Matrices and scaffolds	● Provide 3D support that mimics *in vivo* ● Some incorporate growth factors	● Can be expensive for large-scale production ● Can have difficulty in retrieving cells following 3D culture formation
Microfluidic cell culture platforms	● Described as suitable for high-throughput testing	● Specialized equipment required adding expense ● Further analysis of 3D culture produced may be difficult

(BRESLIN; O'DRISCOLL, 2013)

Matrices and scaffolds can be synthetic or natural are a good system for three-dimensional culture once important molecules for cells (such as growth factors) can be incorporated to them (LIU et al., 2018;REIS et al., 2017), in addition to the structure offered to the cells.

Nowadays, commercial products (such as Matrigel® and Cultrex®) are available and can be used as a scaffold to different cells (including tumor) but they do not intend to mimicking a 3D tumor-specific model (ANGUIANO et al., 2017;BENTON et al., 2011).

These products derive from Engelbreth-Holm-Swarm murine sarcoma (EHS) and for this reason present a large number of growth factors, transcription factors, ligand proteins, among other constituents which function is not explained (HUGHES; POSTOVIT; LAJOIE, 2010) making the interpretation of the results derived from the cells culture in those matrices more challenging (VUKICEVIC et al., 1992). Moreover, due to animal origin, there is an intrinsic variation among batches as described by the Matrigel® fabricant (QUESTIONS, [s.d.]) as also by other scientists (HANAHAN; WEINBERG, 2011;HUGHES; POSTOVIT; LAJOIE, 2010).

In fact, a proteomic study of the reproducibility of the constituents of Matrigel® and identified only 53% of the proteins agreed in three distinct batches (HUGHES; POSTOVIT; LAJOIE, 2010). This result suggests caution in the conclusions of experiments derived from cell culture in Matrigel® since this variation can be an important source of inconsistency. So, despite the importance of these materials and their scientific relevance, developing alternative structures that solve those issues is already considered (NGUYEN et al., 2017). In this context, one promising biopolymer to be applied in tumor engineering is the bacterial nanocellulose (BNC) whose importance will be discussed in the following section.

3.3 Bacterial nanocellulose (BNC)

BNC is a highly crystalline linear polysaccharide produced by some bacteria such as of the genus *Komagataeibacter* (formerly *Acetobacter* and *Gluconacetobacter*) and composed of monomers of β-D-glucopyranose through β-1,4-glycosidic linkages (JACEK et al., 2019;JOZALA et al., 2016). It was first described by Brown, in 1886,

who observed the production of cellulose by the bacteria *Acetobacter xylinum* in the presence of glucose and oxygen (BROWN, 1988). Its current genus name was proposed by Yamada, after a molecular study of 16S rRNA (YAMADA et al., 2012).

The genus *Komagataeibacter* comprises multiple species (for example *K. xylinus* and *K. hansenii*) but not all of them can produce cellulose (MATSUTANI et al., 2015). Furthermore, it is observed the natural occurrence of mutants that lost their ability to produce cellulose, especially in shaken conditions, as firstly observed by Hestrin and Scharamm, in 1954 (JACEK et al., 2019). The bacterial colonies Cel^+ and Cel^- (cellulose positive and cellulose negative, respectively) show different morphologies, being Cel^+ colonies convex and with smooth edges and the Cel^- colonies large, flat and with wave edges (JACEK et al., 2019;MATSUTANI et al., 2015).

The conversion of glucose into cellulose occurs in two stages, the production of β-1,4-glucan chains and their crystallization (JACEK et al., 2019). The last stage is orchestrated by the cellulose synthase (Bcs), a complex of four protein subunits encoded by three or four genes (JACEK et al., 2019).

Differently from the cellulose plant, BNC has no hemicellulose, lignin, or pectin (LIN; DUFRESNE, 2014). Its production occurs inside the bacteria before been secreted through cell envelope pores (LIN; DUFRESNE, 2014) and consists of a defensive barrier against “enemies” such as fungus and UV (XUE; MOU; XIAO, 2017a).

3.3.1 BNC and tissue engineering

The BNC has been largely used as scaffold to the animal cell culture *in vitro* (BERTI et al., 2013a;HU et al., 2014;OLIVEIRA et al., 2012;ZABOROWSKA et al., 2010) and, more recently, it has been explored as scaffold in tumor engineering studies (REIS et al., 2017;WANG, J. et al., 2018;XIONG et al., 2013). Their physical properties such as crystallinity (84-89%) (XUE; MOU; XIAO, 2017b) and tension force (79-88 GPa) (XIONG et al., 2013), are highly relevant to tissue engineering. Moreover, BNC is biocompatible, showing no genotoxicity, nor immunogenicity, or cytotoxicity but presenting high tissue-integration capacity (CZAJA et al., 2006;SIONKOWSKA; MĘŻYKOWSKA; PIĄTEK, 2019). In addition, bacterial nanocellulose displays some

characteristics similar to collagen, such as the size of nanofibers and the water holding capacity (WHC), the reason why sometimes BNC is referred as collagen-like in some studies (XUE; MOU; XIAO, 2017b).

In face to apply the BNC in tissue engineering projects, it is frequently necessary to enhance some of its biological assets. These driven-changing properties have been focus of attention in the recent years (FU et al., 2012;GODINHO et al., 2016;INNALA et al., 2013;RECOUVREUX, D., 2008;REIS et al., 2017;SILVA, DA, 2012;XIONG et al., 2013;ZANG et al., 2015).

Under static culturing, BNC derived from *K. hansenii* ATCC 23769 exhibits differences in the top and bottom surfaces (dense and porous, respectively), inducing changes in the adhesion and growth rate of HUVECs cells cultured in both sides (BERTI et al., 2013a). It occurs because of the variation in the size porous of each surface that allows differences in the diffusivity of nutrients and signaling molecules. So, the ability of cells to adhere, grow and migrate in the extension of nanofibers is intimately related to the size porous.

In 2013, Xiong and coworkers published a study reporting the culture of MDA-MB-231, a TNBC cell lineage, in the BNC submitted to the laser to display macro-porous (XIONG et al., 2013). Innala and collaborators (2013) demonstrate that BNC hydrogels (after surface modifications) were efficient in culturing neuroblastoma cells (SH-SY5Y) that maintained cell viability and were able to differentiate into mature neural cells. Zaborowska et al. (2010) used paraffin microspheres ranging from 300 to 500 μm diameter to produce a BNC structure that had a proper diameter of pores to allow the growth of murine osteoblast (MC3T3-E1).

Birkheur and coworkers (2017) incorporated mannose to the cellulose and observed increasing growth of fibroblasts when compared to non-modified cellulose. Ramani and Sastri (2014) applied graphene oxide and hydroxyapatite to reinforce the BNC produced by *Acetobacter aceti* and used this material as a scaffold to bone cells. These authors demonstrated that, in addition to the proper support of the material, the cultured cells were osteoinduced.

Another relevant aspect of BNC regards its ability to produce different macrostructures according to culture parameters. In static culture, for example, the

bacteria move to the higher oxygen interface, producing a membrane that limits this gas diffusion to the internal medium (GAMA; GATENHOLM; KLEMM, 2012). On the other hand, under specific agitated conditions, it is possible to produce larger three-dimensional structures as cocoons (RECOUVREUX, D. O. S. et al., 2011). Knowing those aspects gave the scientists the chance to produce blood vessels into BNC macrostructures, BNC membranes and also many other composites (KONDAGESKI, 2016). However, the current literature shows that the using of BNC for tissue engineering or tumor engineering purposes is somehow limited to hydrogels or membranes (**Table 3**).

Table 3: A summary of BNC modifications described in the literature and their applications in tissue culture.

Modification	Scaffold structure	Application
Manosilated	Membranes	Increasing fibroblasts growth
Cationization and oxidation	Membranes	Protein free cell adhesion
Silanization	Lyophilized membrane	Wound healing
TEMPO oxidation	Hydroxyapatite and glutaraldehyde crosslink	Bone tissue
Heparin modification	Porous scaffold with endothelial growth factor (VEGF)	Tissue repair
Peptides fused to carbohydrates ligand modules (CBM3)	Membranes	Neural and mesenchymal stem cells (MSCs)
Tri-calcium phosphate and hydroxyapatite blends	Hydrogels	Bone implant

(Adapted from COURTENAY; SCOTT, 2018)

Using different media composition is also an approach used by several research groups. In this respect, recently, the group headed by Dr. Porto (UFSC/Brazil) developed a culture media chemically defined, named DMCM, that allowed the formation of translucent hydrogels by *K. hansenii* ATCC 23769 (SOUZA et al., 2018), a property sought by other groups that, differently from us, achieved it only through composite forms. For this reason, the process was patented under the number BR1020190185.

3.3.2 Stacking layers of BNC: why?

Stacking multiple layers of platforms or scaffolds is now a quite well-established idea (FU et al., 2012;GINESTRA; PANDINI; CERETTI, 2019;MARTÍNEZ ÁVILA et al., 2015;SILVA, DA, 2012). The proposed models go from micropattern sheets (PAPENBURG et al., 2009) to the adoption of static and culture conditions of *Gluconacetobacter* to form more layers of BNC (FU et al., 2012). Nonetheless, they face problems such as being time-consuming or lacking applicability.

To supplant these issues, a scaffold formed by BNC-multilayered is proposed in this thesis by culturing *K. hansenii* (formerly *Gluconacetobacter*) (YAMADA et al., 2012) in a minimum defined media (SOUZA et al., 2018). The platform consists of pure bacterial nanocellulose made in a simple and straightforward way. Additionally, it forms chambers that can be used for indirect cell culturing. In fact, after initial characterization, the applicability of the scaffold was assessed by a multi-co-culture of three distinctive cell types to mimic a breast cancer tumor microenvironment. Finally, advantages and limitations are discussed, as well as other possible uses.

Methods

4 MATERIAL AND METHODS

4.1.1 Obtaining the bacteria

The bacteria *Komagataeibacter hansenii* ATCC 23769 used in this study was obtained from Tropical Culture Collection (CCT, Portuguese acronym) André Tosello (Campinas, SP. Brazil). The aliquots were maintained at the ultra-freezer (-80°C) available at the LiEB/UFSC until needed.

4.1.2 Culture medium and growth conditions

An aliquot of *K. hansenii* was thawed and cultured in Mannitol medium (25 g/L mannitol, 5 g/L yeast extract, and 3 g/L of peptone). After preparation, the pH was adjusted to 6.5 (Digimed, model DM-23), the medium was autoclaved for 20 min at 121ºC, and its manipulation was performed at a biological safety cabinet (BSC) to keep sterility.

The culture of bacteria strain was performed in Petri dishes containing Agar Mannitol (10 g/L mannitol, 2 g/L yeast extract, 1.2 g/L peptone, and 6 g/L agar). Similarly, the pH was adjusted to 6.5, sterilized and strictly manipulated in BSC.

Some experiments were performed using Hestrin & Schramm (HS) (HESTRIN; SCHRAMM, 1954) medium which composition is: 20 g/L glucose, 5 g/L peptone, 5 g/L yeast extract, 2.7 g/L disodium phosphate (Na_2HPO_4), and 1.15 g/L citric acid.

The platform's production was performed using DMCM medium (SOUZA et al., 2018). All cultures were maintained in static conditions under 26°C in the BOD (Bio-Oxygen Demand) incubator (Novatecnica, model NT705).

4.1.3 Standardization

The best condition of the ^{3L}BNC Platform production was chosen after analysis of two different methods of production; recipients for culturing; time of incubation; medium; and volume of media (**Table 4**). All of these methods of production were performed from trial-and-error methods and these steps are described in the following sections for better understanding.

Table 4: Description of standardization procedures.

Experiment ID	Recipient	Time production by layer (days)	Total time production (days)	Volume of inoculum to form 1st layer (µL)	Volume of bacteria culture medium 2nd/3rd layers (µL)	Method of production
KP001	• 24-well plates	5 or 10	15 or 30	• 2000	• 1000	Method I: Transferring membranes and adding medium
KP002	• 24-well plates	5 or 10	15 or 30	• 2000	• 1000	Method I: Transferring membranes and adding medium
KP003	• 96-well plates • Conical tubes • (Eppendorf-like)	15	45	• 250 • 450 or 1000	• 250 • Not applicable	Method I: Transferring membranes and adding medium
KP004	• 96-well plates • 24-well plates • Borosilicate tubes • Conical tubes (Falcon-like)	15	45	• 280 • 2000 • 300 • 3500	• 150 • 1000 • 100 • 1000	Method II: Adding medium only
KP005	48-well plates	15	45	• 1000	• 250	Method II: Adding medium only
KP006	• 96-well plates • 24-well plates	7, 10 or 15	21, 30 or 45	• 280 • 2000	• 50, 75 or 100 • 500, 750 or 1000	Method II: Adding medium only
KP008	• 24-well plates • 48-well plates • Conical tubes (Falcon-like)	7	21	• 1000 • 800 • 3000	• 750 or 1000 • 250 • 750 or 1000	Method II: Adding medium only

4.1.3.1 Methods of production

First of all, two methods of production were tested (**Figure 5** and **Table 4** – Experiment ID KP001 and KP002) of 24-well plates.

It was prepared with 2 mL of inoculum at the concentration of 2.5% (v/v) in bacteria cultured medium (HS, Mannitol or DMCM) followed by 5- or 10-days incubation to form the first layer of BNC (**Figure 5A**). After this period, two methods were tested. The first consisted of transferring the hydrogels to clean wells, followed by addition of 1 mL of cultured media (without inoculum). This procedure was repeated once again, to form the last layer.

The second method consisted of adding 1 mL of the correspondent medium without transferring the previously formed hydrogels (**Figure 5B**). Nonetheless, volume of inoculum and time of incubation remained equal to the method I.

Figure 5: Design of initial production methods in 24-well plates. A) The experiment of transferring and adding medium – method I (**Table 3** – ID KP001). **B)** The experiment of adding-only medium – method II (**Table 3** – ID KP002) and cultured for 5 or 10 days, parts A and B, respectively.

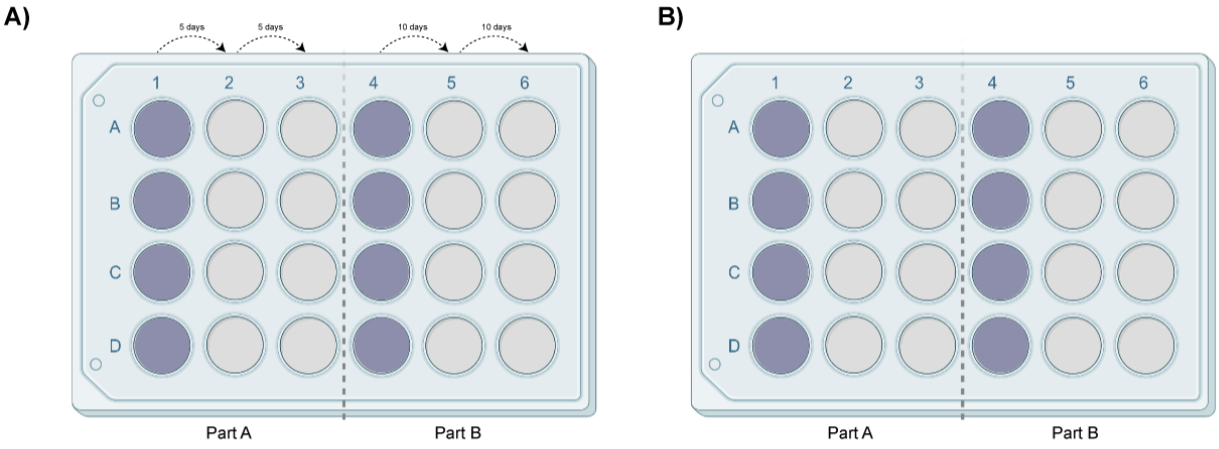

These methods were also tested on the cell-culture 96-well plate (**Figure 6** and **Table 4** – Experiment IDs KP003 and KP004) taking an interval of 15 days for each layer formation to allow the synthesis of BNC by bacteria (**Figure 6**).

Figure 6: Design of initial production methods in 96-well plates. A) The experiment of transferring hydrogels to new cavities and adding medium (**Table 3** – ID KP003). **B)** The experiment of adding medium only (**Table 3** – ID KP004), i.e., layers were not moved from the initial cavity.

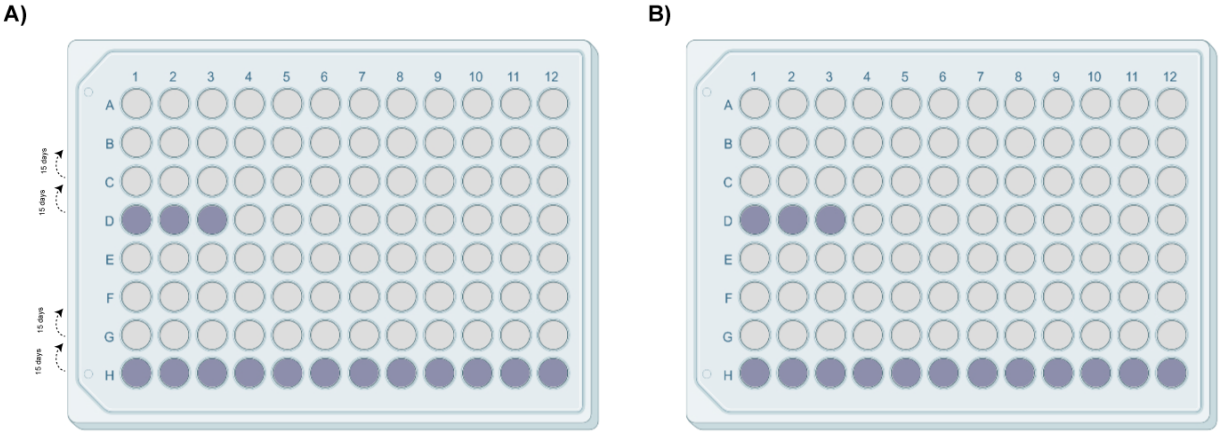

4.1.3.2 Choosing layer-incubation time

The following experiments were performed by the second method. Hereupon, it was tested: three different cell–culture plates (96-well, 48-well, and 24-well), conical tubes (15 mL), and borosilicate tubes (6 mm of diameter and 7.5 cm size) specifically made for this purpose (**Table 4** – Experiments ID KP004 and KP005). These experiments were done with the HS medium, Mannitol medium, and DMCM in an initial time of 15 days' incubation for each layer.

Shorter incubation times were also evaluated. For this purpose, the *K. hansenii* ATCC 23769 was cultured in plates (96-well and 24-well) for an incubation interval of 7-, 10- or 15 days (**Table 4** – Experiment ID KP006).

4.1.3.3 Choosing recipient and media volume to produce ^{3L}BNC Platform

Conical tubes (15 mL), and cell-culture plates (24-wells and 48-wells) were used to ferment bacteria over three different culture media to compare the performance of HS, Mannitol, and DMCM (**Table 4** – Experiment ID KP008). In the 48-well culture plates, bacteria were incubated (7 days, 26°C in BOD incubator) with 800 µL of inoculum 2.5% (v/v) in medium. After 7 and 14 days of bacteria fermentation, 250 µL of the respective culture medium was added to produce the second and third layers, respectively (**Table 5** and **Figure 7**).

Figure 7: Design of the experiments performed in plates (48-well, 24-well) and in conical tubes (Falcon-like 15 mL).

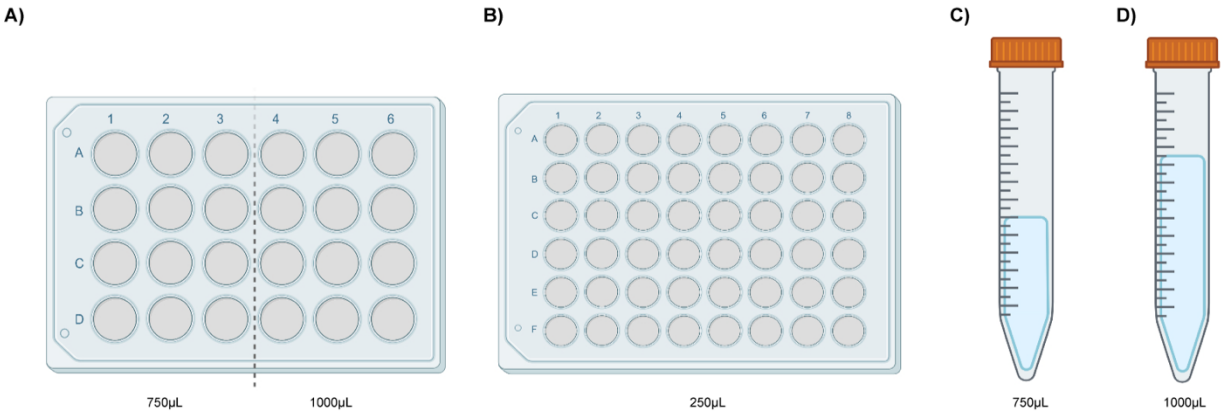

For the 24-well plates, the comparison between the three-culture medium was performed as follows: 1.5 mL of inoculum 2.5% (v/v) in the medium was added and cultivated for 7 days at 26°C. After 7 and 14 days of this initial step, twelve out of 24-well received 750 µL of medium and the other twelve received 1 mL, instead (Table 4 and **Figure 7**).

The last test was performed in conical tubes of 15 mL (TPP, cat. 91014). The culture started with 3 mL of inoculum 2.5% (v/v) in medium. After 7 days' incubation at 26°C, 750 µL or 1 mL of medium were added, and tubes were incubated for the other 7 days at the same conditions. This step was executed once again to form the third and last layer of BNC. This experiment was realized in triplicate (**Table 5** and **Figure 7**).

Table 5: Volume of inoculum and medium tested in different recipients.

Container	1st week	2nd week	3rd week
Cell-culture plate 48-well	800 µL	250 µL	250 µL
Cell-culture plate 24-well	1500 µL	750 µL	750 µL
	1500 µL	1000 µL	1000 µL
Conical tubes (Falcon-like) 15 mL	3000 µL	750 µL	750 µL
	3000 µL	1000 µL	1000 µL

4.1.4 ^{3L}BNC Platform production

After choosing the method, flask (template), and time of bacteria incubation, the ^{3L}BNC Platform production was performed to obtain enough samples for culture cells experiments and platform characterization. So, after bacteria incubation in Agar Mannitol for at least 7 days, an inoculum of *K. hansenii* of optical density varying between 1 and 1.3 (spectrophotometer Thermoplate, λ = 630 nm) were obtained by eluting few bacteria colonies in DMCM medium followed by lysis on vortex at maximum speed. This inoculum was diluted in a proportion of 2.5% (v/v) in DMCM medium and 3 mL of this solution was distributed to each polystyrene' conical tube followed by culturing at 26ºC to form the first layer of ^{3L}BNC Platform.

After 7 and 14 days, 750 µL of medium (DMCM) was gently added to each tube by pipetting (except ^{SL}BNC – controls) to form the 2nd and 3rd layers of the ^{3L}BNC Platform. The controls were removed, washed in distilled water, and kept in the fridge until purification.

Afterward, ^{3L}BNC Platform was gently removed from conical tubes by tweezers and rinsed with distilled water. Then, the samples were purified through incubation at 50ºC for 24 hours in 0.1M sodium hydroxide (NaOH) followed by several rinses with distilled water until the pH reached approximately 6.5. Next, they were sterilized at 121 ºC for 20 min by autoclaving.

The above-mentioned protocol was adapted to produce platforms with different numbers of layers to perform different tests (**Table 6**). Additionally, when necessary, individual layers of the ^{3L}BNC Platform were detached and their number indicated, being 1st the bottom layer and 3rd the upper (**Figure 8**).

Table 6: Tests performed in each platform and/or individual layers.

Analysis	^{SL}BNC	^{2L}BNC	^{3L}BNC	Individual Layers
	Single Layer (7d incubation)	Two layers (14d incubation)	Three layers (21d incubation)	
Transparency	✓	✓	✓	n/r
Thickness	✓	n/r	✓	✓
Pore size	✓	n/r	✓	✓
Nutrient Transport	✓	✓	n/r	n/r
Rheology	n/r	✓	✓	n/r
Cell viability	n/r	✓	✓	n/r
Cell metabolic activity	n/r	✓	n/r	n/r
Confocal microscopy	n/r	n/r	✓	n/r
Gene expression	n/r	n/r	✓	n/r

n/r: not realized

Figure 8: ^{3L}BNC Platform structure. The oldest layer (first to be formed) is named 1st layer. The medium-age layer is called the 2nd layer and the last layer formed is called the 3rd layer. Between the 1st and 2nd layers there is an interlayer 1. The 2nd interlayer is formed between the 2nd layer and 3rd layer.

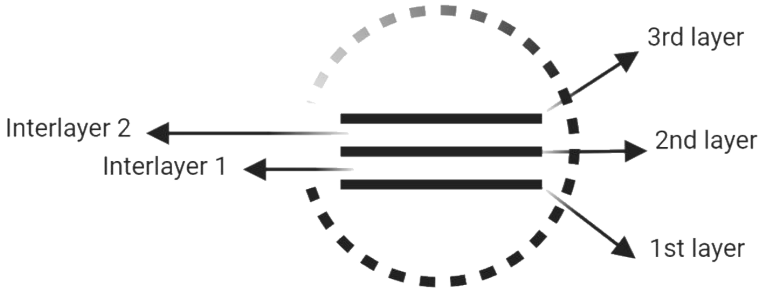

4.1.5 Dimensional analysis

Diameter and thickness of ^{3L}BNC Platform were evaluated through a digital micrometer (Mitutoyo 293-561-30), kindly provided by the Laboratory of Food Physical Properties (Profi/UFSC). To perform these measurements, ^{3L}BNC Platform samples were carefully dried using an absorbent paper towel before analysis and individual layers were detached using tweezers and compared to ^{SL}BNC. The measurements were executed in triplicate for two independently batches (n=6).

The interlayers height region was inferred by subtracting the sum of each layer of the system from the height of the whole platform and by dividing it by the number of interlayers as indicated by the author developed Equation 1:

$$interlayer_{thickness} = \frac{[platform_{thickness} - (\Sigma layer_{thickness})]}{n_{interlayers}} \quad \text{[Eq.1]}$$

where $platform_{thickness}$, is the thickness of the entire platform, $\Sigma layer_{thickness}$ refers to the sum of thickness measured of each layer of the platform, and $n_{interlayers}$ is the number of interlayers of the measured platform.

4.1.6 Transparency

Transparency of ^{SL}BNC, ^{2L}BNC and ^{3L}BNC samples were measured according to (SAITO et al., 2003), In brief, the percentage of transmittance was divided by the scaffold average thickness for three scaffold samples. These results were compared to hydrogels of bacteria cultured in mannitol media. For this analysis it was used two spectrophotometers: SpectraMax i3 Platform, Molecular Devices (from Biomat'X) and Tecan, Infinite 2000 (from LAMEB/UFSC), both at λ = 550 nm.

4.1.7 Alcohol dehydration and supercritical drying

Purified samples were dehydrated by an increasing ethanol concentration (15% to 100%, 15 min/each) to remove water from ^{3L}BNC Platform. Then, they were submitted to carbon dioxide supercritical drying point (CPD) since it is a technique that maintains BNC structure in an ideal condition to perform SEM analysis (BERTI, 2012). The drying step was performed in two different laboratories, the Central Laboratory of Electron Microscopy (LCME/UFSC) or the Electrical Materials Laboratory (LAMATE/UFSC) – coordinated by Prof. Dr. Carlos Renato Rambo.

4.1.8 Scanning Electron Microscopy (SEM)

After CPD, samples were immersed in liquid nitrogen (N_2) for 1 minute and 30 seconds, blade-crossed and immobilized in carbon-strip stubs for gold recovery. Scanning electron microscopy was performed using a JEOL JSM-6390LV microscope

(LCME/UFSC) and images were captured with 10kV acceleration using a secondary electron image (SEI) under augments of 100x, 500x, 1000x, 3000x and 5000x.

4.1.9 Pore size analysis

Porous size analysis was performed by the software ImageJ (version 1.52) available on https://imagej.nih.gov/ij/download.html through the “analyze particles” function using SEM micrographs at 5000x amplification.

4.1.10 Rheology

To determine how the number of layers affects material assets, rheological properties were evaluated. ^{2L}BNC and the ^{3L}BNC samples were characterized by uniaxial compression tests and shear stress analyses using a torsional rheometer (Discovery HR-2, TA Instruments) fitted with a circular plate of 20 mm and a Peltier stage set to 37 °C. Measurements for compression were attained by applying 90% of the compressive strain with a rate of 10μm/s. The Young’s modulus *E* was obtained plotting strain-stress curves using the range of 5-10% strain. All tests were performed in triplicate and analyzed using the TRIOS software (version 4.5.0.42498).

For shear stress analysis, amplitude sweep tests were performed at an angular frequency of 10 rad/s over a strain range of 0.01% to 500%, with a constant temperature of 37ºC and 10 points collected per decade. The storage modulus (G’) of the ^{2L}BNC and ^{3L}BNC platforms were obtained from the linear area under the plotted oscillatory strain/modulus graph, with all tests performed in triplicate.

4.1.11 Glucose permeability

The glucose permeability was evaluated according to previous studies (PAPENBURG et al., 2007). In brief, two polystyrene conical flasks communicated through a 5 mm center hole and sealed with samples were vertically aligned. 20 mL of full DMEM media (i.e., supplemented with 10% FBS and 1% Pen-Strep) was added to the upper flask and the same volume of PBS was added to the bottom flask (acceptor). As control, 1 g/L glucose solution and deionized water were added to donor and acceptors, respectively.

Samples of 500µL were taken from donors and acceptors at different time points as follows: 0 h (prior to starting); 15 min; 30 min; 1h; 2h; 4h; 8h; and 24 h, unless there was no volume remaining. The concentration of glucose for each sample was determined by an enzymatic assay (PGO Enzyme Preparation, Sigma, # P7119-10CAP) and the absorbance was read using a spectrophotometer (SpectraMax i3 Platform, Molecular Devices, λ = 450 nm). The concentration of glucose was calculated according to the manufacturer.

4.1.12 Obtaining cells

4.1.12.1 Mouse Hemangioendothelioma Endothelial cell line (EOMA)

One aliquot of EOMA cells (ATCC CRL-2586) available at Biomat'X Research Laboratories (McGill University) was cultured in DMEM (Gibco, #11885-084) supplemented with 10% Fetal Bovine Serum – FBS (Neuromics, #FBS001), and 1% Pen/Strep – Penicillin Streptomycin (Gibco, #15140122) in a humidified incubator (37ºC, 5% CO_2). Media was replaced every 2-3 days.

4.1.12.2 Triple-negative breast cancer cell MDA-MB-231

One aliquot of MDA-MB-231 cell line was purchased by ATCC (Lot: 70015968) and cultured in complete DMEM (Gibco, #11885-084) supplemented with 10% FBS (Neuromics, #FBS001), and 1% Pen/Strep (Gibco, #15140122) in a humidified incubator (37ºC, 5% CO_2). Media was replaced every 2-3 days. DMEM derived from MDA-MB-231 cell culture was filtered (0.22µm) to prepare conditioned media.

4.1.12.3 Cancer-associated fibroblasts (CAFs)

One aliquot of Human Breast Cancer Associated Fibroblasts (BC-CAFs) was purchased from Neuromics company (Lot: 003A) and cultured in manufacturer indicated media (MSC-GRO® – Neuromics, #PC00B1) in a humidified incubator (37ºC, 5% CO_2). Media was replaced every 2-3 days.

4.1.12.4 M2 macrophages

Two aliquots of THP-1 cell line were gently provided by Dr. Cerruti – Biointerface Lab, McGill University – and cultured in suspension with RPMI-1640 media (Gibco, #11875-093) supplemented with 10% FBS (Neuromics, #FBS001), 1% Pen/Strep (Gibco, #15140122), and 50μM β-mercapthoetanol (Sigma, #M6250) followed by 0.22μm filtration (Stericup, Sigma, #S2GVU05RE). Cultures were kept into a humidified incubator (37ºC, 5% CO_2) and media was replaced every 2-3 days.

The polarization and differentiation of THP-1 cell line was performed as described by Lund and collaborators (2016). In summary, THP-1 was polarized into M0 macrophages by adding 10ng/mL PMA to $1x10^6$ cells and culturing them for 48h. Then, the media was replaced, and the macrophages were kept in incubation for 24h. On the next day, 20ng/mL of IL-4 and IL-13 were added to the culture, and cells were incubated for 72h, to perform the differentiation into M2 macrophages (GENIN et al., 2015).

4.1.13 Cell culture into platforms

Different cell lines were used to perform biological experiments using ^{2L}BNC or ^{3L}BNC platforms (**Table 6**). However, for all tests, the scaffold was put in 24-well non-treated plates, quickly washed once with 1 mL of PBS, and incubated with the same volume of the respective media in a humidified incubator (37°C and 5% CO_2) for at least one hour.

The media was then aspirated, and the cells were seeded on the bottom of the platform or injected into the designated interlayer by using insulin syringe and 25G 1 ½” needles (BD, #305127). After, the cells were incubated for at least one hour prior to the addition of 1mL of their respective media. On the next day, the platforms were put in new wells and 1 mL of complete media was added followed by new incubation at the same conditions. The media was changed every 2-3 days until the end of the analysis.

4.1.13.1 Multi-cell culture onto ^{3L}BNC Platforms

For gene expression analysis, the BC-CAFs were cultured for two days in MSC-GRO® conditioned media (1:1) to prepare the cells for seeding onto the ^{3L}BNC Platform. Approximately 9 x10^4 cells were seeded on the bottom of the platform – 1st layer (**Figure 9**), which was then maintained in a humidified incubator (37°C, 5% CO_2) in non-treated 24-well cell culture plates. The conditioned media was used until the MDA-MB-231 injection. After 3 days of BC-CAFs seeding, approximately 2x10^6 MDA-MB-231 cells were injected in the 1st interlayer of the ^{3L}BNC Platform (**Figure 9**), using a 25G 1 ½" needle. The cells cultured in the scaffolds were incubated with MSC-GRO® / Supplemented DMEM at a ratio of 1:1.

Then, after 7 days of the initial cell culturing in ^{3L}BNC Platform, approximately 9x10^4 M2-macrophages were injected in the 2nd interlayer of the platform (**Figure 9)**, which was maintained in media composed of: Supplemented DMEM / MSC-GRO® / Supplemented RPMI-1640 (at a ratio of 1:1:1). This media was replaced every 2-3 days. This system was maintained in culture and three samples were removed after 1, 5, 10, and 15 days of seeding/injecting for further analysis.

For confocal analysis, approximately 9x10^4 BC-CAFs cultured in conditioned media (MSC-GRO® and DMEM, at 1:1 ratio) and stained with 25 µM red cell tracker (ThermoFisher, #C34552) were seeded in the bottom (1st layer) of the ^{3L}BNC platform. After two days, approximately 2x10^6 MDA-MB-231 cells stained with 25 µM green cell tracker (ThermoFisher, #C7025) were injected in the 1st interlayer (**Figure 9**). Finally, after other two days (4 days since initial BC-CAFs seeding), approximately 4x10^5 M2 macrophages stained by 25µM blue cell tracker (ThermoFisher, #C2110) were injected at the 2nd interlayer of the ^{3L}BNC (**Figure 9**). One sample of ^{3L}BNC Platform was removed after seeding/injecting all cells at 1, 5, 10 and 15-days, followed by preparation for confocal microscopy.

Figure 9: Cell culture onto ^{3L}BNC Platform.

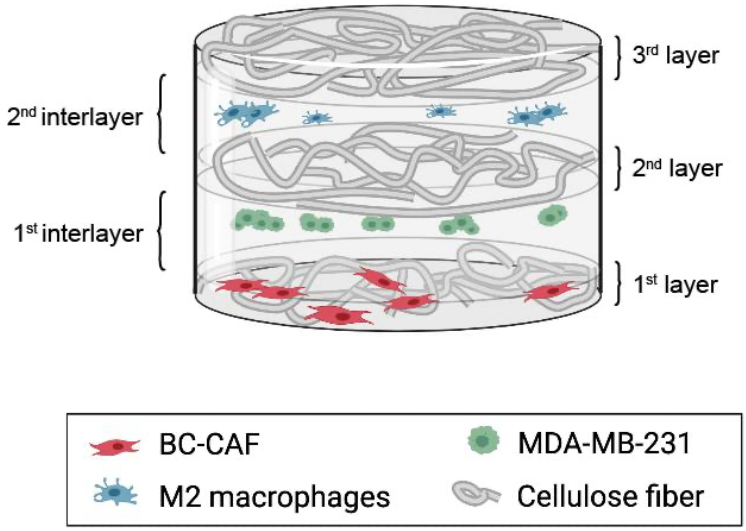

It is worth noting that co-culture of MDA-MB-231 cell line, BC-CAFs and M2 macrophages was also performed in cell culture plates to proper compare the effects of cell culture method (3D model or 2D).

4.1.14 Biological Properties

4.1.14.1 Cell viability

The cell viability of cells grown into the platforms was assessed by Live/Dead assay (Biotium, #30002-T) according to the manufacturer's protocol. For this aim, $1x10^4$ or $1x10^5$ EOMA cells were cultured in ^{2L}BNC and ^{3L}BNC platforms for one week, followed by 45 min incubation with calcein AM and ethidium homodimer III (EthD-III) at room temperature. The experiment was then visualized under fluorescence using an inverted microscope (Nikon Eclipse TE2000-U, software NIS Element D 4.11.00 software). Dead cells were stained by calcein in red and live cells were stained by EthD-III in green.

4.1.14.2 Metabolic activity

To evaluate the metabolic activity of cells cultured into BNC multilayer platforms, $2x10^6$ cells of the lineage MDA-MB-231 were injected in ^{2L}BNC Platform and

tested for the colorimetric assay MTS [3-(4,5-dimethylthiazol-2-yl)-5-(3-carboxymethoxyphenyl)-2-(4-sulfophenyl)-2H-tetrazolium] at different time points (3-, 5-, 7-, 10- and 15-days post-injection) according to manufacturer's indication. Briefly, the cell culture medium was removed, and the samples were washed twice with 1 mL PBS. Next, they were incubated for 4h (37°C, 5% CO_2, humified atmosphere) in a new well with 400 µL of complete culture medium and 80 µL of MTS reagent (Promega # G3580). After that, the BNC samples were smashed, the solution were homogenized by pipetting, 100 µL of this solution was transferred to 96-well plate in triplicate, and the absorbance was assessed by spectrophotometer (SpectraMax i3 Platform) at 490 nm.

4.1.14.3 Cell-cell interaction

Cell-cell interaction was evaluated by confocal microscopy. Samples were rinsed twice with PBS followed by fixation with paraformaldehyde 4% in PBS for 1h at room temperature. Samples were then washed 3 times with PBS (5 min/each), mounted with Aqua-Poly/Mount (Polysciences, #18606-20), and kept at 4°C until imaging at the Advanced BioImaging Facility (ABIF/McGill University). The confocal microscopy was performed using ABIF Opera Phenix High Content Screening at 5x objective and 20x water immersion objective, at 30µm and 15µm interval, respectively. Images were stitched on Imaris.

4.1.14.4 Gene expression

The gene expression of MDA-MB-231 cells was tested by RT-qPCR. For this purpose, the samples were submitted to RNA extraction by Trizol (ThermoFisher, #15596026) according to the manufacturer's protocol. The concentration and purity of RNA was evaluated by Nanodrop spectrophotometer (ThermoFisher) at Dr. Juncker's lab (McGill University).

Then, the RT-qPCR assay was performed in triplicate on the recovered RNA using a commercial kit – GoTaq® 2-Step RT-qPCR System (Promega, #A6010), according to the manufacturer's instructions using three different genes whose expression was normalized by GAPDH (**Table 7**).

Table 7: MDA-MB-231 genes used in the present study.

NCBI ID	Gene	Forward/ Reverse	Sequence (5' → 3')	Start	End
NM_002046.7	GAPDH	F	CACCCACTCCTCCACCTTTG	943	963
		R	CCACCACCCTGTTGCTGTAG	1052	1032
NM_002229.3	JUNB	F	TTCAAGGAGGAACCGCAGAC	1001	1021
		R	TGAGCGTCTTCACCTTGTCC	1196	1176
NM_004419.4	DUSP5	F	CCAACTTTGGCTTCATGGGC	1120	1140
		R	GCTCAGTGTCTGCAAATGGC	1253	1233
Z13009.1	E-cad	F	GGTCTCTCTCACCACCTCCA	1483	1503
		R	GGATGTGATTTCCTGGCCCA	1615	1595

4.1.14.5 Imaging analysis

SEM images were processed on ImageJ (version 1.52). Confocal microscopy volumetric images were snapped on ImarisViewer (version 9.7.2). Panels were assembled on Adobe Illustrator 2021.

4.1.14.6 Statistical analysis

The Mann-Whitney test was used for comparison between porous and dense surfaces for each layer. Paired t test was used for comparison between the glucose Diffusion Coefficient of ^{SL}BNC and ^{2L}BNC Platform. One-way or two-way analysis of variance (ANOVA) with Tukey's post-hoc test was used for the comparison of multiple groups. Data presented is shown as the average ± standard deviation of the results from three independent experiments unless otherwise stated. $P < 0.05$ was considered statistically significant (*$0.01 < P < 0.05$, **$0.001 < P < 0.01$, ***$P < 0.001$, and **** $P < 0.0001$). All analyses were performed using GraphPad (version 9.1.0.221). As previously described, panels were assembled on Adobe Illustrator 2021.

5 RESULTS AND DISCUSSION

5.1 Platform production - Standardization

5.1.1 The best method is adding-only medium after the 1st layer production

First, two methods of scaffold production were evaluated: transference of hydrogels and addition of media to form 2nd and 3rd layers (method I) and addition of media without transference of prior formed hydrogels (method II).

In method I, it was not possible to standardize the volume to form 2nd and 3rd layers due to space restriction in the plates used. For this reason, most membranes dried out due to the absence of an adequate volume for a long time of incubation (up to 45 days) (**Table 3**). For this reason, the second method was then chosen.

5.1.2 The ideal interval of layer production is 7 days

Next, the interval of incubation to obtain each BNC layer was verified. To achieve this, 24-well plates, 48-well plates, 96-well plates, conical tubes of 15 mL (Falcon-like), and borosilicate tubes were tested starting with 15 days of incubation (**Table 3** – Experiment ID KP004 and KP005). Unfortunately, most layers dried out or moved to the recipients' walls, indicating that this time was inappropriate.

To confirm previous results, bacteria were incubated in cell-culture plates (24-well and 96-well) at different times of incubation (7-, 10- and 15 days) using different incubation volumes of HS, Mannitol or DMCM media (50µL, 75µL, and 100µL – for 96-well plates; 500µL, 750µL, and 1000µL – for 24-well plates) (**Table 3** – Experiment ID KP006, and **Figure 10**).

Figure 10: Varying interval of incubation of cultures in 96-well plate and 24-well plate. The values refer to volume in a microliter (µL). To the blank circles, the medium was not added. C: control.

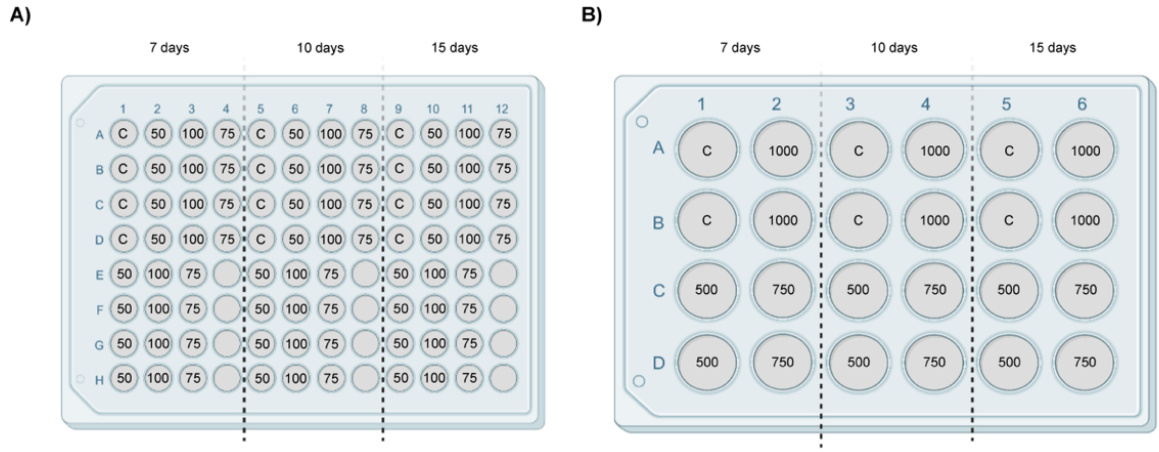

Both intervals of 7- and 10- days of incubation were appropriate to produce the ^{3L}BNC Platform and individual layers could be distinguished (24-well plate). So, the 7 days' interval was chosen for further experiments. The 96-well plates, on the other hand, were not suitable for production due to the small capacity of wells.

5.1.3 Conical tube (Falcon-like) was the best recipient of production

To decide which recipient was more adequate to ^{3L}BNC Platform' production, cell-culture plates (24-well and 48-well) and conical tubes of 15 mL were then used (**Table 4** – Experiment ID KP008 and **Figure 7)**.

In a 24-well plate, 1.5 mL of inoculum (2.5% v/v) was added to form the 1st individual layer of BNC. After 7 days' incubation (26°C), 750µL or 1000µL of culture medium was gently added and the system was kept under 26°C for 7 days, forming the 2nd individual layer. This procedure was repeated once. The same volumes were tested in experiments performed in conical tubes (**Figure 7)**.

In 48-well tissue-culture plates, 800 µL of inoculum (2.5% v/v) was added to produce the 1st individual layer, followed by addition of 250µL medium after 7 and 14 days, making 2nd and 3rd individual layers, respectively.

We observed that BOD generates an air flowing causing rapid evaporation of the culture medium and fast dryness when small recipients were used. Therefore, the use of tissue-culture plates (which material is permeable to oxygen and other gasses) is not adequate (**Table 8)**. To standardize all the parameters to produce the platforms,

such as stable temperature to bacteria growth (which is possible by using BOD) and keep the same volume of media to make additional layers, we choose to test the production in conical flasks.

In fact, the conical tubes showed the best harnessing of production (**Table 8**) since it allowed the assembly of ^{3L}BNC by DMCM and Mannitol medium using different volumes (750 µL and 1 mL) of incubation. Unlike, the HS medium was not indicated for ^{3L}BNC Platform production (**Table 8**)

Table 8: Number of membranes submitted to purification for each medium. Production of ^{3L}BNC Platform performed in the BOD incubator.

Medium: DMCM	**Volume added to form 2nd and 3rd layers**		
	250 µL	**750 µL**	**1 mL**
24-well plate	N/A	4/12	2/12
48-well plate	24/48	N/A	N/A
Conical tubes	N/A	3/3	3/3

Medium: Mannitol	**Volume added to form 2nd and 3rd layers**		
	250 µL	**750 µL**	**1 mL**
24-well plate	N/A	4/12	4/12
48-well plate	24/48	N/A	N/A
Conical tubes	N/A	3/3	3/3

Medium: HS	**Volume added to form 2nd and 3rd layers**		
	250 µL	**750 µL**	**1 mL**
24-well plate	N/A	3/12	1/12
48-well plate	24/48	N/A	N/A
Conical tubes	N/A	0/3	0/3

A comparison between different volumes of production of DMCM-derived samples (i.e., 750µL and 1mL) shows a slightly higher distance of layers produced using more volume. Moreover, it was possible to verify quite easily the layers produced by the addition of 750µL, which was the most stable ^{3L}BNC Platform samples. For stability, it is referred to the observation that individual layers of BNC did not easily detach from each other.

Taking together, the method to produce ^{3L}BNC Platform starts by adding 3 mL of inoculum (2.5% in medium) in conical tubes (Falcon-like of 15 mL) and adding 750µL of bacteria culture medium every 7 days' incubation, twice (**Figure 11**). The time spent in the production of each ^{3L}BNC Platform is, so, 21 days. The 1st layer formed (basal)

is called the 1st layer, the middle is named the 2nd layer, and the last (upper) is called the 3rd layer (**Figure 8**).

Figure 11: Defined method of ^{3L}BNC Platform production.

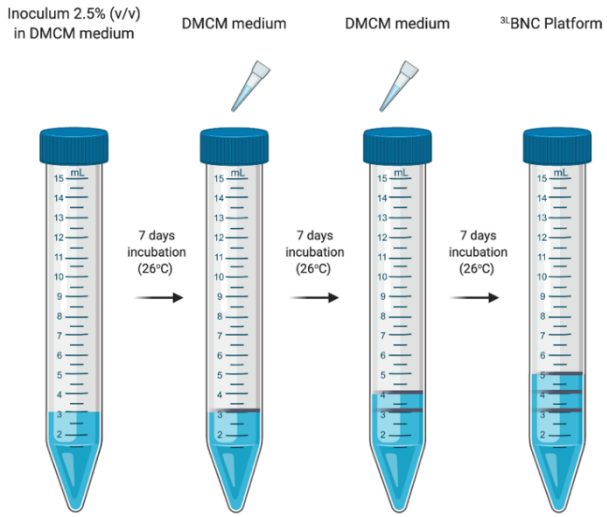

The internal diameter of the conical tubes used is approximately 13 mm – very similar to the diameter of cell-culture plates 24-well (15 mm). However, these flasks avoid medium evaporation rapidly. Once *K. hansenii* is an aerobic bacterium, the amount of medium and gasses (oxygen) accessible is intimately related to the BNC formation. To confirm this hypothesis on those experiments, we tried different ways to close the tubes and noted that there is a balance between evaporation range and the amount of oxygen available. In other words, the cap of the conical tube is also important to allow oxygen transference. This result is in accordance with previous works from Budhiono *et al.* (1999) that have demonstrated the importance of oxygen availability in the medium surface considering BNC production on static conditions. Furthermore, Masaoka and collaborators (1993) have showed that cellulose yield is proportional to the surface area used to produce the biomaterial.

5.2 Platform physical characterization

5.2.1 Dimensional analysis

After defining the producing method, we measured the thickness of the ^{3L}BNC Platform's individual layers produced in DMCM, which was compared with control groups (^{SL}BNC). To aim this, the samples were kindly dried using an absorbent paper towel, followed by measurements using a digital micrometer.

The diameter of the six measured samples was, on average, 14.6005 ± 0.2078mm. Regarding the thickness, the ^{3L}BNC Platform samples presented an average of 7.0385 ± 0.6146mm. The thinner platform was 6.248 mm and the thickest was 7.739 mm. Although quantitative, this analysis hides an issue: the BNC membranes derived from the DMCM medium have approximately 99.5% of water (effect related to their water holding capacity) (SOUZA et al., 2018) that makes it difficult to uniformly dry samples.

Then, the individual layers of ^{3L}BNC samples were detached by tweezers and re-evaluated (**Figure 12**). Both thickness, and diameters were highly comparable to ^{SL}BNC and amongst themselves (i.e., no statistically significant differences were observed). This result indicates that individual layers of ^{3L}BNC Platform correspond to hydrogels of 7-days incubation and, for this reason, should have similar properties.

Figure 12: Dimension analysis of ^{3L}BNC individual layers compared to ^{SL}BNC. A) Thickness. B) Diameter.

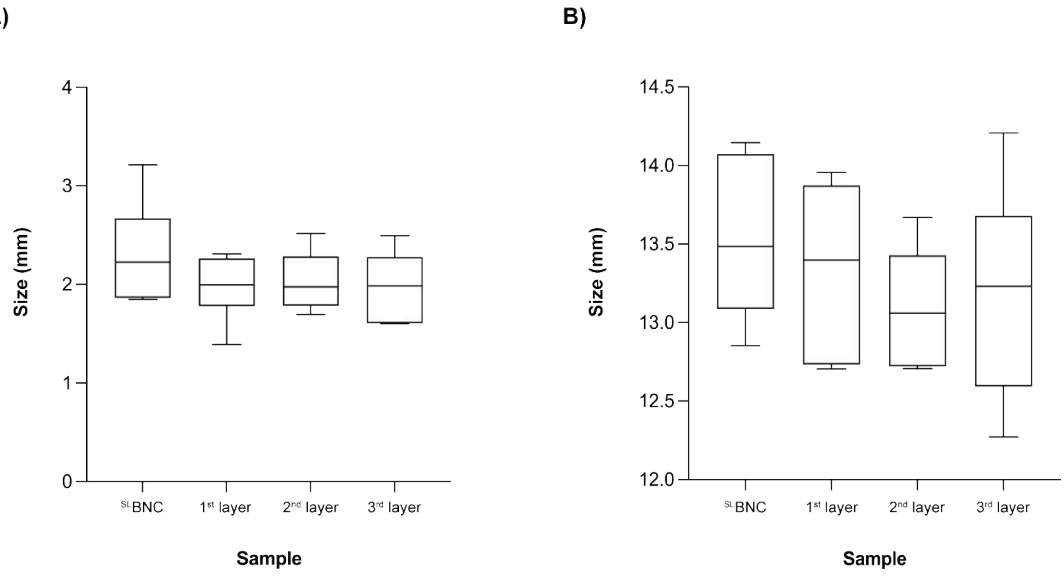

Furthermore, through this analysis it was possible to infer the inter-layers' region (that will be used to culturing cells), which presented 0.5265 ± 0.2739 mm. The high standard deviation observed was caused by one sample that presented an interlayer region of approximately 1.081 mm. After excluding this sample of the analysis, it was obtained an average of 0.4157 ± 0.0396mm, confirming the reproducibility of the method to produce ^{3L}BNC Platform.

^{SL}BNC samples had a percentage of transmittance (%T) from 56.3% to 72.0% and their average transparency was 31.3 ± 4.2%. For ^{2L}BNC scaffolds, %T varied from 57.5% to 67.6% and transparency of 14.2 ± 1.3% which is approximately half of ^{SL}BNC transparency. For layers produced in mannitol media, %T varied from 47.3% to 52.5% and transparency value was 24.7 ± 1.4%.

5.2.2 Transparency

Samples remained translucent even with the increasing number of layers (**Figure 13**). ^{SL}BNC samples had a percentage of transmittance (%T) from 56.3% to 72.0% and their average transparency was 31.3 ± 4.2%. For ^{2L}BNC scaffolds, %T varied from 57.5% to 67.6% and average transparency was 14.2 ± 1.3%, which is approximately half of ^{SL}BNC transparency. Finally, ^{3L}BNC samples had a %T from 47.6% to 50.6% and transparency was 7.0±0.2%.

Figure 13: Translucency of ^{SL}BNC and ^{3L}BNC Platform visualized und stereo microscope.

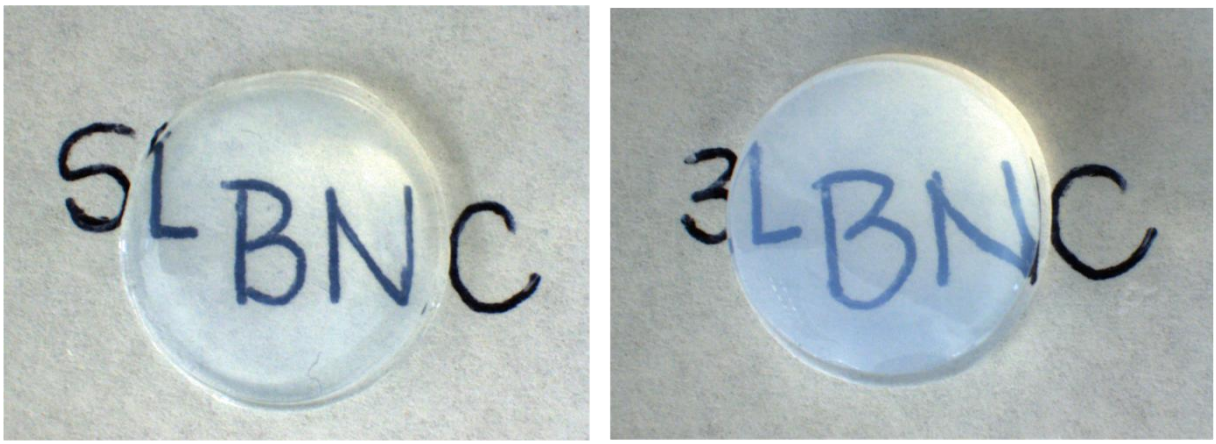

5.2.3 Structural characteristics

The SEM micrographs of ^{3L}BNC scaffolds indicate individual layers within different nanofiber densities surfaces (dense and porous) and like control (^{SL}BNC) (**Figure 14**). These observations are in accordance with the information previously reported by Berti and collaborators (2013b).

The cross-section of the ^{3L}BNC Platform attested the existence of compartmentalization, as expected (**Figure 15**), being possible to identify the distinct layers (arrows) and interlayers regions that remains attached to the layers but have a lower density of nanofibers (*). Micrographs showed two independent environments (detached detail). On the left, the micrograph revealed interlayer regions, due to crossing issues. On the other hand, the right image (higher magnification) allows identifying all parts that comprise the ^{3L}BNC Platform.

It seems that each membrane is, in fact, a sum of tiny membranes that are secreted “one-by-one”, until reaching the final layer format (**Figure 16**). This result agrees with Klemm *et al.*, (2001) that added colored twines on the surface of the nanocellulose supernatant and showed their retention over time.

The interlayer’s region, on the other hand, seems to be composed of dispersed fibers of cellulose that maintain the intact structure (**Figure 17**). The pores of this area are more “opened”, indicating that this region is suitable for culturing cells.

Figure 14: Comparison of bottom and top surfaces amongst the individual layers of ^{3L}BNC Platforms and ^{SL}BNC.

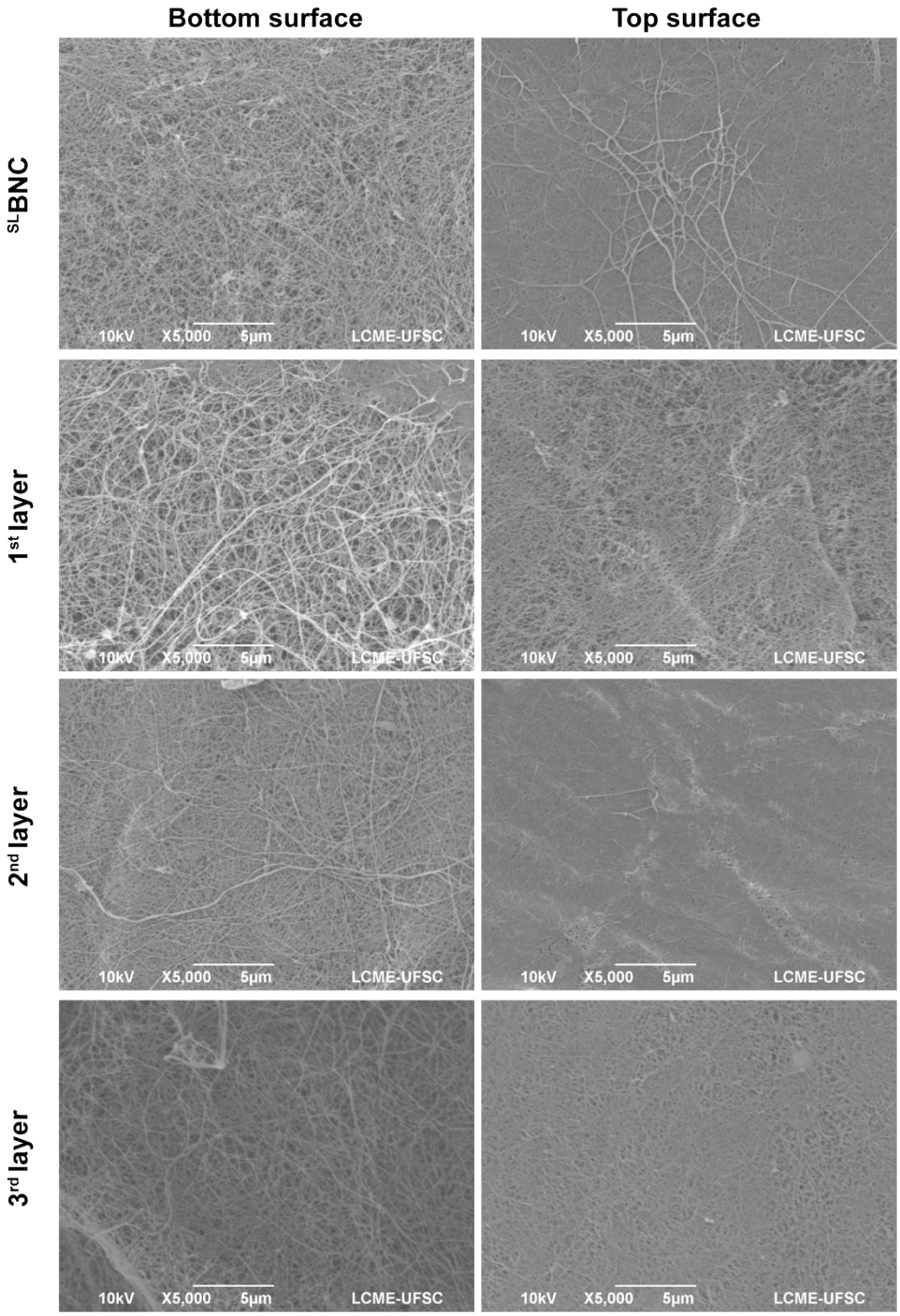

Figure 15: Cross-section of ^{3L}BNC Platform showing individual layers (arrows) and interlayers' area (*).

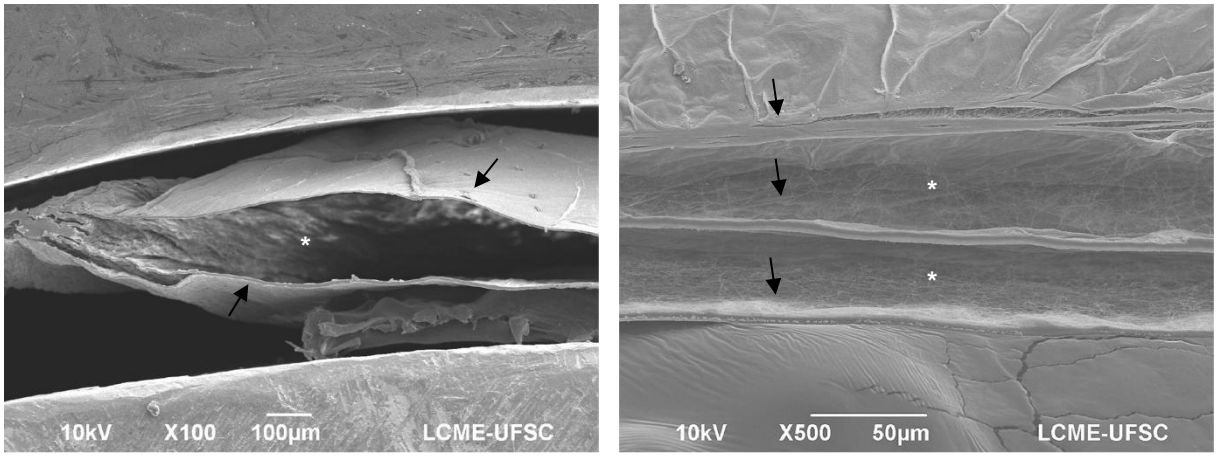

Figure 16: Deposition of tiny cellulose fibers to form the final layer of the platform.

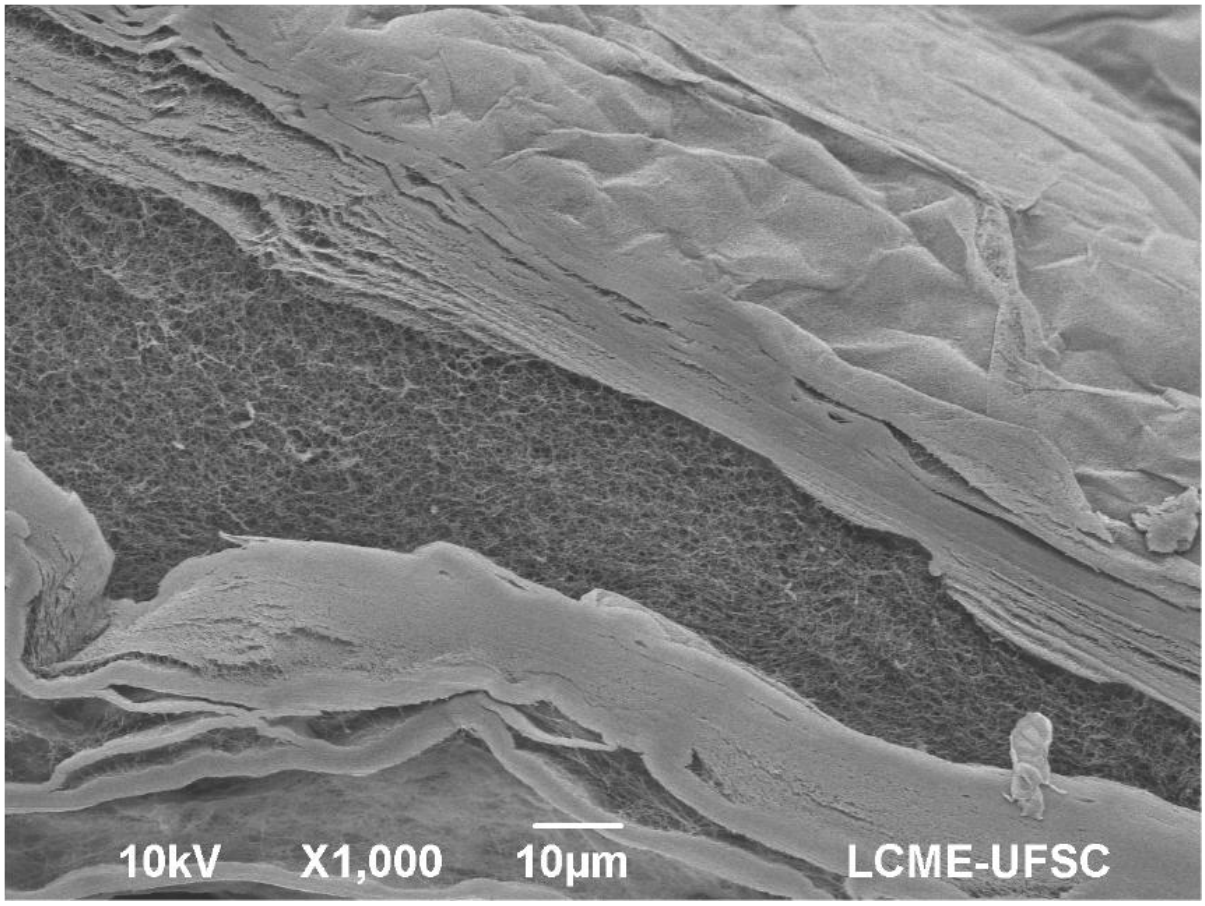

Figure 17: The interlayer structure.

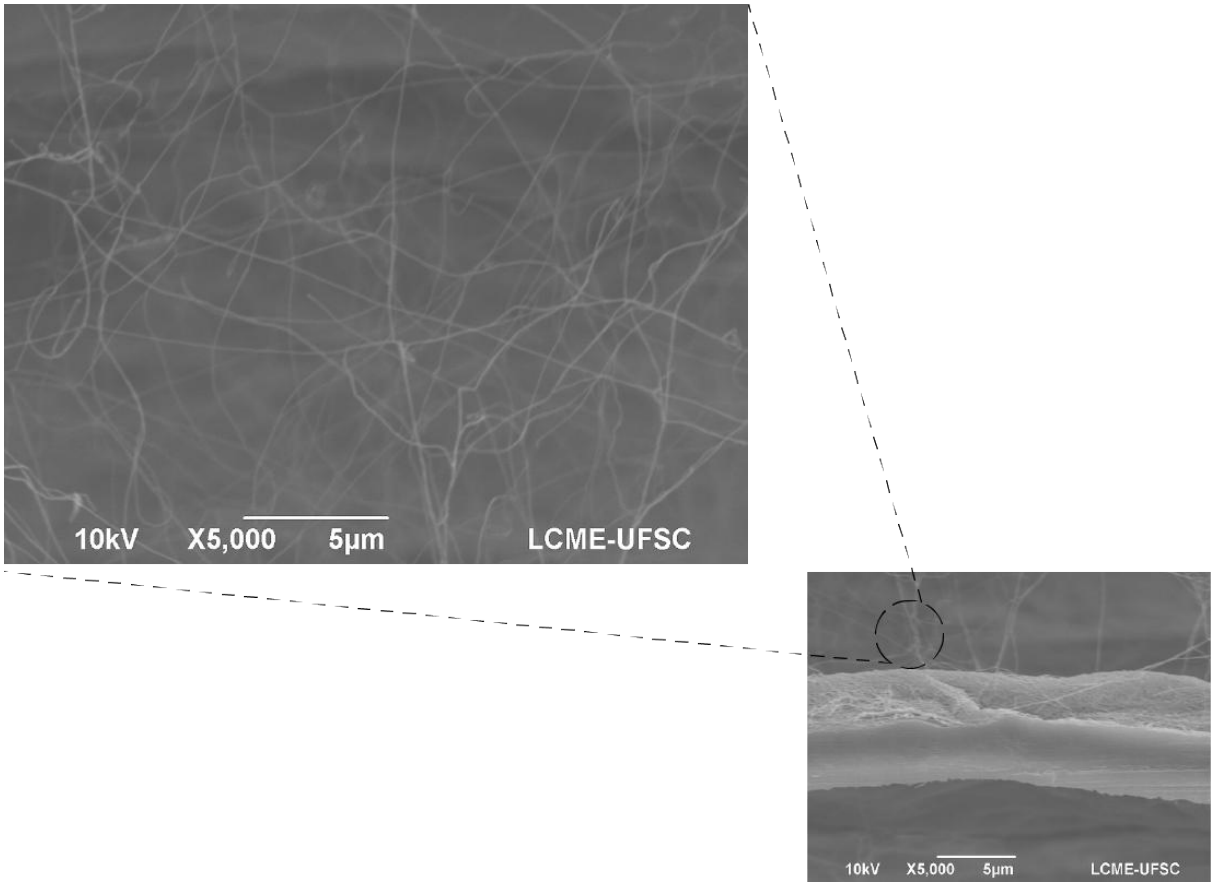

5.2.4 Pore size and nutrient transport

Pore size is an important characteristic to be considered in tissue engineering since it directly influences cell attachment (MATSIKO; GLEESON; O'BRIEN, 2015; O'BRIEN et al., 2005), morphology (MATSIKO; GLEESON; O'BRIEN, 2015), nutrient supply (LIEN; KO; HUANG, 2009), cell growth (WHANG et al., 1999), ECM secretion (LIEN; KO; HUANG, 2009), cell invasion (TIEN et al., 2020) and gene expression (MATSIKO; GLEESON; O'BRIEN, 2015).

In fact, pore' size has been subject of multiple works (ANNABI et al., 2010;LIEN; KO; HUANG, 2009;LOH; CHOONG, 2013;MURPHY; O'BRIEN, 2010;O'BRIEN et al., 2005;TIEN et al., 2020) and many groups have been pursuing strategies to produce more opened BNC porous which could improve cell culture onto

those scaffold (JACEK et al., 2018;SUNDBERG; GÖTHERSTRÖM; GATENHOLM, 2015;XIONG et al., 2013;ZABOROWSKA et al., 2010).

In the present study, the pore size was evaluated by Feret diameter that calculates the average of pairs of parallel tangents to the periphery of a particle (or pore) (TOMLINS et al., 2006). Only micropores (< 100 µm) were identified in the individual layers, in accordance with previous work that demonstrated this type of pore represents 92% of all pores of pristine bacterial cellulose (XIONG et al., 2013).

Additionally, as previously demonstrated by SEM micrographs (**Figure 14**), there are differences between both surfaces of each individual layer of ^{3L}BNC Platform and they are statistically significant **(Figure 18** and **Table 9)**. In other words, in all individual layers, the porous surface presented larger pore size when compared to their counterparts.

Figure 18: Feret diameter analysis of ^{SL}BNC and individual layers' surfaces (porous and dense). For individual layers, the data corresponds to analysis of 3 images (*n=3*) and their corresponding standard deviation (±). For ^{SL}BNC, data corresponds to the average analysis of 1 image (n=1) and their corresponding standard deviation (±). ** : P < 0.01; **** : P < 0.0001; **std:** standard deviation.

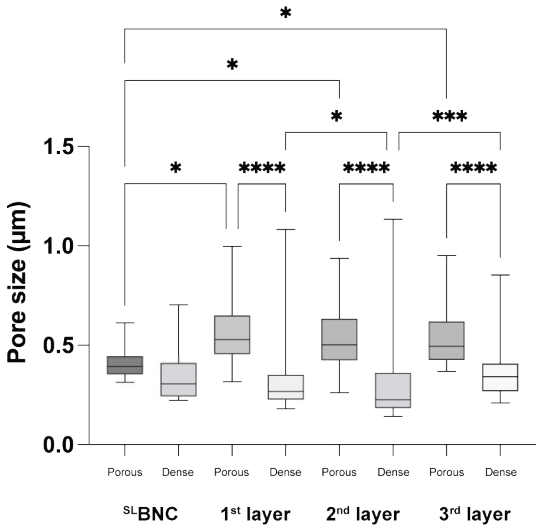

Considering the porous surface of all samples, the ^{SL}BNC presents the lower pore size. On the other hand, all individual layers showed more similar results. When dense surfaces are considered, the second interlayer differed from their counterparts (1st and 3rd individual layers).

Table 9: Descriptive statistics of Feret diameter of surfaces of individual layers and ^{SL}BNC.
Data in micrometer (μm). CI: confidence interval.

	^{SL}BNC		1st layer		2nd layer		3rd layer	
	Porous	Dense	Porous	Dense	Porous	Dense	Porous	Dense
Number of values	19	13	75	70	39	82	37	45
Minimum	0.3130	0.2236	0.3162	0.1789	0.2608	0.1414	0.3677	0.2088
25% Percentile	0.3544	0.2429	0.4561	0.2269	0.4238	0.1844	0.4265	0.2694
Median	0.3929	0.3053	0.5280	0.2668	0.5016	0.2258	0.4940	0.3418
75% Percentile	0.4441	0.4110	0.6478	0.3506	0.6315	0.3605	0.6187	0.4064
Maximum	0.6122	0.7034	0.9964	1.082	0.9364	1.133	0.9508	0.8528
Range	0.2992	0.4798	0.6802	0.9028	0.6756	0.9915	0.5831	0.6440
Mean	0.4084	0.3465	0.5568	0.3274	0.5416	0.2809	0.5371	0.3588
Std. Deviation	0.07974	0.1345	0.1439	0.1688	0.1714	0.1450	0.1495	0.1169
Std. Error of Mean	0.01829	0.03729	0.01661	0.02018	0.02744	0.01601	0.02458	0.01743
Lower 95% CI of mean	0.3700	0.2653	0.5237	0.2871	0.4860	0.2490	0.4873	0.3237
Upper 95% CI of mean	0.4468	0.4278	0.5899	0.3676	0.5971	0.3127	0.5870	0.3940

The minimum pore size was observed in the dense surface of the 2nd individual layer (0.1414μm) and the largest was seen at the porous surface of the same layer (1.133μm).

For the interlayers (**Figure 17**), the Feret diameter was 2.386 ± 0.981μm, which is approximately 5x bigger that average of pore size observed on the 2nd layer and 8x larger than average pore size from 1st layer. Despite these substantial increasing on pore size of interlayers when compared with individual layers, their size remains smaller than mammalian cells' size (GINZBERG; KAFRI; KIRSCHNER, 2015;LAN et al., 2019;SHASHNI et al., 2018). In fact, the interlayers' pore size was approximately 83%, 86% and 89% smaller than BC-CAFs (13.8μm), MDA-MB-231 (16.78μm) and M2 macrophages (20.98μm), respectively.

The small pore size of ^{3L}BNC Platform favors the increase of surface area and their interconnectivity (OSORIO et al., 2019) which is important for successful cell culture in scaffolds and for their nutrition (ROUWKEMA et al., 2009). For this reason, the permeability to nutrients was assessed by comparing glucose concentration samples sealed with ^{2L}BNC Platform and compared to ^{SL}BNC (**Figure 19**).

The ^{SL}BNC allowed both solutions – glucose solution and supplemented media – passed through it up to 12 hours faster than in the ^{2L}BNC Platform. In fact, the time for glucose to pass from donor to acceptor chambers was 2 hours, contrasting to 8

hours when supplemented media was being used. In contrast, for the ^{2L}BNC Platform, both solutions took 24 hours to fully go from donor to acceptor chambers due to more resistance generated by the increased number of layers..

Furthermore, independently of the analyzed sample (i.e., ^{SL}BNC or ^{2L}BNC Platform for both glucose control and supplemented media) the glucose concentration of the acceptor chambers did not reach the concentration of the donors' chambers. In other words, although supplemented media and glucose solution of acceptor chambers were 1mg/mL, most glucose molecules were retained by the hydrogels since the concentration in acceptor chambers did not attain values higher than 0.03mg/mL (**Figure 19**).

Taking together these results indicated that the increasing number of layers does not prevent platforms from being permeable to important nutrients to cells and, hence, to signaling molecules, since they usually have a nanometer size (MÜLLER; SCHIER, 2011). Additionally, considering that pore size of individual layers is smaller than of the interlayers (as previously discussed), it is hypothesized that cells cultured inside interlayers chambers can be trapped, allowing signaling molecules be studied without cell-cell contact.

Figure 19: Concentration of glucose in acceptor flasks communicated with donor and sealed by ^{2L}BNC Platform or ^{SL}BNC. Control – glucose solution (glu); Sample – supplemented DMEM (media); 0 min – prior starting analysis; Initial concentration (in donor chambers) 1mg/mL.

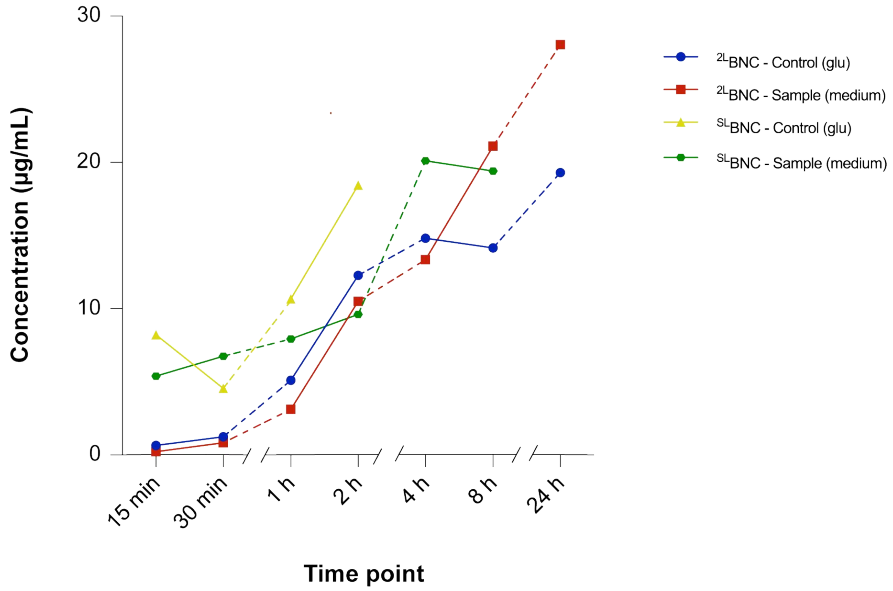

5.2.5 Rheological properties

Another major actor in tissue engineering regards mechanical properties, especially stiffness – a material property that does not depend on structure. Kashani and Packirisamy (2020) created a migratory speed (μ) of cells based on substrate mechanical properties. Their results showed that MDA-MB-231 cells are able to adjust themselves in terms of phenotype. Furthermore, Geiger and collaborators (2019) showed that MDA-MB-231 cells presented larger displacement in a hydrogel with Young's modulus of 584 ± 296 Pa (measured by an AFM assay).

Stiffness is an important factor and it differs amongst components of the analyzed tissue *in vivo*, including several healthy tissues (GEFEN; DILMONEY, 2007). However, their values are related to the technique and model applied in the analysis (GUIMARÃES et al., 2020;RAMIÃO et al., 2016;SAMANI; ZUBOVITS; PLEWES, 2007), making comparisons between studies somehow difficult. Furthermore, it is frequently impaired in disease tissues (BAHCECIOGLU et al., 2020;DEPTUŁA et al., 2020;SAMANI; ZUBOVITS; PLEWES, 2007).

Bahcecioglu and colleagues (BAHCECIOGLU et al., 2020) reviewed the literature and stated that the elastic modulus of breast cancer tissue is approximately ten times higher than the normal mammary gland reaching 1000-4000 Pa. In their work, Gefen and Dilmoney (GEFEN; DILMONEY, 2007) reported elastic modulus varying between 200-3000 kPa for breast skin and 2000-14000 MPa for the ribs, in healthy normal breast tissue. Samani et al. (SAMANI; ZUBOVITS; PLEWES, 2007) calculated the Young's modulus of normal and diseased breast tissue, which varied considerably from 3.24 ± 0.61 kPa (normal fibroglandular tissue) to 42.52 ± 12.47 kPa (high-grade IDC).

It is worth noting that the mechanical characteristics of soft tissues go beyond the stiffness defined by the Young's (or elastic) modulus. Indeed, there are other properties related to the elastic and viscous components that should be considered (COX, T. R.; ERLER, 2011) and all biological structures can be rheologically characterized (DEPTUŁA et al., 2020).

For reasons above, stiffness (E), storage modulus (G'), and loss modulus (G") of ^{2L}BNC and ^{3L}BNC platforms were measured and reported (**Table 10**). It was verified

that ^{3L}BNC Platform presents Young's modulus 75.5% higher than ^{2L}BNC Platform and this difference is statistically significant ($P < 0.05$).

Table 10: Platforms' rheological properties.

	Young's modulus (*E*) – Pa	Storage Modulus (G') – Pa	Loss Modulus (G") – Pa
^{2L}BNC Platform	124.78 (± 31.96)	2067.95 (± 291.46)	309.21 (± 8.49)
^{3L}BNC Platform	509.07 (± 74.37)	3257.93 (± 551.22)	540.28 (± 80.94)

The stiffness observed on ^{2L}BNC and ^{3L}BNC platforms resembles data in normal breast tissue (epithelium and stroma) and in breast tumor-associated stroma (reviewed by: BAHCECIOGLU et al., 2020), respectively. Additionally, the results are in accordance with data obtained by Rijal and collaborators (RIJAL; LI, 2017) who identified values of 366 ± 61 Pa for decellularized porcine breast using Atomic Force Microscopy (AFM).

With respect to storage modulus (i.e., the ability of the hydrogel to store deformation energy in an elastic manner), it has been proposed to be a mechano-marker of cancer by Deptuła and coworkers (2020).

Here, ^{3L}BNC Platform presented a storage modulus 36.5% higher than ^{2L}BNC Platform ($P < 0.05$). The high storage modulus observed for both materials indicate a high degree of cross-linking of glucose chains and values observed in ^{2L}BNC are similar to state in previous works (GAMA; GATENHOLM; KLEMM, 2012). Nonetheless, an increase was observed when an additional BNC layer was produced.

5.3 ^{3L}BNC Platform: take-home message and what to expect next

Taken together, the previous results indicate that it is possible to produce a platform made of stacked-multilayered BNC hydrogels in a successful and standardized manner. A previous work from our group showed two layers of BNC by culturing 20% inoculum of *K. hansenii* in a mannitol media with addition of dextrin or gluclose (SILVA, DA, 2012).

However, from the best of our knowledge, it is the first time that a pristine platform of multilayered BNC is produced in an optical translucid format. Among many characterized properties, it can be highlighted the translucency that is in accordance

with previous works (SOUZA et al., 2018) and it was not affected by the number of layers (**Figure 13).** Additionally, the number of layers does not seem to impact the ability of nutrient transport since there is pore interconnectivity. Nonetheless, it is expected a “trapping” feature of cells was also evaluated here.

Regarding the mechanical properties it seems that ^{3L}BNC Platform reflects what is expected for the study of breast tumor-associated stroma (BAHCECIOGLU et al., 2020) and for further studies with cells and cells signal biological molecules.

5.4 Platform biological characterization

5.4.1 Visual characterization, Cell viability and Metabolic activity

After physical characterization, different densities of EOMA cells were injected in ^{2L}BNC and ^{3L}BNC platforms and their viability were evaluated one week after injection by Live/Dead assay (**Figure 20**).

Due to platforms translucency (**Figure 13**), it was possible to visualize injected cells in both layered platforms (^{2L}BNC and ^{3L}BNC) using a microscope (**Figure 20A** and **B** – first column) and the increasing number of cells could sometimes be seen with naked eyes, since the platform became opaquer with the growth of proliferative cells. This is an important property that makes the injection more controllable and facilitates the day-by-day evaluation.

EOMA cells remained viable in the entire period of analysis (**Figure 20A** and **B** – second column) independently of the type of platform used. That is, the number of layers did not affect cell viability. Those results corroborate what obtained from physical characterization, especially after diffusivity of glucose’ analysis (**Figure 19**).

It was also possible to identify a few dead cells (**Figure 20A** and **B**, third column) compared to the number of alive cells of the same field. Additionally, this analysis pointed out the need of culturing a relatively large number of cells into the ^{3L}BNC Platform to obtain meaningful results. That is, the small number of cells cultured inside those platforms made it difficult to observe them under fluorescence microscope (**Figure 20B – II)**, which was solved by increasing the number of cells seeding (**Figure 20B – VI**). Nonetheless, the same challenge was not observed when EOMA cells were cultured inside ^{2L}BNC Platform (**Figure 20A – II** and **VI**). In this initial phase we

observed that the interlayers have approximately 596.0158 mm^2 of area and using a reduced number of cells could make the cell-cell communication difficult at all.

Since the platforms were suitable for cell culturing, the metabolic activity of cells grown in the ^{2L}BNC Platforms was next determined. For this aim, cells from the triple-negative breast cancer cell line MDA-MB-231 were cultured in this scaffold up to 15 days and their activity was measured by MTS assay.

The data acquired (**Figure 21**) indicated that the cells were metabolically active (and viable) for up to 15 days when cultured on the ^{2L}BNC Platform. In other words, the existence of multiple layers of BNC does not prevent cell growth. Those results confirmed the cells' capability to live on ^{2L}BNC Platform as observed with EOMA cells by Live/Dead Assay (**Figure 20**), and supports the results obtained for physical characterization, especially nutrient diffusiveness (**Figure 19**).

When metabolic activity of cells cultured in platforms (a 3D environment) was compared to that of cells cultured in plates (a 2D environment), statistically significant differences were observed (**Figure 21**) for all time points, which is in accordance with previous works (BÄCKDAHL et al., 2006;FALLICA et al., 2012;LUCA et al., 2013). These distinctions might be related to unlimited nutrient availability characterized by 2D models and by the spatial distribution of cells, which alters cell-cell communication. Nonetheless, previous works have showed differences between metabolomes of 2D and 3D culture cells (IKARI et al., 2021;LAGIES et al., 2020) and more similarity between cells cultured in 3D when compared to cells derived from original tissue (LAGIES et al., 2020). Additionally, 2D cultures are conducted in parallel to confirm cells viability in vitro (control group) and not as a comparative.

No statistically significant differences were observed between the time-points (3- and 5-; and 7- and 10- days) for the platform. For this reason, the following experiments were realized at 1-, 5-, 10- and 15 days' time point.

Figure 20: Live/Dead assay of one-week EOMA cells culture into ^{2L}BNC Platform (A) and into ^{3L}BNC Platform (B) at two different densities (1x10^4 and 1x10^5 cells). Green: live cells; red: dead cells; last column: merged images. Scale bars: 100µm.

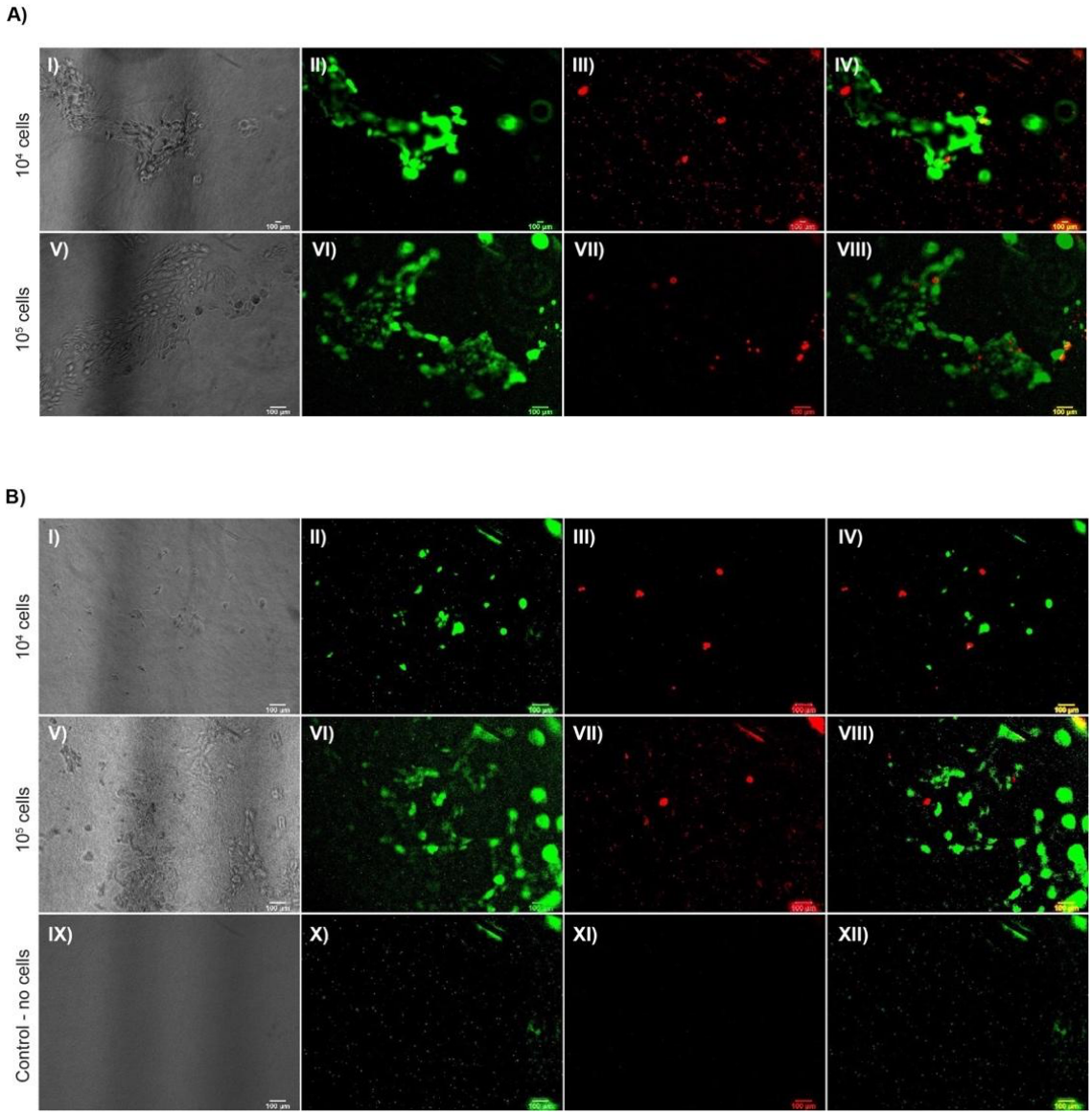

Figure 21: MTS assay of MDA-MB-231 cultured into ^{2L}BNC Platform ($2x10^6$ cells/platform) and in cell culture plate ($8x10^4$ cells/well).

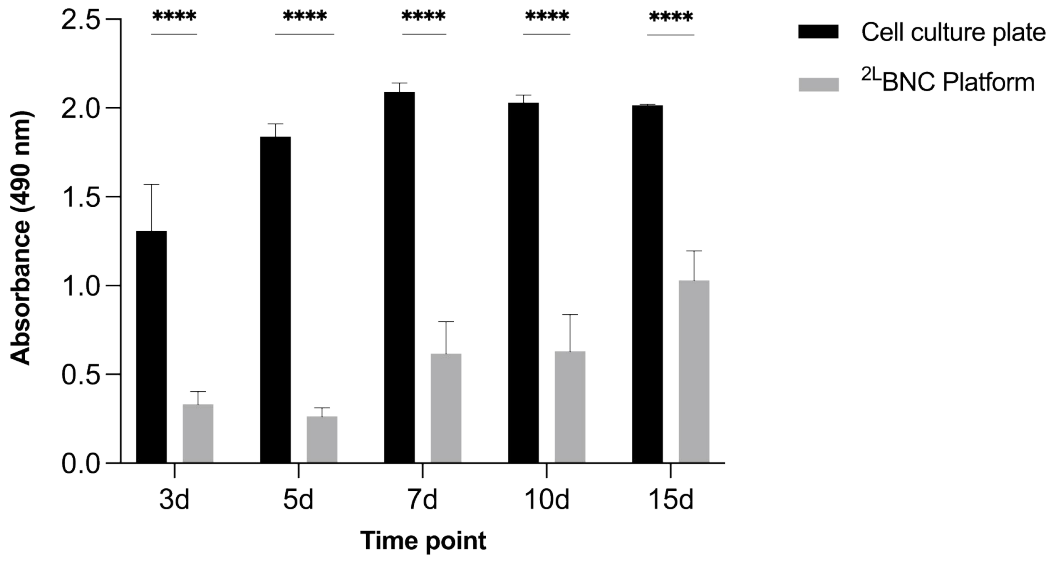

5.5 Co-culturing: challenging ^{3L}BNC Platform

5.5.1 Microscopic analysis

As will be further explained in the "Challenges' section", using specific antibodies for each cell type followed by confocal microscopy was a herculean and not successful work. For this reason, the best option was to use cell trackers.

However, to perform experiments with cell trackers, two aspects were verified namely: a) the spectral view of reagents; and b) their stability. Spectral view (**Figure 22**) displays a good separation between emission wavelengths (filled lines) for all three colors. Nonetheless, the emission wavelength (dashed line) shows a small overlap between dyes. This means that we cannot completely discard the existence of spectral bleed-through artifacts (also known as crossover or crosstalk) although some precautions can minimize them.

Figure 22: Fluorescence SpectraViewer of CellTrackers used in this project. In blue: CellTracker™ Blue CMAC (# C2110); in green: CellTracker™ Green CMFDA (# C7025); in red: CellTracker™ Red CMTPX (# C34552). Dashed lines: excitation wavelength; filled lines: emission wavelength.

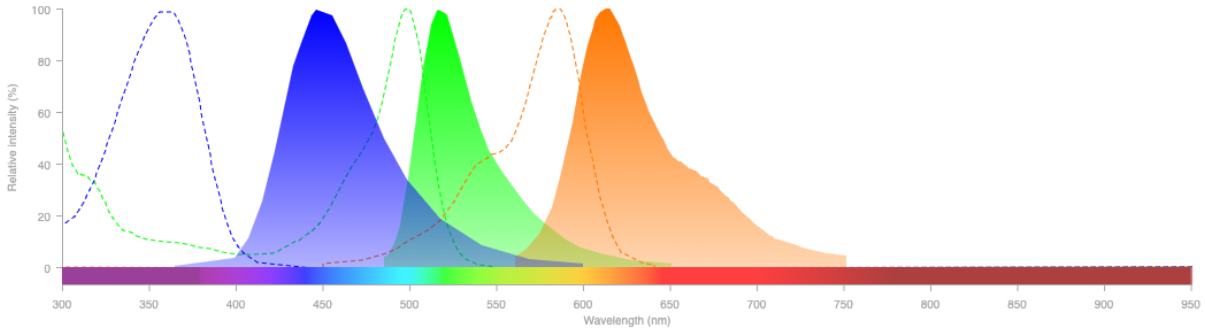

The second aspect checked was if those reagents used could be seen after 15 days in culture. To aim it, different groups of MDA-MB-231 cell line was stained by 25μM of green or red cell trackers and visualized under fluorescence microscopy (**Figure 23**). This comparison showed prolonged fluorescence for red cell tracker. In other words, red dye remains brighter for long period of time when compared to the green dye (which fluorescence started to diminish after 10d – data not shown). Unfortunately, no similar test was performed for blue cell dye, due to a delay of shipment for this reagent.

With both aspects in mind, the next step on this study was performing co-culture of triple-negative breast cancer cell line (MDA-MB-231) and tumor-associated cells (CAFs and M2 macrophages) into ^{3L}BNC Platform.

Cells were successfully seeded/injected into the ^{3L}BNC Platform, as easily visualized by confocal microscopy at 1d time point (**Figure 24,** 1st row) at both magnification (5x and 20x). BC-CAFs and MDA-MB-231 cells remained in their respective sites up to this day. Nonetheless, there was no distinction of M2 macrophages in their respective sites. In fact, these cells seemed associated with the other two cell types, as visualized by co-localization with green and red colors.

Figure 23: Fluorescence microscopy after 15 days of culture MDA-MB-231 in cell culture plates. A) Cells stained by 25µM cell tracker green and Hoescht. B) Cells stained by 25µM cell tracker red and Hoescht. Bars: 100µm.

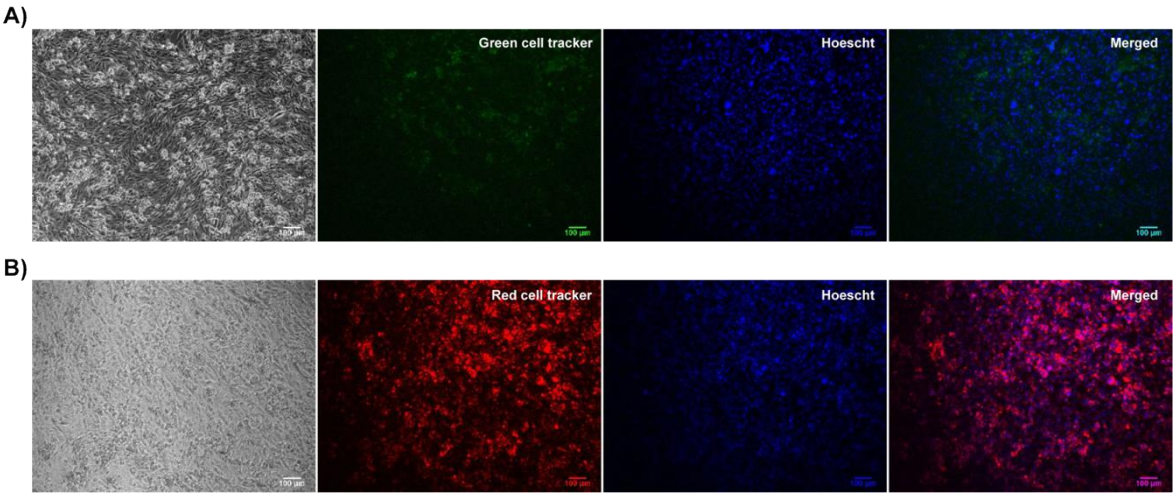

Different cell areas were not visualized at 5- and 10d time points (**Figure 24**, 2nd and 3rd rows). In fact, for both periods, green dots were identified exclusively on the bottom of the 3LBNC Platform. On the other hand, the 15d time point indicates a slightly different result (4th row). Both BC-CAFs and MDA-MB-231 areas could be seen at a low magnification (5x) but not at the higher (20x).

To check M2' presence, we displayed them alone and compared them to an exhibition of all cells (**Figure 25**). In fact, only the 5d time point did not exhibit blue dots compatible with M2 macrophages staining.

Figure 24: Tridimensional confocal microscopy of cells seeded/injected into ^{3L}BNC Platform of different time points (1-, 5-, 10- and 15d) and at low- (5x, left column) and high magnification (20x, right column). In green: MDA-MB-231; in red: BC-CAFs; in blue: M2 macrophages.

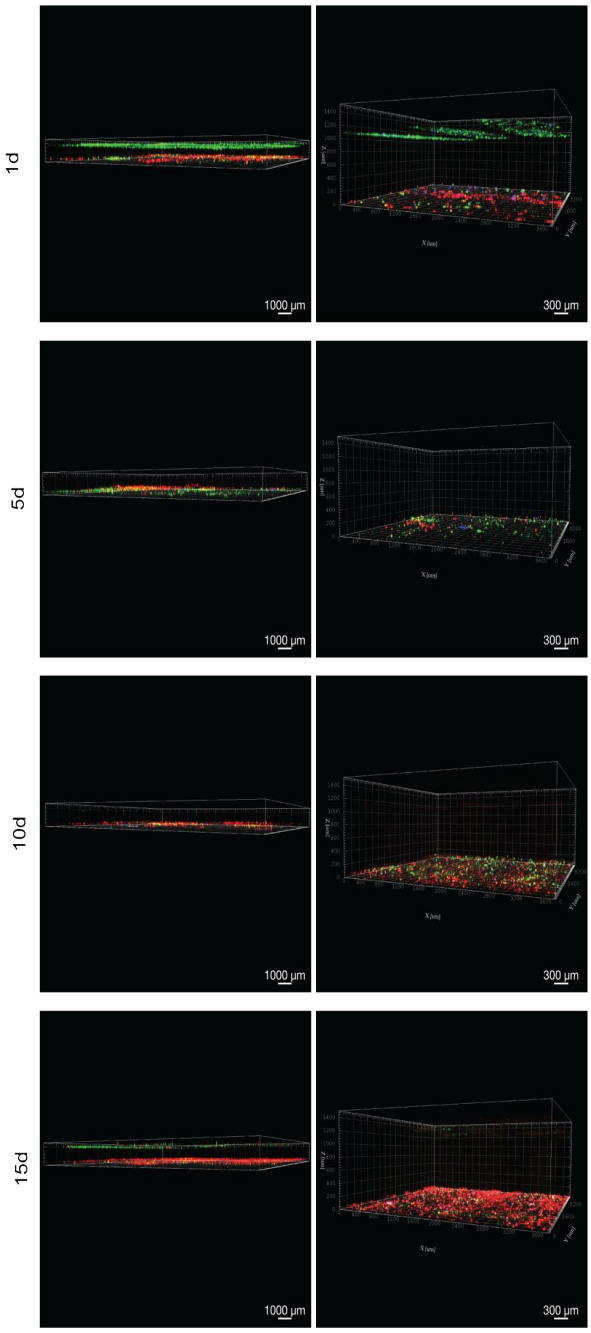

Figure 25: Exhibition of M2 macrophages alone (first column) and comparison with display of all cells at the same time (second column) at different time-points (1-, 5-, 10- and 15d) at high magnification (20x). In green: MDA-MB-231; in red: BC-CAFs; in blue: M2 macrophages.

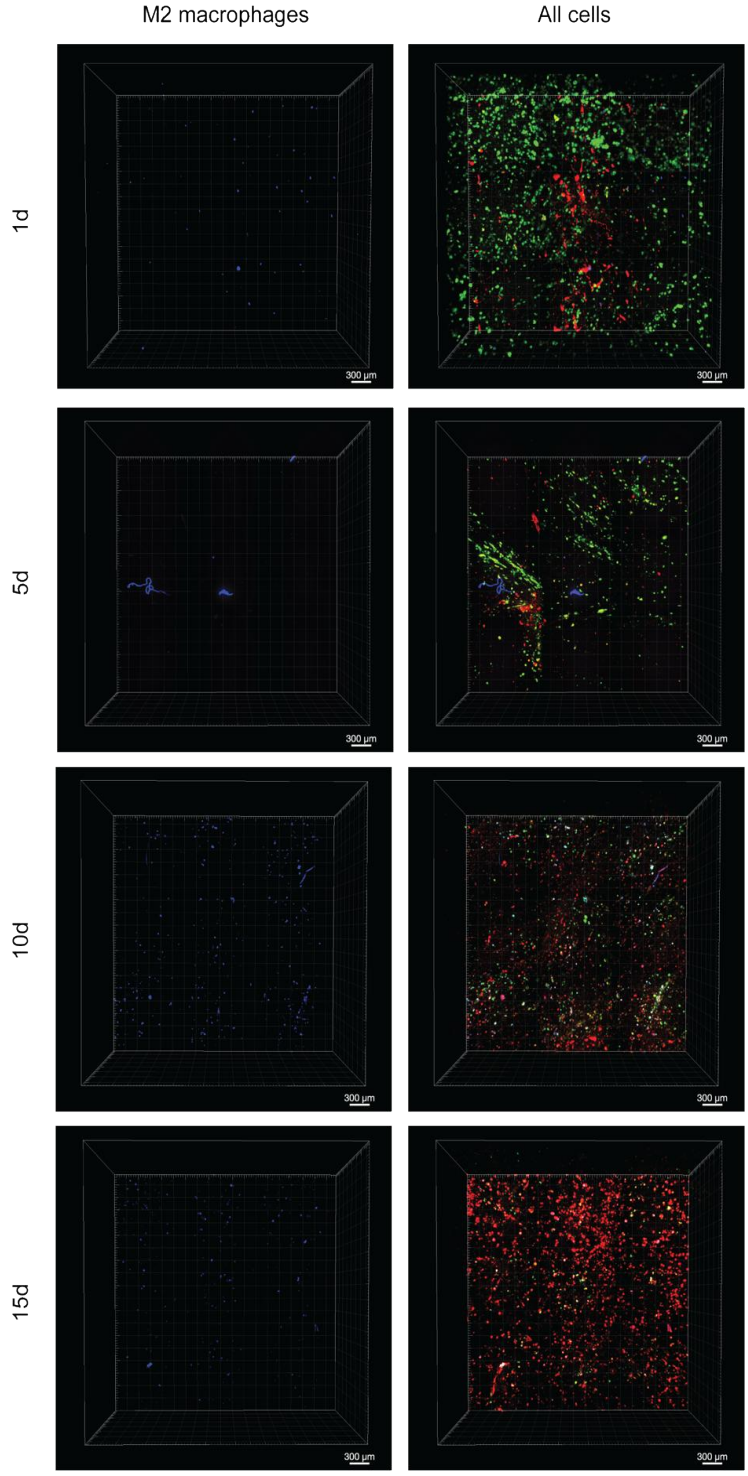

The vertical migration was also evaluated at all time points (**Figure 26**). This analysis was performed using different volume rendering modes in ImarisViewer

(version 9.7.2). Briefly, MIP (maximum intensity pixel) shows the maximum intensity of all images of the sample. Blend rendering blocks images in the background, prioritizing what is seen in the front. The normal shading, on the other hand, is better for visualizing the surface of what is being displayed.

No cells were visualized at the z-axis for the confocal microscopy of ^{3L}BNC Platform in any of the rendering modes (**Figure 26**). As previously discussed, all three cell types could be seen at 1d time point, although M2 macrophages did not stay in their injected compartment (i.e., 2nd interlayer).

At the 5d time point, an increasing number of MDA-MB-231 cell lines were seen in the bottom of ^{3L}BNC and almost no BC-CAFs were visualized. This could be the result of technical problems, such as a layer detachment that was not identified on time (i.e., the 1st layer could be folded during the manipulation and later detached), releasing fibroblasts and causing troubles to interpret this data. This also could explain the absence of M2 macrophages at 5d time point (**Figure 25**) since they seemed much more associated with fibroblasts.

Similarly, at 10d we do not identify cancer cells at the 1st interlayer (i.e., where they were injected) but exclusively at the bottom of the platform (1st layer). However, at this time a good number of BC-CAFs were also identified. Surprisingly, the normal shading rendering indicates that cancer cells seemed to be involved by fibroblasts and few of them are also reported at the area corresponding to MDA-MB-231 injection.

At the final time point, very few cancer cells were observed, agreeing with the lack of fluorescence previously discussed. Nonetheless, normal shading indicates higher red dots (BC-CAFs) at the initial position of breast cancer cells and higher zoom in the image shows few fibroblasts between the two regions (**Figure 26** – bottom image on the right).

Figure 26: Migration of cells into ^{3L}BNC Platform at 1-, 5-, 10-, and 15d time points and using different rending volume modes (MIP, Blend and Normal Shading). In green: MDA-MB-231; in red: BC-CAFs; in blue: M2 macrophages. Augment: 20x.

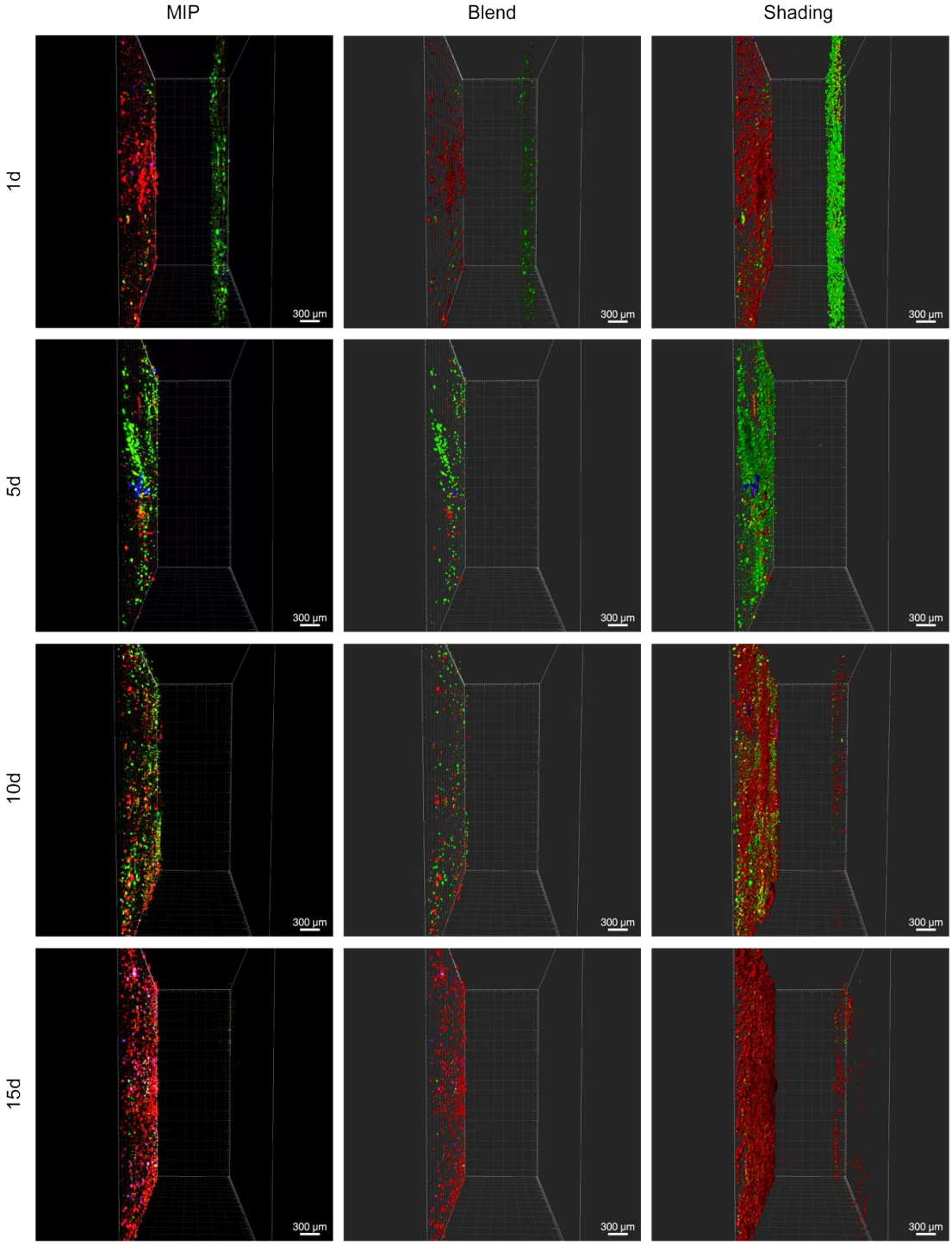

To explain these results some factors must be considered. First of all, BNC does not naturally allow cell penetration into hydrogels, which prompts extensive

studies for increasing its porosity (SÄMFORS et al., 2019;SUNDBERG; GÖTHERSTRÖM; GATENHOLM, 2015;XIONG et al., 2013;ZABOROWSKA et al., 2010).

Secondly, MDA-MB-231 cells presents high motility and invasiveness when cultured in CAFs conditioned media (in a mechanism influenced by mDia2 protein regulation by CXCL12), both in 2D and 3D environments (DVORAK, K. M. et al., 2018). Furthermore, this high invasiveness can be observed as early as 24h.

Third, CAFs are present in primary and metastatic tumor stroma (MCCARTHY; EL-ASHRY; TURLEY, 2018) and can circulate to bring the “soil” for cancer cells (the seed) (DUDA et al., 2010). Their subtypes display differential ability to move towards oral squamous cell carcinoma (COSTEA et al., 2013). In breast cancer, normal fibroblasts acquired CAFs properties by delivering miR-9 (BARONI et al., 2016), which directly targets E-cadherin (MA et al., 2010) and is upregulated in MDA-MB-231 cells (SHI; YE; LONG, 2017).

Fourth, monocytes are recruited by CAFs by the SDF-1, also known as CXCL12 (YAVUZ et al., 2019), that in addition to CXCL14, has a role on M2 polarization (GUNAYDIN, 2021). In fact, macrophages are frequently found at the same area of CAFs (YAVUZ et al., 2019) and their M2 polarization seems to confer advantage to their long survival in TME (GEORGIEVA et al., 2020). It is also important to point out the lower M2 adhesion and higher motility when compared to classically activated macrophages (M1) (CUI et al., 2018).

Lastly, expansion of tumor-associated macrophages (TAMs, M2 polarized) is not a well-defined subject once different authors found different growth rates. For example, Tymoszuk and colleagues demonstrate the ability of fully TAMs to expand in the tumor but they also discuss the existence of nondividing TAMs, found by other groups (TYMOSZUK et al., 2014). Nonetheless, one important factor to have in mind is the macrophage source, since macrophages derived from THP-1 cell line and bone-marrow monocytes mismatch in many phenotypical and molecular aspects (TEDESCO et al., 2018).

Based on the factors listed above, we cannot affirm that the ^{3L}BNC Platform allows cell invasion. In fact, the absence of cell penetration (invasion) into BNC can be

easily explained by comparing the average Feret diameter of porous of ^{3L}BNC Platform' individual layers (**Figure 18**) and average size of cells used in this work (MDA-MB-231: 16µm; BC-CAFs: 14µm; and M2 macrophages: 21µm).

So, the simplest explanation for the high number of breast cancer seen at 1st layer of the platform would be their detachment and migration towards to fibroblasts due to cell signaling, which could be facilitated by the smaller diameter of ^{3L}BNC Platforms (14.6005 ± 0.2078 mm) when compared to the well culture plates in which they were placed (17mm) and by media replacement every 2-3 days. This hypothesis could also be reasonable to explain by the low number of BC-CAFs that moved towards the 1st interlayer.

Regarding the M2 macrophages, we present the same considering the impact of those cells due to their high motility mentioned earlier. Additionally, we cannot completely discard a lack of efficiency of the cell tracker used to stain these macrophages, since blue dye did not shine as much as the other two dyes.

5.5.2 Gene Expression

After showing that ^{3L}BNC Platform is suitable for co-culturing breast cancer and tumor-associated cells, the next aim was verifying the expression of some breast cancer genes and for this, the total RNA was extracted from all samples (**Table 11**).

For ^{3L}BNC Platform, the released RNA was approximately 3 times lower than samples derived from cell culture plates, ranging from 94.3 ng/µL to 754.0 ng/µL to platforms and from 94.3 ng/µL to 754.0 ng/µL to cell culture plates. This result can be explained by the high-water holding capacity of BNC (up to 99%) (BÄCKDAHL et al., 2006;KLEMM et al., 2001) and by the high degree of swelling of the proposed platforms (reaching 86% for ^{SL}BNC and 233.34% for ^{2L}BNC Platform).

Such characteristics make it difficult to completely liberate hydrophilic molecules (such as RNAs). In fact, to the best of our knowledge, the evaluation of gene expression of cells cultured in BNC scaffolds is not common and easy to perform. Indeed, the characterization of models usually overlooks this aspect, and it is hypothesized that this is due to the difficulties mentioned above.

Table 11: Nanodrop results from RNA extraction by Trizol of cells grown in ^{3L}BNC Platform and cell culture plate. [ ]: concentration; NC: negative control (i.e., no cells)

Cultured in	Sample	Time point	[ ] (ng/µL)	260/280	260/230
^{3L}BNC Platform	1d – Rep 1	1d	7.9	1.54	0.08
	1d – Rep 2	1d	63.1	1.79	0.29
	1d – Rep 3	1d	80.1	1.87	0.33
	5d – Rep 1	5d	70.0	1.87	0.47
	5d – Rep 2	5d	222.4	1.86	0.73
	5d – Rep 3	5d	117.1	1.86	0.59
	10d – Rep 1	10d	219.6	1.85	1.22
	10d – Rep 2	10d	167.6	1.91	0.79
	10d – Rep 3	10d	22.4	1.94	0.21
	15d – Rep 1	15d	172.5	1.91	0.87
	15d – Rep 2	15d	235.0	1.91	1.10
	15d – Rep 3	15d	38.6	1.83	0.27
	NC – Rep 1	15d	5.9	1.67	0.10
Cell culture plate	1d – Rep 1	1d	94.3	1.80	0.24
	5d – Rep 1	5d	243.8	1.77	0.74
	5d – Rep 2	5d	358.8	1.89	1.02
	10d – Rep 1	10d	626.4	1.83	1.30
	10d – Rep 2	10d	640.2	1.86	1.27
	15d – Rep 1	15d	691.7	1.81	0.98
	15d – Rep 2	15d	754.0	1.79	1.29
	NC – Rep 1	15d	9.1	1.89	0.03
	NC – Rep 2	15d	65.3	1.57	0.16

The RNA extracted presented a ration A_{260}/A_{280} higher than 1.8 for most samples, as indicated as a quality parameter for this technique, although this method is questionable (FLEIGE; PFAFFL, 2006). The ratio A_{260}/A_{230}, on the other hand, was low, which prompts possible contaminants as nanocellulose fibers. In fact, the quality of the RNA has important implications in the downstream techniques. In our tests, GAPDH was used as a reference gene and its amplification had an averaged Ct of 20.73 ± 0.19 and 17.91 ± 0.36 for samples derived from ^{3L}BNC Platform and cell culture plates, respectively.

Then, the GAPDH relative expression of *e-cadherin*, DUSP5, and *Junb* genes were comparable across similar time-points and cell culture conditions by RT-qPCR essay (**Figure 27**).

E-cad gene encodes the tumor suppressor glycoprotein E-cadherin involved in cell-to-cell adhesion and which role in tumor progression and metastasis has been extensively discussed (LIU, Y. N. et al., 2005;NA et al., 2020;ONDER et al., 2008;PADMANABAN et al., 2019;PETROVA; SCHECTERSON; GUMBINER, 2016). *E-cad* is frequently impaired in cancers and its lost/low expression in TNBC patients it is related to poorer overall survival (KASHIWAGI et al., 2010), reason why it's prognostic value has been postulated (KASHIWAGI et al., 2010;SHEN et al., 2016).

The MDA-MB-231 is an *e-cad*⁻ TNBC cell line that presents a highly proliferative phenotype (RUSSO et al., 2020). In this work, breast cancer cells cultured in ^{3L}BNC Platform presented lower expression of *e-cad* when compared to cells cultured in plates (**Figure 27**) that were statistically significant for days 1 and 5 ($P<0.05$, two-way ANOVA). The lower expression of *e-cad* in cells cultured in our scaffold compared to those cultured in plates suggests that our model is suitable to mimic the complexity of the TME and agrees with the results of MDA-MB-231 migration.

With respect to DUSP5, this gene belongs to a family of dual-specificity phosphatase and is downregulated on MDA-MB-231 paclitaxel (PTX) resistant cell line (LIU, T. et al., 2018). Further, it seems low expressed in the basal subtype of breast cancer patients, negatively correlated to high histological grades, and associated with a poor prognosis (LIU, T. et al., 2018).

To understand why DUSP5 was chosen for gene expression analysis, it is important to point out two things. First, approximately 70-80% of TNBC are classified as basal-like breast cancer (NEDELJKOVI; DAMJANOVIC, 2019). The second aspect regards PTX being an antimitotic taxane class of anticancer drug frequently used to strike breast cancer and which mechanism of action is reviewed by Abu and colleagues (2019).

Our data shows a decrease of DUSP5 expression from day 1 followed by an increasing trend in ^{3L}BNC (**Figure 27**). Additionally, its less expression in our scaffold when compared with plates suggests a behavior of drugs' resistance, similarly to state

by literature and might indicate that our model is suitable for drug's test. However, further experiments would be necessary to support this hypothesis.

With regards to *Junb*, it belongs to AP-1 transcription factor and exerts a critical role for TGFβ-induced invasion and breast cancer progression (SUNDQVIST et al., 2018). Their expression was upregulated in MDA-MB-231 cell lines (SHI; YE; LONG, 2017) and in circulating tumor cells, which was associated with poor prognosis in breast cancer (KALLERGI et al., 2019). In the data presented here, *Junb* was the most expressed gene in ^{3L}BNC Platform (**Figure 27**) which corroborates literature data.

Figure 27: GAPDH relative gene expression of *e-cadherin*, DUSP5, and *Junb* in MDA-MB-231 cell line. ^{3L}BNC Platform: 3 samples ± std. Cell culture plate: 2 samples ± std. Statistical analysis refers to the same time-point in different models of culture (3D vs 2D).

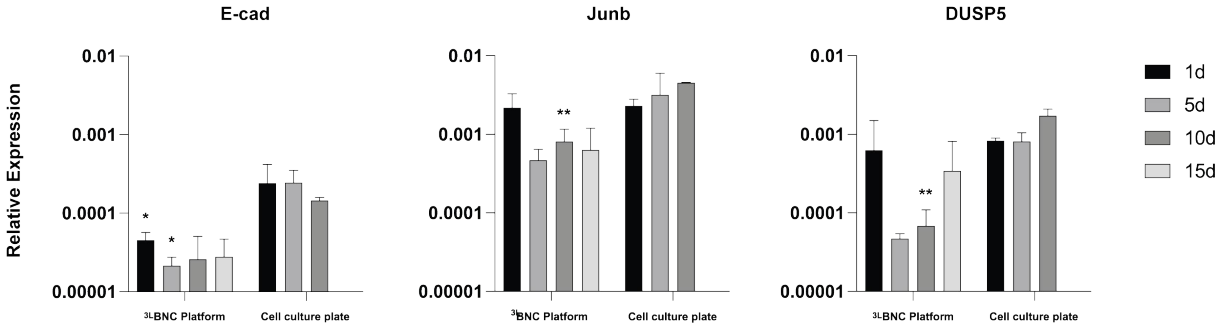

Comparing the expression of all three genes of cells cultured into ^{3L}BNC Platform, it seems they perform a similar trend to what is reported in the literature (i.e., *e-cad* < DUSP5 < *Junb*). Nonetheless, it is clear the need for improvement of gene expression analysis in the proposed 3D cell culture model since all genes of interest showed lower expression compared to cell plates, even the up-regulated *Junb*.

Conclusion

6 CONCLUSION: LIMITATIONS AND ADVANTAGES OF ^{3L}BNC PLATFORM

In respect to limitations of ^{3L}BNC Platform, it can be mentioned: a) the platform's diameter demands a high number of cells in comparison to other 3D cell culture methods, such as spheroids; b) the mode of production, although simple, requires an incubator that allows storage of Falcon-like tubes, since it was not possible to prepare the platform in plates; c) the production of individual layers is influenced by the way of closing recipients' caps; d) cell culturing inside the platforms requires injection of cells and for this reason need skilled workers; e) excessive manipulation of the platform may result in detachment of layers. Taking together, scaling-up the process of ^{3L}BNC Platform production and adopting its routinely use can be especially challenging.

Notwithstanding these drawbacks, the ^{3L}BNC Platform was successfully standardize and validated *in vitro.* It is the first time that a pristine stacked-multilayered BNC platform was successfully produced and characterized, especially in a minimal media. Different cell types were cultured but did not remain compartmentalized in our system due to technical limitations. From the best of our knowledge, it is the first time that those transparent multi-compartmentalized BNC platforms were proposed and validated *in vitro*, which make us confident of its further applicability allowing several studies of paracrine cell signaling.

Challenges and Closing Remarks

7 CHALLENGES AND CLOSING REMARKS: ADJUSTING BOAT' SAILS

Research projects are a non-linear process that requires constant adjustment according to faced situations and the discoveries we find by the way. However, "talking about research failures" is quite a taboo.

Although graduate students frequently have "bad days" and discuss their experimental failures with their lab teams, formally addressing this topic seems a shame. In fact, to make science more honest and transparent, "Negative results" journals (such as "Positively Negative" and "The Missing Pieces: A Collection of Negative; Null and Inconclusive Results", both from PlosOne) have been created.

This project is no exception. In fact, during its development, unexpected situations emerged, and results did not always come as expected. The most logical attitude was to re-think and adapt. This section lists troubles not directly related to limitations but, instead, to the frustrations related to not so well-succeeded experiments, in a very honest manner.

First, during the platform's preparation, some contamination of bacteria culture happened, which resulted in delays. Also, the manipulation of platforms to remove bacteria sometimes caused layers' detachment. Further, during transport from Brazil to Canada, an expressive number of platforms also had detached layers (pressure impacts the stability of the platforms). Altogether, these problems made the availability of samples lower than first expected and experiment priorities adjusted.

During material characterization, the plan was to perform analysis of AFM and μCT to address questions of cell-platform interaction and pore size, respectively. Nonetheless, due to unavailability of equipment, these needed to be replaced.

Still about characterization, glucose diffusivity essays presented an unexpected issue: due to the platforms' height, keeping communication of donors and acceptor chambers only through samples was challenging and requested multiple attempts to find an acceptable solution.

Another important puzzle regards confocal microscopy. Initially, the plan was to stain cells with specific markers (**Table 12**), but this idea had to be replaced. Indeed, different combinations of different primary antibodies (one for each cell type) were tested, but for all of them it was observed some crosstalk – even after following

recommended guidelines. The crosstalk also happened when samples were stained with only one antibody (such as EpCAM, for MDA-MB-231 cell line) which made analysis a very laborious process.

Finally, doing an international internship in the middle of the SARS-CoV-2 pandemic breakout was not the ideal scenario. Fortunately, an agreement between advisors and the institutions involved in this project made it possible for me to stay longer in Canada to perform further analysis. However, as expected, access to some facilities and shipment of important reagents were affected.

It is worth mentioning that many aspects of the platform must be improved to make its application more appealing to scientists. Despite these circumstances, it is possible to verify the success of this project where the production and characterization of a stacked-multilayered BNC platform was addressed, including an applicability proposal. It is hypothesized that this system can address, at least, important questions about multi-co-culture cell signaling, and drugs' tests (once it becomes possible to use patients-derived' cells for an individualized medicine). Moreover, different downstream analysis can be achieved, and we are convinced of the ^{3L}BNC Platform potential for further uses.

Table 12: Antibodies tested for cell visualization in ^{3L}BNC Platform.

Primary Antibody						Secondary Antibody			
Antibody	**Manufacturer (cat. Number)**	**Conjugated?**	**Clonality**	**Host**	**Cell target**	**Antibody**	**Host**	**Target**	**Color**
Anti-CD163	Biolegend (# 326507)	Yes	Monoclonal	Mouse	Macrophages	Alexa Fluor 647	N/A	N/A	Red
Anti-CD206	Biolegend (# 321101)	No	Monoclonal	Mouse	Macrophages	Alexa Fluor 594	Goat	Mouse	Orange
Anti-EpCAM	CellSignaling (# 5198S)	Yes	Monoclonal	Mouse	Cancer cells	Alexa Fluor 488	N/A	N/A	Green
PDGF	Abcam (# ab61219)	No	Polyclonal	Rabbit	Fibroblasts	Alexa Fluor 555	Goat	Rabbit	Orange
Anti-αSMA	GeneTex (# GTX100034)	No	Polyclonal	Rabbit	Fibroblasts	Alexa Fluor 555	Goat	Rabbit	Orange

Bibliographic references

8 BIBLIOGRAPHIC REFERENCES

(INCA), I. N. de C. J. A. G. da S. C. de P. e V. / M. da S. **Estimativa 2018: Incidência de Câncer no Brasil**. 2017. Rio de Janeiro: [s.n.], 2017. 190 p. ISBN: 9788573183627.

ABERCROMBIE, M. **Fibroblasts**. *J. clin. Path.*, [s.l.], v. 31, nº 12, p. 1–6, 1978.

ABU SAMAAN, T. M. et al. **Paclitaxel's Mechanistic and Clinical Effects on Breast Cancer**. *Biomolecules*, [s.l.], v. 9, nº 12, p. 1–22, 2019. ISSN: 2218273X, DOI: 10.3390/biom9120789.

ANDERBERG, C.; PIETRAS, K. **Cell Cycle Features: cancer-associated fibroblasts**. *Cell Cycle*, [s.l.], nº May, p. 1461–1465, 2009. ISBN: 1551-4005 (Electronic)n1551-4005 (Linking), ISSN: 1538-4101, DOI: 10.4161/cc.8.10.8557.

ANGUIANO, M. et al. **Characterization of three-dimensional cancer cell migration in mixed collagen-Matrigel scaffolds using microfluidics and image analysis**. *PLoS ONE*, [s.l.], p. 1–24, 2017. ISBN: 1111111111, DOI: 10.1371/journal.pone.0171417.

ANNABI, N. et al. **Controlling the Porosity and Microarchitecture of Hydrogels for Tissue Engineering**. *Tissue Engineering Part B-Reviews*, [s.l.], v. 16, nº 4, 2010. DOI: 10.1089/ten.teb.2009.0639.

ARAS, S.; RAZA ZAIDI, M. **TAMeless traitors: Macrophages in cancer progression and metastasis**. *British Journal of Cancer*, [s.l.], v. 117, nº 11, p. 1583–1591, 2017. ISSN: 15321827, DOI: 10.1038/bjc.2017.356.

BÄCKDAHL, H. et al. **Mechanical properties of bacterial cellulose and interactions with smooth muscle cells**. *Biomaterials*, [s.l.], v. 27, nº 9, p. 2141–2149, 2006. ISSN: 01429612, DOI: 10.1016/j.biomaterials.2005.10.026.

BAHCECIOGLU, G. et al. **Breast cancer models: Engineering the tumor microenvironment**. *Acta Biomaterialia*, [s.l.], v. 106, p. 1–21, 2020. ISSN: 18787568, DOI: 10.1016/j.actbio.2020.02.006.

BALKWILL, F. R.; CAPASSO, M.; HAGEMANN, T. **The tumor microenvironment at a glance**. *Journal of Cell Science*, [s.l.], v. 125, nº 23, p. 5591–5596, 2012. ISSN: 00219533, DOI: 10.1242/jcs.116392.

BARCELLOS-DE-SOUZA, P. et al. **Mesenchymal Stem Cells are Recruited and Activated into Carcinoma-Associated Fibroblasts by Prostate Cancer Microenvironment-Derived TGF-beta1**. *Stem Cells*, [s.l.], v. 34, p. 2536–2547, 2016. ISBN: 1066-5099.

BARECHE, Y. et al. **Unravelling triple-negative breast cancer molecular heterogeneity using an integrative multiomic analysis**. *Annals of Oncology*, [s.l.], v. 29, nº 4, p. 895–902, 2018. ISSN: 15698041, DOI: 10.1093/annonc/mdy024.

BARONI, S. et al. **Exosome-mediated delivery of miR-9 induces cancer-Associated fibroblast-like properties in human breast fibroblasts**. *Cell Death and Disease*, [s.l.], v. 7, nº 7, p. 1–9, 2016. ISSN: 20414889, DOI: 10.1038/cddis.2016.224.

BARTOSCHEK, M. et al. **Spatially and functionally distinct subclasses of breast cancer-associated fibroblasts revealed by single cell RNA sequencing**.

Nature Communications, [s.l.], v. 9, nº 1, 2018. ISSN: 20411723, DOI: 10.1038/s41467-018-07582-3.

BEACHLEY, V. Z. et al. **Tissue matrix arrays for high-throughput screening and systems analysis of cell function**. *Nature Methods*, [s.l.], nº October, 2015. DOI: 10.1038/nmeth.3619.

BENNER, B. et al. **Generation of monocyte-derived tumor-associated macrophages using tumor-conditioned media provides a novel method to study tumor-associated macrophages in vitro**. *Journal for ImmunoTherapy of Cancer*, [s.l.], v. 7, nº 1, p. 1–14, 2019. ISSN: 20511426, DOI: 10.1186/s40425-019-0622-0.

BENTON, G. et al. **Multiple uses of basement membrane-like matrix (BME/Matrigel) in vitro and in vivo with cancer cells**. *International Journal of Cancer*, [s.l.], v. 128, p. 1751–1757, 2011. DOI: 10.1002/ijc.25781.

BERTI, F. V. et al. **Nanofiber density determines endothelial cell behavior on hydrogel matrix**. *Materials Science & Engineering C*, [s.l.], v. 33, nº 8, p. 4684–4691, 2013a. ISSN: 0928-4931, DOI: 10.1016/j.msec.2013.07.029.

BERTI, F. V. **Desenvolvimento de Estruturas Vasculares Endotelizadas em Scaffolds de Celulose Bacteriana**. - Universidade Federal de Santa Catarina, 2012.

_____. **Nanofiber density determines endothelial cell behavior on hydrogel matrix**. *Materials Science and Engineering: C*, [s.l.], v. 33, nº 8, p. 4684–4691, 2013b. ISSN: 0928-4931.

BIELECKA, Z. F. et al. **Three-dimensional cell culture model utilization in cancer stem cell research**. *Biological Reviews*, [s.l.], v. 92, nº 3, p. 1505–1520, 2017. ISBN: 0006-3231, ISSN: 1469185X, DOI: 10.1111/brv.12293.

BIRKHEUR, S. et al. **Enhancement of fibroblast growing on the mannosylated surface of cellulose membranes**. *Materials Science & Engineering C*, [s.l.], v. 77, p. 672–679, 2017. ISSN: 0928-4931, DOI: 10.1016/j.msec.2017.04.006.

BONNANS, C.; CHOU, J.; WERB, Z. **Remodelling the extracellular matrix in development and disease**. *Nature Reviews Molecular Cell Biology*, [s.l.], v. 15, nº 12, p. 786–801, 2014. ISSN: 1471-0072, DOI: 10.1038/nrm3904.

BRESLIN, S.; O'DRISCOLL, L. **Three-dimensional cell culture: the missing link in drug discovery**. *Drug Discov Today*, [s.l.], v. 18, nº 5–6, p. 240–249, 2013. ISBN: 1359-6446, DOI: 10.1016/j.drudis.2012.10.003.

BROWN, A. J. **On an acetic ferment which forms cellulose**. *Journal of the Chemical Society, Transactions*, [s.l.], v. 49, nº 432, p. 432–439, 1988. ISSN: 03681645, DOI: 10.1039/CT8864900432.

BUDHIONO, A. et al. **Kinetic aspects of bacterial cellulose formation in nata-de-coco culture system**. *Carbohydrate Polymers*, [s.l.], v. 40, nº 2, p. 137–143, 1999. ISSN: 01448617, DOI: 10.1016/S0144-8617(99)00050-8.

BURRELL, R. A. et al. **The causes and consequences of genetic heterogeneity in cancer evolution**. *Nature*, [s.l.], v. 501, nº 19 September 2013, p. 338–345, 2013. DOI: 10.1038/nature12625.

CAMARGO, S. et al. **Paracrine signaling from a three-dimensional model of bladder carcinoma and from normal bladder switch the phenotype of stromal fibroblasts**. *Cancers*, [s.l.], v. 13, nº 12, p. 1–15, 2021. ISSN: 20726694, DOI: 10.3390/cancers13122972.

CARMONA-FONTAINE, C. et al. **Metabolic origins of spatial organization in the tumor microenvironment**. *Proceedings of the National Academy of Sciences of the United States of America*, [s.l.], v. 114, nº 11, p. 2934–2939, 2017. ISSN: 10916490, DOI: 10.1073/pnas.1700600114.

CASSETTA, L. et al. **Human Tumor-Associated Macrophage and Monocyte Transcriptional Landscapes Reveal Cancer-Specific Reprogramming, Biomarkers, and Therapeutic Targets**. *Cancer Cell*, [s.l.], v. 35, nº 4, p. 588-602.e10, 2019. ISSN: 18783686, DOI: 10.1016/j.ccell.2019.02.009.

CASWELL, D. R.; SWANTON, C. **The role of tumour heterogeneity and clonal cooperativity in metastasis, immune evasion and clinical outcome**. *BMC Medicine*, [s.l.], v. 15, nº 1, p. 1–9, 2017. ISSN: 17417015, DOI: 10.1186/s12916-017-0900-y.

CATHCART, J.; PULKOSKI-GROSS, A.; CAO, J. **Targeting matrix metalloproteinases in cancer: Bringing new life to old ideas**. *Genes and Diseases*, [s.l.], v. 2, nº 1, p. 26–34, 2015. ISSN: 23523042, DOI: 10.1016/j.gendis.2014.12.002.

COHEN, N. et al. **Fibroblasts drive an immunosuppressive and growth-promoting microenvironment in breast cancer via secretion of Chitinase 3-like 1**. *Oncogene*, [s.l.], v. 36, nº 31, p. 4457–4468, 2017. ISSN: 14765594, DOI: 10.1038/onc.2017.65.

COLOMBO, E.; CATTANEO, M. G. **Multicellular 3d models to study tumour-stroma interactions**. *International Journal of Molecular Sciences*, [s.l.], v. 22, nº 4, p. 1–19, 2021. ISSN: 14220067, DOI: 10.3390/ijms22041633.

COSTEA, D. E. et al. **Identification of two distinct carcinoma-associated fibroblast subtypes with differential tumor-promoting abilities in oral squamous cell carcinoma**. *Cancer Research*, [s.l.], v. 73, nº 13, p. 3888–3901, 2013. ISSN: 00085472, DOI: 10.1158/0008-5472.CAN-12-4150.

COURTENAY, J. C.; SCOTT, J. **Recent Advances in Modified Cellulose for Tissue Culture Applications**. *Molecules*, [s.l.], v. 23, nº March, 2018. DOI: 10.3390/molecules23030654.

COX, G.; O'BYRNE, K. J. **Matrix metalloproteinases and cancer**. *Anticancer Research*, [s.l.], v. 21, nº 6 B, p. 4207–4219, 2001. ISSN: 02507005.

COX, T. R.; ERLER, J. T. **Remodeling and homeostasis of the extracellular matrix: Implications for fibrotic diseases and cancer**. *DMM Disease Models and Mechanisms*, [s.l.], v. 4, nº 2, p. 165–178, 2011. ISSN: 17548403, DOI: 10.1242/dmm.004077.

CRUSZ, S. M.; BALKWILL, F. R. **Inflammation and cancer: Advances and new agents**. *Nature Reviews Clinical Oncology*, [s.l.], v. 12, nº 10, p. 584–596, 2015. ISSN: 17594782, DOI: 10.1038/nrclinonc.2015.105.

CUI, K. et al. **Distinct migratory properties of M1, M2, and resident**

macrophages are regulated by αdβ2and αmβ2integrin-mediated adhesion. *Frontiers in Immunology*, [s.l.], v. 9, nº NOV, p. 1–14, 2018. ISSN: 16643224, DOI: 10.3389/fimmu.2018.02650.

CZAJA, W. et al. **Microbial cellulose — the natural power to heal wounds**. *Biomaterials*, [s.l.], v. 27, p. 145–151, 2006. DOI: 10.1016/j.biomaterials.2005.07.035.

DAS, A. et al. **MMP proteolytic activity regulates cancer invasiveness by modulating integrins**. *Scientific Reports*, [s.l.], v. 7, nº 1, p. 1–13, 2017. ISBN: 4159801714, ISSN: 20452322, DOI: 10.1038/s41598-017-14340-w.

DAVIS, M. J. et al. **Macrophage M1 / M2 Polarization Dynamically Adapts to Changes in Cytokine Microenvironments in Cryptococcus neoformans Infection**. *MBio*, [s.l.], v. 4, nº 3, p. 1–10, 2013. ISBN: 2150-7511 (Electronic), ISSN: 2150-7511, DOI: 10.1128/mBio.00264-13.Editor.

DELNERO, P.; SONG, Y. H.; FISCHBACH, C. **Microengineered tumor models: insights & opportunities from a physical sciences-oncology perspective**. *Biomed Microdevices*, [s.l.], v. 15, p. 583–593, 2013. DOI: 10.1007/s10544-013-9763-y.

DEPTUŁA, P. et al. **Tissue Rheology as a Possible Complementary Procedure to Advance Histological Diagnosis of Colon Cancer**. *ACS Biomaterials Science and Engineering*, [s.l.], v. 6, nº 10, p. 5620–5631, 2020. ISSN: 23739878, DOI: 10.1021/acsbiomaterials.0c00975.

DIMANCHE-BOITREL, M. T. et al. **In vivo and in vitro invasiveness of a rat colon-cancer cell line maintaining E-cadherin expression: An enhancing role of tumor-associated myofibroblasts**. *International Journal of Cancer*, [s.l.], v. 56, nº 4, p. 512–521, 1994. ISSN: 10970215, DOI: 10.1002/ijc.2910560410.

DIREKZE, N. C. et al. **Bone marrow contribution to tumor-associated myofibroblasts and fibroblasts**. *Cancer Research*, [s.l.], v. 64, nº 23, p. 8492–8495, 2004. ISSN: 00085472, DOI: 10.1158/0008-5472.CAN-04-1708.

DUDA, D. G. et al. **Malignant cells facilitate lung metastasis by bringing their own soil**. *Proceedings of the National Academy of Sciences of the United States of America*, [s.l.], v. 107, nº 50, p. 21677–21682, 2010. ISSN: 00278424, DOI: 10.1073/pnas.1016234107.

DULUC, D. et al. **Interferon-γ reverses the immunosuppressive and protumoral properties and prevents the generation of human tumor-associated macrophages**. *International Journal of Cancer*, [s.l.], v. 125, nº 2, p. 367–373, 2009. ISSN: 00207136, DOI: 10.1002/ijc.24401.

DVORAK, H. F. **Tumors: wounds that do not heal. Similarities between tumor stroma generation and wound healing.** *The New England journal of medicine*, [s.l.], v. 315, nº 26, p. 1650–9, 1986. ISSN: 0028-4793, DOI: 10.1056/NEJM198612253152606.

DVORAK, K. M. et al. **Carcinoma associated fibroblasts (CAFs) promote breast cancer motility by suppressing mammalian Diaphanous-related formin-2 (mDia2)**. *PLoS ONE*, [s.l.], v. 13, nº 3, p. 1–22, 2018. ISBN: 1111111111, ISSN: 19326203, DOI: 10.1371/journal.pone.0195278.

ELIAS, A. D. **Triple-negative breast cancer: A short review**. *American Journal of Clinical Oncology: Cancer Clinical Trials*, [s.l.], v. 33, nº 6, p. 637–645, 2010. ISSN: 02773732, DOI: 10.1097/COC.0b013e3181b8afcf.

FALLICA, B. et al. **Alteration of Cellular Behavior and Response to PI3K Pathway Inhibition by Culture in 3D Collagen Gels**. *PLoS ONE*, [s.l.], v. 7, nº 10, p. 1–11, 2012. ISSN: 19326203, DOI: 10.1371/journal.pone.0048024.

FARHANGFAR, C. J. et al. **The impact of tumor heterogeneity on patient treatment decisions**. *Clinical Chemistry*, [s.l.], v. 59, nº 1, p. 38–40, 2013. ISSN: 00099147, DOI: 10.1373/clinchem.2012.194712.

FARMAKI, E. et al. **A CCL8 gradient drives breast cancer cell dissemination**. *Oncogene*, [s.l.], v. 35, nº 49, p. 6309–6318, 2016. ISSN: 14765594, DOI: 10.1038/onc.2016.161.

FERNANDEZ-GARCIA, B. et al. **Expression and prognostic significance of fibronectin and matrix metalloproteases in breast cancer metastasis**. *Histopathology*, [s.l.], v. 64, nº 4, p. 512–522, 2014. ISSN: 03090167, DOI: 10.1111/his.12300.

FERREIRA, L. P.; GASPAR, V. M.; MANO, J. F. **Bioinstructive microparticles for self-assembly of mesenchymal stem Cell-3D tumor spheroids**. *Biomaterials*, [s.l.], v. 185, p. 155–173, 2018. DOI: 10.1016/j.biomaterials.2018.09.007.

FLEIGE, S.; PFAFFL, M. W. **RNA integrity and the effect on the real-time qRT-PCR performance**. *Molecular Aspects of Medicine*, [s.l.], v. 27, nº 2–3, p. 126–139, 2006. ISSN: 00982997, DOI: 10.1016/j.mam.2005.12.003.

FORNIER, M.; FUMOLEAU, P. **The paradox of triple negative breast cancer: Novel approaches to treatment**. *Breast Journal*, [s.l.], v. 18, nº 1, p. 41–51, 2012. ISSN: 1075122X, DOI: 10.1111/j.1524-4741.2011.01175.x.

FU, L. et al. **Skin tissue repair materials from bacterial cellulose by a multilayer fermentation method**. *Journal of Materials Chemistry*, [s.l.], v. 22, p. 12349–12357, 2012. DOI: 10.1039/c2jm00134a.

GAMA, M.; GATENHOLM, P.; KLEMM, D. (Dieter). **Bacterial NanoCellulose : a sophisticated multifunctional material**. 2012. CRC Press. [s.l.]: CRC Press, 2012. 309 p. ISBN: 9781439869925.

GAO, Q. et al. **Heterotypic CAF-tumor spheroids promote early peritoneal metastatis of ovarian cancer**. *Journal of Experimental Medicine*, [s.l.], v. 216, nº 3, p. 688–703, 2019. ISSN: 15409538, DOI: 10.1084/jem.20180765.

GEFEN, A.; DILMONEY, B. **Mechanics of the normal woman's breast**. *Technology and Health Care*, [s.l.], v. 15, nº 4, p. 259–271, 2007. ISSN: 09287329, DOI: 10.3233/thc-2007-15404.

GEIGER, F. et al. **Fiber stiffness, pore size and adhesion control migratory phenotype of MDA-MB-231 cells in collagen gels**. *PLoS ONE*, [s.l.], v. 14, nº 11, p. 1–13, 2019. ISBN: 1111111111, ISSN: 19326203, DOI: 10.1371/journal.pone.0225215.

GENIN, M. et al. **M1 and M2 macrophages derived from THP-1 cells differentially modulate the response of cancer cells to etoposide**. *BMC Cancer*,

[s.l.], v. 15, nº 1, p. 1–14, 2015. ISSN: 14712407, DOI: 10.1186/s12885-015-1546-9.

GEORGIEVA, P. B. et al. **Long-lived tumor-associated macrophages in glioma**. *Neuro-Oncology Advances*, [s.l.], v. 2, nº 1, p. 1–12, 2020. DOI: 10.1093/noajnl/vdaa127.

GILMORE, A. C. et al. **An in vitro tumorigenesis model based on live-cell-generated oxygen and nutrient gradients**. *Communications Biology*, [s.l.], v. 4, nº 1, p. 1–13, 2021. ISBN: 4200302101, ISSN: 23993642, DOI: 10.1038/s42003-021-01954-0.

GINESTRA, P.; PANDINI, S.; CERETTI, E. **Hybrid multi-layered scaffolds produced via grain extrusion and electrospinning for 3D cell culture tests**. *Rapid Prototyping Journal*, [s.l.], v. 26, nº 3, p. 593–602, 2019. ISSN: 13552546, DOI: 10.1108/RPJ-03-2019-0079.

GINZBERG, M. B.; KAFRI, R.; KIRSCHNER, M. **On being the right (cell) size**. *Science*, [s.l.], v. 348, nº 6236, 2015.

GODINHO, J. F. et al. **Incorporation of Aloe vera extracts into nanocellulose during biosynthesis**. *Cellulose*, [s.l.], v. 23, p. 545–555, 2016. DOI: 10.1007/s10570-015-0844-3.

GONÇALVES, H. et al. **Survival Study of Triple-Negative and Non–Triple-Negative Breast Cancer in a Brazilian Cohort**. *Clinical Medicine Insights: Oncology*, [s.l.], v. 12, 2018. ISSN: 11795549, DOI: 10.1177/1179554918790563.

GONZALEZ, H.; HAGERLING, C.; WERB, Z. **Roles of the immune system in cancer: From tumor initiation to metastatic progression**. *Genes and Development*, [s.l.], v. 32, nº 19–20, p. 1267–1284, 2018. ISSN: 15495477, DOI: 10.1101/GAD.314617.118.

GREAVES, M.; MALEY, C. C. **Clonal evolution in cancer**. *Nature*, [s.l.], v. 481, nº 7381, p. 306–313, 2012. ISSN: 00280836, DOI: 10.1038/nature10762.

GRETEN, F. R.; GRIVENNIKOV, S. I. **Inflammation and Cancer: Triggers, Mechanisms, and Consequences**. *Immunity*, [s.l.], v. 51, nº 1, p. 27–41, 2019. ISSN: 10747613, DOI: 10.1016/j.immuni.2019.06.025.

GRZYWA, T. M.; PASKAL, W.; WŁODARSKI, P. K. **Intratumor and Intertumor Heterogeneity in Melanoma**. *Translational Oncology*, [s.l.], v. 10, nº 6, p. 956–975, 2017. ISSN: 19365233, DOI: 10.1016/j.tranon.2017.09.007.

GUIMARÃES, C. F. et al. **The stiffness of living tissues and its implications for tissue engineering**. *Nature Reviews Materials*, [s.l.], v. 5, nº 5, p. 351–370, 2020. ISSN: 20588437, DOI: 10.1038/s41578-019-0169-1.

GUNAYDIN, G. **CAFs Interacting With TAMs in Tumor Microenvironment to Enhance Tumorigenesis and Immune Evasion**. *Frontiers in Oncology*, [s.l.], v. 11, nº July, p. 1–29, 2021. ISSN: 2234943X, DOI: 10.3389/fonc.2021.668349.

HAN, S. J.; KWON, S.; KIM, K. S. **Challenges of applying multicellular tumor spheroids in preclinical phase**. *Cancer Cell International*, [s.l.], v. 21, nº 1, p. 1–19, 2021. ISSN: 14752867, DOI: 10.1186/s12935-021-01853-8.

HANAHAN, D.; WEINBERG, R. A. **The hallmarks of cancer**. *Cell*, [s.l.], v. 10,

p. 57–70, 2000. ISSN: 15685888, DOI: 10.1007/BF03091804.

HANAHAN, D.; WEINBERG, R. A. **Hallmarks of cancer: The next generation**. *Cell*, [s.l.], v. 144, nº 5, p. 646–674, 2011a. ISSN: 00928674, DOI: 10.1016/j.cell.2011.02.013.

HANAHAN, D.; WEINBERG, R. A. **Hallmarks of Cancer: The Next Generation**. *Cell*, [s.l.], v. 144, nº 5, p. 646–674, 2011b. ISSN: 0092-8674, DOI: 10.1016/j.cell.2011.02.013.

HE, Y. et al. **Classification of triple-negative breast cancers based on Immunogenomic profiling**. *Journal of Experimental and Clinical Cancer Research*, [s.l.], v. 37, nº 1, p. 1–13, 2018. ISSN: 17569966, DOI: 10.1186/s13046-018-1002-1.

HESTRIN, S.; SCHRAMM, M. **Synthesis of cellulose by Acetobacter xylinum. II. Preparation of freeze-dried cells capable of polymerizing glucose to cellulose.** *The Biochemical journal*, [s.l.], v. 58, nº 2, p. 345–352, 1954. ISSN: 02646021, DOI: 10.1042/bj0580345.

HORNING, J. L. et al. **3-D Tumor Model for In Vitro Evaluation of Anticancer Drugs**. *Molecular Pharmaceutics*, [s.l.], v. 5, nº 5, p. 849–862, 2008.

HU, Y. et al. **Engineering of porous bacterial cellulose toward human fi broblasts ingrowth for tissue engineering**. *Journal of Materials Research*, [s.l.], v. 29, nº 22, 2014. DOI: 10.1557/jmr.2014.315.

HUANG, G. et al. **Functional and Biomimetic Materials for Engineering of the Three-Dimensional Cell Microenvironment**. *Chemical Reviews*, [s.l.], v. 117, nº 20, p. 12764–12850, 2017. ISSN: 15206890, DOI: 10.1021/acs.chemrev.7b00094.

HUGHES, C. S.; POSTOVIT, L. M.; LAJOIE, G. A. **Matrigel : A complex protein mixture required for optimal growth of cell culture**. *Proteomics*, [s.l.], v. 10, p. 1886–1890, 2010. DOI: 10.1002/pmic.200900758.

IKARI, R. et al. **Differences in the central energy metabolism of cancer cells between conventional 2d and novel 3d culture systems**. *International Journal of Molecular Sciences*, [s.l.], v. 22, nº 4, p. 1–13, 2021. ISSN: 14220067, DOI: 10.3390/ijms22041805.

IMAMURA, Y. et al. **Comparison of 2D- and 3D-culture models as drug-testing platforms in breast cancer**. *Oncology Reports*, [s.l.], v. 33, p. 1837–1843, 2015. DOI: 10.3892/or.2015.3767.

INNALA, M. et al. **3D Culturing and differentiation of SH-SY5Y neuroblastoma cells on bacterial nanocellulose scaffolds**. *Artificial Cells, Nanomedicine and Biotechnology*, [s.l.], nº April, p. 1–7, 2013. DOI: 10.3109/21691401.2013.821410.

INSUA-RODRÍGUEZ, J.; OSKARSSON, T. **The extracellular matrix in breast cancer**. *Advanced Drug Delivery Reviews*, [s.l.], v. 97, p. 41–55, 2016. ISSN: 18728294, DOI: 10.1016/j.addr.2015.12.017.

ISHII, G. et al. **Bone-marrow-derived myofibroblasts contribute to the cancer-induced stromal reaction**. *Biochemical and Biophysical Research Communications*, [s.l.], v. 309, nº 1, p. 232–240, 2003. ISSN: 0006291X, DOI: 10.1016/S0006-291X(03)01544-4.

JACEK, P. et al. **Scaffolds for chondrogenic cells cultivation prepared from bacterial cellulose with relaxed fibers structure induced genetically**. *Nanomaterials*, [s.l.], v. 8, nº 12, 2018. ISSN: 20794991, DOI: 10.3390/NANO8121066.

_____. **Molecular aspects of bacterial nanocellulose biosynthesis**. *Microbial Biotechnology*, [s.l.], v. 12, nº 4, p. 633–649, 2019. ISSN: 17517915, DOI: 10.1111/1751-7915.13386.

JIANG, Y. et al. **Assessing intratumor heterogeneity and tracking longitudinal and spatial clonal evolutionary history by next-generation sequencing**. *Proceedings of the National Academy of Sciences of the United States of America*, [s.l.], v. 113, nº 37, p. E5528–E5537, 2016. DOI: 10.1073/pnas.1522203113.

JOHANSSON, A. C. et al. **Cancer-associated fibroblasts induce matrix metalloproteinase-mediated cetuximab resistance in head and neck squamous cell carcinoma cells**. *Molecular Cancer Research*, [s.l.], v. 10, nº 9, p. 1158–1168, 2012. ISSN: 15417786, DOI: 10.1158/1541-7786.MCR-12-0030.

JOTZU, C. et al. **Adipose tissue derived stem cells differentiate into carcinoma-associated fibroblast-like cells under the influence of tumor derived factors**. *Cellular Oncology*, [s.l.], v. 33, nº 1, p. 61–79, 2010. ISSN: 22113428, DOI: 10.1007/s13402-011-0012-1.

JOZALA, A. F. et al. **Bacterial nanocellulose production and application: a 10-year overview**. *Applied Microbiology and Biotechnology*, [s.l.], v. 100, nº 5, p. 2063–2072, 2016. ISSN: 1432-0614.

KALLERGI, G. et al. **The prognostic value of JUNB-positive CTCs in metastatic breast cancer: From bioinformatics to phenotypic characterization**. *Breast Cancer Research*, [s.l.], v. 21, nº 1, p. 1–13, 2019. ISBN: 1305801911, ISSN: 1465542X, DOI: 10.1186/s13058-019-1166-4.

KALLURI, R. **The biology and function of fibroblasts in cancer**. *Nature Reviews Cancer*, [s.l.], v. 16, nº 9, p. 582–598, 2016. ISSN: 14741768, DOI: 10.1038/nrc.2016.73.

KALLURI, R.; ZEISBERG, M. **Fibroblasts in cancer**. *Nature Reviews Cancer*, [s.l.], v. 6, nº 5, p. 392–401, 2006. ISSN: 1474175X, DOI: 10.1038/nrc1877.

KAMINKA, K. et al. **The role of the cell – cell interactions in cancer progression Cancer cell – fibroblast interaction in cancer progression**. *Journal of Cellular and Molecular Medicine*, [s.l.], v. 19, nº 2, p. 283–296, 2015. DOI: 10.1111/jcmm.12408.

KAPAŁCZYŃSKA, M. et al. **2D and 3D cell cultures – a comparison of different types of cancer cell cultures**. *Archives of Medical Science*, [s.l.], v. 14, nº 4, p. 910–919, 2018. ISSN: 18969151, DOI: 10.5114/aoms.2016.63743.

KASHANI, A. S.; PACKIRISAMY, M. **Cancer cells optimize elasticity for efficient migration: Migratory index**. *Royal Society Open Science*, [s.l.], v. 7, nº 10, 2020. ISSN: 20545703, DOI: 10.1098/rsos.200747.

KASHIWAGI, S. et al. **Significance of E-cadherin expression in triple-negative breast cancer**. *British Journal of Cancer*, [s.l.], v. 103, nº 2, p. 249–255,

2010. ISSN: 00070920, DOI: 10.1038/sj.bjc.6605735.

KATT, M. E. et al. **In Vitro Tumor Models : Advantages , Disadvantages , variables , and Selecting the Right Platform**. *Frontiers in Bioengineering and Biotechnology*, [s.l.], v. 4, nº February, p. 1–14, 2016. DOI: 10.3389/fbioe.2016.00012.

KELLY, P. M. A. et al. **Macrophages in human breast disease: A quantitative immunohistochemical study**. *British Journal of Cancer*, [s.l.], v. 57, nº 2, p. 174–177, 1988. ISSN: 15321827, DOI: 10.1038/bjc.1988.36.

KLEMM, D. et al. **Bacterial synthesized cellulose - Artificial blood vessels for microsurgery**. *Progress in Polymer Science (Oxford)*, [s.l.], v. 26, nº 9, p. 1561–1603, 2001. ISSN: 00796700, DOI: 10.1016/S0079-6700(01)00021-1.

KONDAGESKI, C. **Compósito Polimérico de nanocelulose bacteriana e poli(ácido L-lático-co-trimetileno carbonato) para aplicações biomédicas**. 134 p. - Universidade Federal de Santa Catarina, 2016.

KULAR, J. K.; BASU, S.; SHARMA, R. I. **The extracellular matrix: Structure, composition, age-related differences, tools for analysis and applications for tissue engineering**. *Journal of Tissue Engineering*, [s.l.], v. 5, 2014. DOI: 10.1177/2041731414557112.

KWA, M. Q.; HERUM, K. M.; BRAKEBUSCH, C. **Cancer-associated fibroblasts: how do they contribute to metastasis?** *Clinical and Experimental Metastasis*, [s.l.], v. 36, nº 2, p. 71–86, 2019. ISBN: 1058501909, ISSN: 15737276, DOI: 10.1007/s10585-019-09959-0.

LAGIES, S. et al. **Cells grown in three-dimensional spheroids mirror in vivo metabolic response of epithelial cells**. *Communications Biology*, [s.l.], v. 3, nº 1, 2020. ISSN: 23993642, DOI: 10.1038/s42003-020-0973-6.

LAN, X. et al. **Dental pulp stem cells: An attractive alternative for cell therapy in ischemic stroke**. *Frontiers in Neurology*, [s.l.], v. 10, nº JUL, p. 1–10, 2019. ISSN: 16642295, DOI: 10.3389/fneur.2019.00824.

LEBLEU, V. S.; KALLURI, R. **A peek into cancer-associated fibroblasts: Origins, functions and translational impact**. *DMM Disease Models and Mechanisms*, [s.l.], v. 11, nº 4, p. 1–9, 2018. ISBN: 0000000221, ISSN: 17548411, DOI: 10.1242/dmm.029447.

LEHMANN, B. D. et al. **Identification of human triple-negative breast cancer subtypes and preclinical models for selection of targeted therapies**. *Journal of Clinical Investigation*, [s.l.], v. 121, nº 7, p. 2750–2767, 2011. DOI: 10.1172/JCI45014.2750.

LIEN, S.; KO, L.; HUANG, T. **Effect of pore size on ECM secretion and cell growth in gelatin scaffold for articular cartilage tissue engineering**. *Acta Biomaterialia*, [s.l.], v. 5, nº 2, p. 670–679, 2009. ISSN: 1742-7061, DOI: 10.1016/j.actbio.2008.09.020.

LIN, N.; DUFRESNE, A. **Nanocellulose in biomedicine: Current status and future prospect**. *EUROPEAN POLYMER JOURNAL*, [s.l.], v. 59, p. 302–325, 2014. ISSN: 0014-3057, DOI: 10.1016/j.eurpolymj.2014.07.025.

LITTLE, A. C. et al. **IL-4/IL-13 stimulated macrophages enhance breast**

cancer invasion via rho-GTPase regulation of synergistic VEGF/CCL-18 signaling. *Frontiers in Oncology*, [s.l.], v. 9, nº MAY, p. 1–13, 2019. ISSN: 2234943X, DOI: 10.3389/fonc.2019.00456.

LITTLEPAGE, L. E.; EGEBLAD, M.; WERB, Z. **Coevolution of cancer and stromal cellular responses**. *Cancer Cell*, [s.l.], v. 7, nº 6, p. 499–500, 2005. ISSN: 15356108, DOI: 10.1016/j.ccr.2005.05.019.

LIU, T. et al. **The suppression of DUSP5 expression correlates with paclitaxel resistance and poor prognosis in basal-like breast cancer**. *International Journal of Medical Sciences*, [s.l.], v. 15, nº 7, p. 738–747, 2018. ISSN: 14491907, DOI: 10.7150/ijms.24981.

LIU, Y. N. et al. **Regulatory mechanisms controlling human E-cadherin gene expression**. *Oncogene*, [s.l.], v. 24, nº 56, p. 8277–8290, 2005. ISSN: 09509232, DOI: 10.1038/sj.onc.1208991.

LOH, Q. L.; CHOONG, C. **Three-dimensional scaffolds for tissue engineering applications: Role of porosity and pore size**. *Tissue Engineering - Part B: Reviews*, [s.l.], v. 19, nº 6, p. 485–502, 2013. ISSN: 19373368, DOI: 10.1089/ten.teb.2012.0437.

LOVITT, C. J.; SHELPER, T. B.; AVERY, V. M. **Doxorubicin resistance in breast cancer cells is mediated by extracellular matrix proteins**. *BMC Cancer*, [s.l.], p. 1–11, 2018. DOI: 10.1186/s12885-017-3953-6.

LUCA, A. C. et al. **Impact of the 3D Microenvironment on Phenotype, Gene Expression, and EGFR Inhibition of Colorectal Cancer Cell Lines**. *PLoS ONE*, [s.l.], v. 8, nº 3, 2013. ISSN: 19326203, DOI: 10.1371/journal.pone.0059689.

LUND, M. E. et al. **The choice of phorbol 12-myristate 13-acetate differentiation protocol influences the response of THP-1 macrophages to a pro-inflammatory stimulus**. *Journal of Immunological Methods*, [s.l.], v. 430, p. 64–70, 2016. ISSN: 18727905, DOI: 10.1016/j.jim.2016.01.012.

LYSSIOTIS, C. A.; KIMMELMAN, A. C. **Metabolic Interactions in the Tumor Microenvironment**. *Physiology & behavior*, [s.l.], v. 27, nº 11, p. 863–875, 2017. DOI: 10.1016/j.tcb.2017.06.003.

MA, L. et al. **MiR-9, a MYC/MYCN-activated microRNA, regulates E-cadherin and cancer metastasis**. *Nature Cell Biology*, [s.l.], v. 12, nº 3, p. 247–256, 2010. ISSN: 14657392, DOI: 10.1038/ncb2024.

MARTINCORENA, I. et al. **Universal Patterns of Selection in Cancer and Somatic Tissues**. *Cell*, [s.l.], v. 171, nº 5, p. 1029-1041.e21, 2017. ISSN: 10974172, DOI: 10.1016/j.cell.2017.09.042.

MARTÍNEZ ÁVILA, H. et al. **Novel bilayer bacterial nanocellulose scaffold supports neocartilage formation invitro and invivo**. *Biomaterials*, [s.l.], v. 44, p. 122–133, 2015. ISSN: 18785905, DOI: 10.1016/j.biomaterials.2014.12.025.

MASAOKA, S.; OHE, T.; SAKOTA, N. **Production of cellulose from glucose by Acetobacter xylinum**. *Journal of Fermentation and Bioengineering*, [s.l.], v. 75, nº 1, p. 18–22, 1993. ISSN: 0922338X, DOI: 10.1016/0922-338X(93)90171-4.

MATSIKO, A.; GLEESON, J. P.; O'BRIEN, F. J. **Scaffold mean pore size**

influences mesenchymal stem cell chondrogenic differentiation and matrix deposition. *Tissue Engineering - Part A*, [s.l.], v. 21, nº 3–4, p. 486–497, 2015. ISSN: 1937335X, DOI: 10.1089/ten.tea.2013.0545.

MATSUTANI, M. et al. **Adaptive mutation related to cellulose producibility in Komagataeibacter medellinensis (Gluconacetobacter xylinus) NBRC 3288**. *Applied Microbiology and Biotechnology*, [s.l.], v. 99, nº 17, p. 7229–7240, 2015. ISSN: 14320614, DOI: 10.1007/s00253-015-6598-x.

MCCARTHY, J. B.; EL-ASHRY, D.; TURLEY, E. A. **Hyaluronan, cancer-associated fibroblasts and the tumor microenvironment in malignant progression**. *Frontiers in Cell and Developmental Biology*, [s.l.], v. 6, nº MAY, p. 1–13, 2018. ISSN: 2296634X, DOI: 10.3389/fcell.2018.00048.

MELISSARIDOU, S. et al. **The effect of 2D and 3D cell cultures on treatment response, EMT profile and stem cell features in head and neck cancer**. *Cancer Cell International*, [s.l.], p. 1–10, 2019. ISSN: 1475-2867, DOI: 10.1186/s12935-019-0733-1.

MISHRA. **Carcinoma associated fibroblast like differentiation of human MSC**. *Cancer Research*, [s.l.], v. 68, nº 11, p. 4331–4339, 2008. DOI: 10.1158/0008-5472.CAN-08-0943.Carcinoma.

MISHRA, P. J. et al. **Carcinoma-associated fibroblast-like differentiation of human mesenchymal stem cells**. *Cancer Research*, [s.l.], v. 68, nº 11, p. 4331–4339, 2008. ISSN: 00085472, DOI: 10.1158/0008-5472.CAN-08-0943.

MITRA, A. K. et al. **MicroRNAs reprogram normal fibroblasts into cancer-associated fibroblasts in ovarian cancer**. *Cancer Discovery*, [s.l.], v. 2, nº 12, p. 1100–1108, 2012. ISSN: 21598274, DOI: 10.1158/2159-8290.CD-12-0206.

MÜLLER, P.; SCHIER, A. F. **Extracellular Movement of Signaling Molecules**. *Developmental Cell*, [s.l.], v. 21, nº 1, p. 145–158, 2011. ISSN: 15345807, DOI: 10.1016/j.devcel.2011.06.001.

MURATA, M. **Inflammation and cancer Environmental Health and Preventive Medicine**. *Environmental Health and Preventive Medicine*, [s.l.], v. 23, p. 50, 2018. DOI: 10.1186/s12199-018-0740-1.

MURDOCH, C.; GIANNOUDIS, A.; LEWIS, C. E. **Mechanisms regulating the recruitment of macrophages into hypoxic areas of tumors and other ischemic tissues**. *Blood*, [s.l.], v. 104, nº 8, p. 2224–2234, 2004. ISSN: 00064971, DOI: 10.1182/blood-2004-03-1109.

MURPHY, C. M.; O'BRIEN, F. J. **Understanding the effect of mean pore size on cell activity in collagen-glycosaminoglycan scaffolds**. *Cell Adhesion and Migration*, [s.l.], v. 4, nº 3, p. 377–381, 2010. ISSN: 19336926, DOI: 10.4161/cam.4.3.11747.

NA, T. Y. et al. **The functional activity of E-cadherin controls tumor cell metastasis at multiple steps**. *Proceedings of the National Academy of Sciences of the United States of America*, [s.l.], v. 117, nº 11, p. 5931–5937, 2020. ISBN: 1918167117, ISSN: 10916490, DOI: 10.1073/pnas.1918167117.

NAVIN, N. et al. **Tumour evolution inferred by single-cell sequencing**.

Nature, [s.l.], v. 472, nº 7341, p. 90–95, 2011. ISSN: 00280836, DOI: 10.1038/nature09807.

NEDELJKOVI, M.; DAMJANOVIC, A. **Mechanisms of Chemotherapy Resistance in Triple-Negative Breast Cancer—HowWe Can Rise to the Challenge**. *Cells*, [s.l.], v. 8, 2019.

NGUYEN, E. H. et al. **Versatile synthetic alternatives to Matrigel for vascular toxicity screening and stem cell expansion**. *Nature Biomedical Engineering*, [s.l.], p. 1–34, 2017. DOI: 10.6084/m9.figshare.c.3791386.

NIK-ZAINAL, S. et al. **The life history of 21 breast cancers**. *Cell*, [s.l.], v. 149, nº 5, p. 994–1007, 2012. ISSN: 10974172, DOI: 10.1016/j.cell.2012.04.023.

NOWELL, P. **The clonal evolution of Tulor Cell Populations - Nowell - 1976.pdf**. *Science*, [s.l.], v. 194, nº 4260, 1976.

O'BRIEN, F. J. et al. **The effect of pore size on cell adhesion in collagen-GAG scaffolds**. *Biomaterials*, [s.l.], v. 26, nº 4, p. 433–441, 2005. ISSN: 01429612, DOI: 10.1016/j.biomaterials.2004.02.052.

OLIVEIRA, C. R. De et al. **Bacterial Cellulose Membranes Constitute Biocompatible Biomaterials for Mesenchymal and Induced Pluripotent Stem Cell Culture and Tissue Engineering**. *Journal of Tissue Science & Engineering*, [s.l.], 2012. DOI: 10.4172/2157-7552.S11-005.

OLUMI, A. F. et al. **Carcinoma-associated fibroblasts direct tumor progression of initiated human prostatic epithelium**. *Cancer Research*, [s.l.], v. 59, nº 19, p. 5002–5011, 1999. ISSN: 00085472.

ONDER, T. T. et al. **Loss of E-cadherin promotes metastasis via multiple downstream transcriptional pathways**. *Cancer Research*, [s.l.], v. 68, nº 10, p. 3645–3654, 2008. ISSN: 00085472, DOI: 10.1158/0008-5472.CAN-07-2938.

OSORIO, M. et al. **Development of novel three-dimensional scaffolds based on bacterial nanocellulose for tissue engineering and regenerative medicine: Effect of processing methods, pore size, and surface area**. *Journal of Biomedical Materials Research - Part A*, [s.l.], v. 107, nº 2, p. 348–359, 2019. ISSN: 15524965, DOI: 10.1002/jbm.a.36532.

ÖSTMAN, A.; AUGSTEN, M. **Cancer-associated fibroblasts and tumor growth - bystanders turning into key players**. *Current Opinion in Genetics and Development*, [s.l.], v. 19, nº 1, p. 67–73, 2009. ISSN: 0959437X, DOI: 10.1016/j.gde.2009.01.003.

PADMANABAN, V. et al. **E-cadherin is required for metastasis in multiple models of breast cancer**. *Nature*, [s.l.], v. 573, nº 7774, p. 439–444, 2019. ISSN: 14764687, DOI: 10.1038/s41586-019-1526-3.

PAGET, S. **Distribution of secondary growths in cancer of the breast**. *The Lancet*, [s.l.], p. 571–573, 1889. ISBN: 9783540773405.

PAPENBURG, B. J. et al. **One-step fabrication of porous micropatterned scaffolds to control cell behavior**. *Biomaterials*, [s.l.], v. 28, nº 11, p. 1998–2009, 2007. ISSN: 01429612, DOI: 10.1016/j.biomaterials.2006.12.023.

_____. **Development and analysis of multi-layer scaffolds for tissue engineering**. *Biomaterials*, [s.l.], v. 30, nº 31, p. 6228–6239, 2009. ISSN: 01429612, DOI: 10.1016/j.biomaterials.2009.07.057.

PETERSEN, O. W. et al. **Interaction with basement membrane serves to rapidly distinguish growth and differentiation pattern of normal and malignant human breast epithelial cells**. *Proc. Natl Acad. Sci. USA*, [s.l.], v. 89, nº October, p. 9064–9068, 1992.

PETROVA, Y. I.; SCHECTERSON, L.; GUMBINER, B. M. **Roles for E-cadherin cell surface regulation in cancer**. *Molecular Biology of the Cell*, [s.l.], v. 27, nº 21, p. 3233–3244, 2016. ISSN: 19394586, DOI: 10.1091/mbc.E16-01-0058.

PICKUP, M. W.; MOUW, J. K.; WEAVER, V. M. **The extracellular matrix modulates the hallmarks of cancer**. *EMBO REPORTS*, [s.l.], v. 15, p. 1243–1253, 2014. ISSN: 22798013.

PROVENZANO, P. P. et al. **Collagen density promotes mammary tumor initiation and progression**. *BMC Medicine*, [s.l.], v. 6, p. 1–15, 2008. ISSN: 17417015, DOI: 10.1186/1741-7015-6-11.

PULS, T. J. et al. **3D collagen fibrillar microstructure guides pancreatic cancer cell phenotype and serves as a critical design parameter for phenotypic models of EMT**. *PLoS ONE*, [s.l.], v. 12, nº 11, 2017. DOI: 10.1371/journal.pone.0188870.

QUANTE, M. et al. **Bone Marrow-Derived Myofibroblasts Contribute to the Mesenchymal Stem Cell Niche and Promote Tumor Growth**. *Cancer Cell*, [s.l.], v. 19, nº 2, p. 257–272, 2011. ISSN: 15356108, DOI: 10.1016/j.ccr.2011.01.020.

QUESTIONS, F. A. **Corning ® Matrigel ® Matrix**. Corning. [s.d.]. Disponível em: <https://www.corning.com/media/worldwide/cls/.../CLS-DL-CC-026 DL.pdf>.

RADISKY, D. C.; KENNY, P. A.; BISSELL, M. J. **Fibrosis and cancer: Do myofibroblasts come also from epithelial cells via EMT?** *Journal of Cellular Biochemistry*, [s.l.], v. 101, nº 4, p. 830–839, 2007. ISSN: 07302312, DOI: 10.1002/jcb.21186.

RAMANI, D.; SASTRY, T. P. **Bacterial cellulose-reinforced hydroxyapatite functionalized graphene oxide : a potential osteoinductive composite**. *Cellulose*, [s.l.], v. 21, p. 3585–3595, 2014. DOI: 10.1007/s10570-014-0313-4.

RAMIÃO, N. G. et al. **Biomechanical properties of breast tissue, a state-of-the-art review**. *Biomechanics and Modeling in Mechanobiology*, [s.l.], v. 15, nº 5, p. 1307–1323, 2016. ISSN: 16177940, DOI: 10.1007/s10237-016-0763-8.

RECOUVREUX, D. **Desenvolvimento de Novos Biomateriais Baseados em Celulose Bacteriana para Aplicações Biomédicas e de Engenharia de Tecidos**. v. Único, 145 p. - Universidade Federal de Santa Catarina, 2008.

RECOUVREUX, D. O. S. et al. **Novel three-dimensional cocoon-like hydrogels for soft tissue regeneration**. *Materials Science and Engineering: C*, [s.l.], v. 31, nº 2, p. 151–157, 2011. ISSN: 0928-4931, DOI: 10.1016/J.MSEC.2010.08.004.

REIS, E. M. et al. **Bacterial nanocellulose-lKVAV hydrogel matrix modulates melanoma tumor cell adhesion and proliferation and induces**

vasculogenic mimicry in vitro. *Journal Biomedical Materials Research Part B*, [s.l.], p. 2741–2749, 2017. DOI: 10.1002/jbm.b.34055.

RIJAL, G.; LI, W. **A versatile 3D tissue matrix scaffold system for tumor modeling and drug screening**. *Science Advances*, [s.l.], v. 3, nº 9, 2017. ISBN: 23752548, DOI: 10.1126/sciadv.1700764.

RINN, J. L. et al. **Anatomic demarcation by positional variation in fibroblast gene expression programs**. *PLoS Genetics*, [s.l.], v. 2, nº 7, p. 1084–1096, 2006. ISSN: 15537390, DOI: 10.1371/journal.pgen.0020119.

ROMA-RODRIGUES, C. et al. **Targeting the tumor microenvironment for cancer therapy**. *International Journal of Molecular Sciences*, [s.l.], v. 20, nº 840, 2019. ISSN: 00099147, DOI: 10.1373/clinchem.2012.185363.

ROUWKEMA, J. et al. **Supply of nutrients to cells in engineered tissues**. *Biotechnology and Genetic Engineering Reviews*, [s.l.], v. 26, nº 1, p. 163–178, 2009. ISSN: 20465556, DOI: 10.5661/bger-26-163.

RUSSO, G. C. et al. **E-cadherin promotes cell hyper-proliferation in breast cancer**. *bioRxiv*, [s.l.], p. 2020.11.04.368746, 2020.

RYE, I. H. et al. **Intratumor heterogeneity defines treatment-resistant HER2+ breast tumors**. *Molecular Oncology*, [s.l.], v. 12, nº 11, p. 1838–1855, 2018. ISSN: 18780261, DOI: 10.1002/1878-0261.12375.

SAITO, H. et al. **Preparation and properties of transparent cellulose hydrogels**. *Journal of Applied Polymer Science*, [s.l.], v. 90, nº 11, p. 3020–3025, 2003. ISSN: 00218995, DOI: 10.1002/app.13015.

SAMANI, A.; ZUBOVITS, J.; PLEWES, D. **Elastic moduli of normal and pathological human breast tissues: An inversion-technique-based investigation of 169 samples**. *Physics in Medicine and Biology*, [s.l.], v. 52, nº 6, p. 1565–1576, 2007. ISSN: 00319155, DOI: 10.1088/0031-9155/52/6/002.

SÄMFORS, S. et al. **Biofabrication of bacterial nanocellulose scaffolds with complex vascular structure**. *Biofabrication*, [s.l.], v. 11, nº 4, 2019. ISSN: 17585090, DOI: 10.1088/1758-5090/ab2b4f.

SANNACHI, L. et al. **Response monitoring of breast cancer patients receiving neoadjuvant chemotherapy using quantitative ultrasound, texture, and molecular features**. *PLoS ONE*, [s.l.], v. 13, nº 1, p. 1–18, 2018. ISBN: 1111111111, ISSN: 19326203, DOI: 10.1371/journal.pone.0189634.

SASAKI, S. et al. **Crucial involvement of the CCL3-CCR5 axis-mediated fibroblast accumulation in colitis-associated carcinogenesis in mice**. *International Journal of Cancer*, [s.l.], v. 135, nº 6, p. 1297–1306, 2014. ISSN: 10970215, DOI: 10.1002/ijc.28779.

SAWA-WEJKSZA, K. et al. **Colon cancer–derived conditioned medium induces differentiation of THP-1 monocytes into a mixed population of M1/M2 cells**. *Tumor Biology*, [s.l.], v. 40, nº 9, p. 1–12, 2018. ISSN: 14230380, DOI: 10.1177/1010428318797880.

SCHWARTZ, R.; SCHÄFFER, A. A. **The evolution of tumour phylogenetics: Principles and practice**. *Nature Reviews Genetics*, [s.l.], v. 18, nº 4,

p. 213–229, 2017. ISSN: 14710064, DOI: 10.1038/nrg.2016.170.

SHALAPOUR, S.; KARIN, M. **Immunity, inflammation, and cancer: an eternal fight between good and evil**. *The Journal of Clinical Investigation*, [s.l.], v. 125, nº 9, p. 3347–3355, 2015. ISBN: 0021-9738, ISSN: 0021-9738, DOI: 10.1172/JCI80007.The.

SHASHNI, B. et al. **Size-based differentiation of cancer and normal cells by a particle size analyzer assisted by a cell-recognition PC software**. *Biological and Pharmaceutical Bulletin*, [s.l.], v. 41, nº 4, p. 487–503, 2018. ISSN: 13475215, DOI: 10.1248/bpb.b17-00776.

SHEN, T. et al. **Prognostic value of E-cadherin and β-catenin in triple-negative breast cancer**. *American Journal of Clinical Pathology*, [s.l.], v. 146, nº 5, p. 603–610, 2016. ISSN: 19437722, DOI: 10.1093/AJCP/AQW183.

SHI, Y.; YE, P.; LONG, X. **Differential Expression Profiles of the Transcriptome in Breast Cancer Cell Lines Revealed by Next Generation Sequencing**. *Cellular Physiology and Biochemistry*, [s.l.], v. 44, p. 804–816, 2017. DOI: 10.1159/000485344.

SHIGA, K. et al. **Cancer-associated fibroblasts: Their characteristics and their roles in tumor growth**. *Cancers*, [s.l.], v. 7, nº 4, p. 2443–2458, 2015. ISSN: 20726694, DOI: 10.3390/cancers7040902.

SILVA, T. R. S. DA. **Desenvolvimento de hidrogeis de celulose bacteriana para cultura de células e permeação de biomoléculas**. - Universidade Federal de Santa Catarina, 2012.

SIONKOWSKA, A.; MĘŻYKOWSKA, O.; PIĄTEK, J. **Bacterial nanocelullose in biomedical applications: a review**. *Polymer International*, [s.l.], v. 68, nº 11, p. 1841–1847, 2019. ISSN: 0959-8103, DOI: 10.1002/pi.5882.

SOUSA, S. et al. **Human breast cancer cells educate macrophages toward the M2 activation status**. *Breast Cancer Research*, [s.l.], v. 17, nº 1, p. 1–14, 2015. ISSN: 1465542X, DOI: 10.1186/s13058-015-0621-0.

SOUZA, S. S. De et al. **Nanocellulose biosynthesis by Komagataeibacter hansenii in a defined minimal culture medium**. *Cellulose*, [s.l.], v. 4, 2018. ISBN: 1057001821, ISSN: 1572-882X, DOI: 10.1007/s10570-018-2178-4.

STANTA, G.; BONIN, S. **Overview on clinical relevance of intra-tumor heterogeneity**. *Frontiers in Medicine*, [s.l.], v. 5, nº APR, p. 1–10, 2018. ISSN: 2296858X, DOI: 10.3389/fmed.2018.00085.

STEWART, B. W.; WILD, C. P. **World Cancer Report 2014**. 2014. Lyon: [s.n.], 2014.

SUNDBERG, J.; GÖTHERSTRÖM, C.; GATENHOLM, P. **Biosynthesis and in vitro evaluation of macroporous mineralized bacterial nanocellulose scaffolds for bone tissue engineering**. *Bio-Medical Materials and Engineering*, [s.l.], v. 25, nº 1, p. 39–52, 2015. ISSN: 18783619, DOI: 10.3233/BME-141245.

SUNDQVIST, A. et al. **JUNB governs a feed-forward network of TGFβ signaling that aggravates breast cancer invasion**. *Nucleic Acids Research*, [s.l.], v. 46, nº 3, p. 1180–1195, 2018. ISSN: 13624962, DOI: 10.1093/nar/gkx1190.

SWANTON, C. **Intratumor heterogeneity: Evolution through space and time**. *Cancer Research*, [s.l.], v. 72, nº 19, p. 4875–4882, 2012. ISSN: 00085472, DOI: 10.1158/0008-5472.CAN-12-2217.

TAKAHASHI, H. et al. **Cancer-associated fibroblasts promote an immunosuppressive microenvironment through the induction and accumulation of protumoral macrophages**. *Oncotarget*, [s.l.], v. 8, nº 5, p. 8633–8647, 2017. DOI: 10.18632/oncotarget.14374.

TEDESCO, S. et al. **Convenience versus biological significance: Are PMA-differentiated THP-1 cells a reliable substitute for blood-derived macrophages when studying in vitro polarization?** *Frontiers in Pharmacology*, [s.l.], v. 9, nº FEB, p. 1–13, 2018. ISSN: 16639812, DOI: 10.3389/fphar.2018.00071.

TIBBITT, M. W.; ANSETH, K. S. **Hydrogels as Extracellular Matrix Mimics for 3D Cell Culture**. *Biotechnology and Bioengineering*, [s.l.], v. 103, nº 4, p. 655–663, 2009. DOI: 10.1002/bit.22361.

TIEN, J. et al. **Matrix Pore Size Governs Escape of Human Breast Cancer Cells from a Microtumor to an Empty Cavity**. *iScience*, [s.l.], v. 23, nº 11, 2020. ISSN: 25890042, DOI: 10.1016/j.isci.2020.101673.

TOMLINS, P. et al. **Characterisation of Polymeric Tissue Scaffolds**. 2006. *a National Measurement Good Practice Guide*. 2006. ISBN: 1368–6550.

TRINCHIERI, G. **Innate inflammation and cancer: Is it time for cancer prevention?** *F1000 Medicine Reports*, [s.l.], v. 3, nº 1, p. 1–6, 2011. ISSN: 17575931, DOI: 10.3410/M3-11.

TYMOSZUK, P. et al. **In situ proliferation contributes to accumulation of tumor-associated macrophages in spontaneous mammary tumors**. *European Journal of Immunology*, [s.l.], v. 44, nº 8, p. 2247–2262, 2014. ISSN: 15214141, DOI: 10.1002/eji.201344304.

UPADHYAY, S. et al. **Role of immune system in tumor progression and carcinogenesis**. *Journal of Cellular Biochemistry*, [s.l.], v. 119, nº 7, p. 5028–5042, 2018. ISSN: 10974644, DOI: 10.1002/jcb.26663.

VOGELSTEIN, B. et al. **Cancer genome landscapes**. *Science*, [s.l.], v. 340, nº 6127, p. 1546–1558, 2013. ISSN: 10959203, DOI: 10.1126/science.1235122.

VU, L. T. et al. **Tumor-secreted extracellular vesicles promote the activation of cancer-associated fibroblasts via the transfer of microRNA-125b**. *Journal of Extracellular Vesicles*, [s.l.], v. 8, nº 1, 2019. ISSN: 20013078, DOI: 10.1080/20013078.2019.1599680.

VUKICEVIC, S. et al. **Identification of Multiple Active Growth Factors in Basement Membrane Matrigel Suggests Caution in Interpretation of Cellular Activity Related to Extracelular Matrix Components**. *Experimental Cell Research*, [s.l.], v. 202, 1992.

WAHBA, H. A.; EL-HADAAD, H. A. **Current approaches in treatment of triple-negative breast cancer**. *Cancer Biology and Medicine*, [s.l.], v. 12, nº 2, p. 106–116, 2015. ISSN: 20953941, DOI: 10.7497/j.issn.2095-3941.2015.0030.

WALKER, C.; MOJARES, E.; HERNÁNDEZ, A. del R. **Role of Extracellular**

Matrix in Development and Cancer Progression. *International Journal of Molecular Sciences*, [s.l.], v. 19, 2018. ISBN: 2075945187, DOI: 10.3390/ijms19103028.

WANG, J. et al. **Novel Bacterial Cellulose/Gelatin Hydrogels as 3D Scaffolds for Tumor Cell Culture**. *Polymers*, [s.l.], v. 10, nº 6, 2018. ISBN: 2073-4360, DOI: 10.3390/polym10060581.

WANG, T. et al. **Melanoma-derived conditioned media efficiently induce the differentiation of monocytes to macrophages that display a highly invasive gene signature**. *Pigment Cell and Melanoma Research*, [s.l.], v. 25, nº 4, p. 493–505, 2012. ISSN: 17551471, DOI: 10.1111/j.1755-148X.2012.01005.x.

WEBB, A. H. et al. **Inhibition of MMP-2 and MMP-9 decreases cellular migration, and angiogenesis in in vitro models of retinoblastoma**. *BMC Cancer*, [s.l.], v. 17, nº 1, p. 1–11, 2017. ISSN: 14712407, DOI: 10.1186/s12885-017-3418-y.

WEI, L. et al. **Cancer-associated fibroblasts promote progression and gemcitabine resistance via the SDF-1/SATB-1 pathway in pancreatic cancer**. *Cell Death and Disease*, [s.l.], v. 9, nº 11, 2018. ISSN: 20414889, DOI: 10.1038/s41419-018-1104-x.

WEIGELT, B et al. **Refinement of breast cancer classification by molecular characterization of histological special types**. *Journal of Pathology*, [s.l.], nº July, p. 141–150, 2008. DOI: 10.1002/path.

WEIGELT, Britta; BAEHNER, F. L.; REIS-FILHO, J. S. **The contribution of gene expression profiling to breast cancer classification, prognostication and prediction: a retrospective of the last decade**. *Journal of Pathology*, [s.l.], v. 220, p. 263–280, 2010. DOI: 10.1002/path.

WHANG, K. et al. **Engineering Bone Regeneration with Bioabsorbable Scaffolds with Novel Microarchitecture**. [s.l.], v. 5, nº 1, p. 35–51, 1999.

XIONG, G. et al. **A Novel in Vitro Three-Dimensional Macroporous Scaffolds from Bacterial Cellulose for Culture of Breast Cancer Cells**. *Journal of Biomaterials and Nanobiotechnology*, [s.l.], v. 4, nº October, p. 316–326, 2013. DOI: 10.4236/jbnb.2013.44040.

XUE, Y.; MOU, Z.; XIAO, H. **Nanocellulose as a sustainable biomass material: structure, properties, present status and future prospects in biomedical applications**. *Nanoscale*, [s.l.], v. 9, nº 39, p. 14758–14781, 2017a. DOI: 10.1039/C7NR04994C.

_____. **Nanoscale structure, properties, present status and future**. *Nanoscale*, [s.l.], v. 9, p. 14758–14781, 2017b. DOI: 10.1039/c7nr04994c.

YAMADA, Y. et al. **Subdivision of the genus Gluconacetobacter Yamada, Hoshino and Ishikawa 1998: The proposal of Komagatabacter gen. nov., for strains accommodated to the Gluconacetobacter xylinus group in the α-Proteobacteria**. *Annals of Microbiology*, [s.l.], v. 62, nº 2, p. 849–859, 2012. ISSN: 15904261, DOI: 10.1007/s13213-011-0288-4.

YANG, J. et al. **Monocytes and macrophage differentiation: circulation inflammatory monocyte as biomarker for inflammatory diseases**. *Biomarker Research*, [s.l.], v. 2, 2014. ISSN: 00368075, DOI: 10.1126/science.312.5782.1868.

YAVUZ, B. G. et al. **Cancer associated fibroblasts sculpt tumour microenvironment by recruiting monocytes and inducing immunosuppressive PD-1 + TAMs**. *Scientific Reports*, [s.l.], v. 9, nº 1, p. 1–15, 2019. ISSN: 20452322, DOI: 10.1038/s41598-019-39553-z.

YERUSHALMI, R.; HAYES, M. M.; GELMON, K. A. **Breast carcinoma - Rare types: Review of the literature**. *Annals of Oncology*, [s.l.], v. 20, nº 11, p. 1763–1770, 2009. ISSN: 09237534, DOI: 10.1093/annonc/mdp245.

YOSHIDA, G. J. et al. **Activated fibroblast program orchestrates tumor initiation and progression; molecular mechanisms and the associated therapeutic strategies**. *International Journal of Molecular Sciences*, [s.l.], v. 20, nº 9, 2019. ISSN: 14220067, DOI: 10.3390/ijms20092256.

YU, X. L. et al. **Overexpression of IL-12 reverses the phenotype and function of M2 macrophages to M1 macrophages**. *International Journal of Clinical and Experimental Pathology*, [s.l.], v. 9, nº 9, p. 8963–8972, 2016. ISSN: 19362625.

YUAN, Y. et al. **Role of the tumor microenvironment in tumor progression and the clinical applications (Review)**. *Oncology Reports*, [s.l.], v. 35, nº 5, p. 2499–2515, 2016. ISSN: 17912431, DOI: 10.3892/or.2016.4660.

ZABOROWSKA, M. et al. **Microporous bacterial cellulose as a potential scaffold for bone regeneration**. *Acta Biomaterialia*, [s.l.], v. 6, nº 7, p. 2540–2547, 2010. ISSN: 1742-7061, DOI: 10.1016/j.actbio.2010.01.004.

ZANG, S. et al. **Investigation on artificial blood vessels prepared from bacterial cellulose**. *Materials Science & Engineering C*, [s.l.], v. 46, p. 111–117, 2015. ISSN: 0928-4931, DOI: 10.1016/j.msec.2014.10.023.

ZEISBERG, E. M. et al. **Discovery of endothelial to mesenchymal transition as a source for carcinoma-associated fibroblasts**. *Cancer Research*, [s.l.], v. 67, nº 21, p. 10123–10128, 2007. ISBN: 6179755663, ISSN: 00085472, DOI: 10.1158/0008-5472.CAN-07-3127.

ZHANG, B. et al. **M2-polarized macrophages promote metastatic behavior of Lewis lung carcinoma cells by inducing vascular endothelial growth factor-C expression**. *Clinics*, [s.l.], v. 67, nº 8, p. 901–906, 2012. ISSN: 18075932, DOI: 10.6061/clinics/2012(08)08.

ZHANG, J.; LIU, J. **Tumor stroma as targets for cancer therapy**. *Pharmacol Ther*, [s.l.], v. 137, nº 2, p. 200–215, 2013. ISBN: 6176321972, ISSN: 15378276, DOI: 10.1038/jid.2014.371.